Fiber composites-based flexible triboelectric nanogenerators: from material design to emerging applications

OPEN ACCESS
IMMT | IOP Publishing
International Journal of Extreme Manufacturing
Int. J. Extrem. Manuf. **8** (2026) 012010 (42pp)
https://doi.org/10.1088/2631-7990/ae0a90

Topical Review

Fiber composites-based flexible triboelectric nanogenerators: from material design to emerging applications

Gang Yu[1,§], Han Hu[1,§], Qianguo Yu[1,§], Chun Li[1,3], Dongdong Zhou[1], Zuankai Wang[2] and Kedong Bi[1,*]

[1] Jiangsu Key Laboratory for Design and Manufacturing of Precision Medicine Equipment, School of Mechanical Engineering, Southeast University, Nanjing 211189, People's Republic of China
[2] Department of Mechanical Engineering, The Hong Kong Polytechnic University, Hong Kong 999077, People's Republic of China
[3] College of Mechanical Engineering, Yangzhou University, Yangzhou 225009, People's Republic of China

E-mail: kedongbi@seu.edu.cn

Received 27 February 2025, revised 11 May 2025
Accepted for publication 22 September 2025
Published 22 October 2025

Abstract

The rise of portable electronic devices and Internet of Things (IoT) has spurred significant interest in flexible triboelectric nanogenerators (TENGs) as sustainable energy solutions. The electrical performance of TENGs is profoundly influenced by nanoscale factors, including interface properties and material characteristics, highlighting the critical need for a comprehensive understanding of these parameters to unlock their full potential. This paper summarizes the recent advances in advanced fiber composite TENGs (FC-TENGs), especially electrospun nanofibers, with a focus on key nanoscale properties, covering triboelectric layer interface characteristics, dielectric constant, electron affinity, and crystal phase, all of which are fundamental to optimizing their output performance. Additionally, it explores emerging applications of FC-TENGs in wearable electronics, self-powered sensors, wireless communication systems, human-machine interfaces, and modern healthcare technologies. The review concludes by addressing existing challenges, evaluating future opportunities, and outlining research directions for advancing FC-TENGs. By bridging foundational material science with innovative applications, this review seeks to inspire the development of high-performance, self-powered electrospun composite tribovoltaic nanogenerators, paving the way for a wireless, artificial intelligence (AI)-enabled IoT era.

§ These authors contributed to this work equally.
* Author to whom any correspondence should be addressed.

Keywords: fiber composite triboelectric nanogenerators, triboelectric lay characteristics, liquid metal nanoparticles, emerging application, TVNG, bulk effect

1. Introduction

Flexible electronic devices, with their unique advantages of seamless connection to the human body, real-time environmental monitoring, and intelligent interaction, are rapidly emerging as one of the most promising technological fields in the era of the Internet of Things (IoT)[1–3]. However, common fuel cells face limitations in biocompatibility and rigidity, making them unsuitable for the application in flexible electronic devices[4–6]. As an emerging energy-capturing technology, triboelectric nanogenerators (TENGs) leverage triboelectric and electrostatic effects to efficiently capture low-entropy energy from environmental sources, including mechanical movements[7,8], human movements[9,10], wind[11,12], and water[13,14], and transform it into electrical energy[15–17]. With its simple structure, low cost, and eco-friendliness, TENG presents a highly promising solution for sustainable energy supply in flexible electronic devices[18–22].

Despite these merits, TENGs still face numerous challenges with respect to energy conversion efficiency, output stability, robustness, etc., which hinder their practical application[23–26]. The performance of TENGs is intricately linked to their material composition and microstructural design, yet existing materials often fail to simultaneously achieve high conversion efficiency, stable performance, and environmental resilience[27–30]. Therefore, it is imperative to make breakthroughs in material design to create novel high-performance materials that address the key bottlenecks of TENG[31–36].

Compared with conventional flexible films, the inherent breathability, light weight, high specific surface area, and excellent mechanical properties of triboelectric layers or electrode layers made of fiber materials have become a research hotspot for improving the performance of flexible TENGs[37–41]. On one hand, fibers can be made from a variety of materials, including natural fibers, synthetic fibers, and nanocomposites, offering flexible material selection to optimize performance according to specific requirements[42–44]. Fiber composite TENGs (FC-TENGs) enable nanoscale structural design, specifically hierarchical[45,46], gradient[47,48], and porous structures[49,50], offering effective ways to optimize TENG performance. To quantitatively demonstrate the superiority of FC-TENGs, Song et al. investigated different film-forming processes of PVDF films and their effects on the triboelectric output performance. By comparing the performance of TENGs using cast PVDF films and electrospun PVDF films as friction layers, the results showed that the output voltage and short-circuit current of the electrospun TENG were 2.3 times and 2.88 times those of the cast TENG, respectively[51]. The primary components of a TENG are the triboelectric layer and electrode layer. Fiber manufacturing processes such as electrospinning, melt spinning, and wet spinning can be used to produce high-performance triboelectric layers and highly conductive electrode layers for flexible TENGs[52–56], which have important potential application prospects in fields such as energy harvesting, sensors, wireless communication, human-machine interfaces, and wearable electronics[57–62]. Figure 1 shows various applications of FC-TENGs.

The materials of flexible TENGs are usually composed of single polymers, such as polyvinyl alcohol (PVA)[63,64], thermoplastic polyurethane (PU)[65,66], polytetrafluoroethylene (PTFE)[67,68], etc.[69–73]. These materials possess good flexibility and electrical properties, making them suitable for the triboelectric layers of TENGs. Although they exhibit satisfactory electrical insulation, their positions in the triboelectric series are relatively fixed, which limits the charge transfer efficiency. Composites composed of polymer matrix and fillers significantly improve the material's performance through the synergistic effect between the matrix and the fillers[74–76]. The introduction of fillers can regulate the physical and chemical properties of materials at the nanoscale or microscale. Researchers have significantly enhanced the conductivity of materials by introducing conductive fillers into the polymer matrix[77,78]. Introducing certain nanoparticles can improve the composites' mechanical strength and thermal stability[79,80]. Additionally, two-dimensional (2-D) materials, by virtue of their large specific surface area and distinctive layered architecture, can substantially enhance the mechanical properties, thermal conductivity, and barrier properties of the materials[81,82]. As a result, fillers can effectively adjust the polymers' position in the triboelectric series, thus boosting the TENG's output performance and opening avenues for TENG applications across various scenarios[83–87]. FC-TENG has been rapidly developed and significantly advanced, achieving numerous milestones and novel applications (Figure 2).

Composites have demonstrated remarkable capabilities in enhancing the performance of flexible TENGs, and significant progress has been made. For example, by mixing conductive nanoparticles with polymer precursor solutions, nanofiber membranes with high-efficiency triboelectric charge collection capabilities can be prepared, which greatly improves the output power of TENGs[88–92]. By incorporating nanoparticles with elevated dielectric properties into the fiber matrix, the electrostatic induction effect can be strengthened, improving energy conversion efficiency of TENGs[93–97]. By incorporating environmentally adaptive functional materials into the fiber structure, the environmental tolerance and long-term stability of TENGs can be enhanced[98–102]. Additionally, researchers have explored various structural design strategies, such as constructing helical[103,104], woven[105,106], and three-dimensional network structures[107–109], to achieve multi-dimensional optimization of TENG performance.

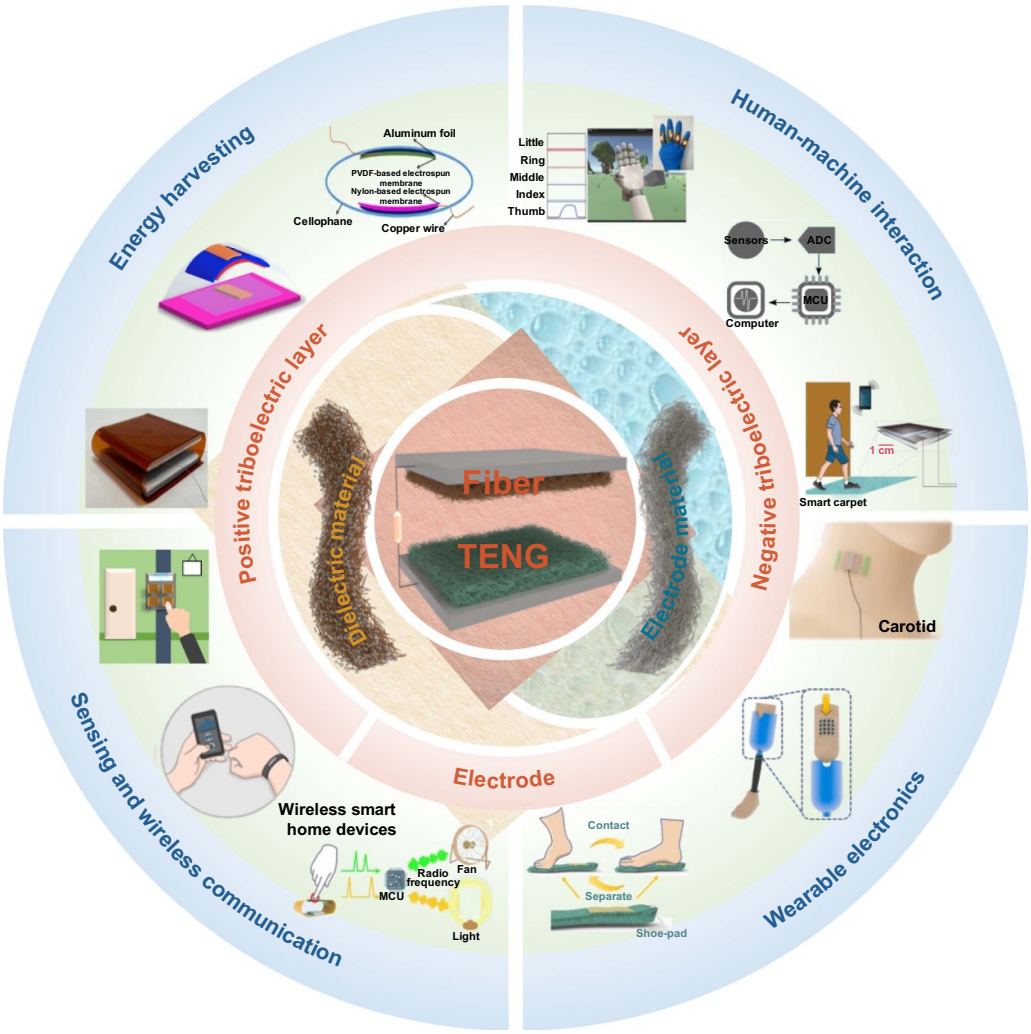

Figure 1. Various applications of fiber composite material TENGs. Energy harvesting. Reprinted from[110], Copyright (2020), with permission from Elsevier. Reprinted from[111], Copyright (2020), with permission from Elsevier. Reproduced from[112]. CC BY 4.0. Human-machine interaction (HMI). Reprinted from[113], Copyright (2022), with permission from Elsevier. Reprinted from[114], Copyright (2024), with permission from Elsevier. Reprinted from[115], Copyright (2024), with permission from Elsevier. Wearable electronics. Reprinted from[116], Copyright (2022), with permission from Elsevier. Reprinted from[117], Copyright (2023), with permission from Elsevier. Reprinted from[118], Copyright (2023), with permission from Elsevier. Sensing and wireless communication. Reprinted from[119], Copyright (2023), with permission from Elsevier. Reprinted from[120], Copyright (2022), with permission from Elsevier.[121] John Wiley & Sons. © 2022 Wiley-VCH GmbH.

To date, several reviews on TENGs, their manufacturing materials, and processes have been published. However, the mechanism by which filler materials in composites affect the performance of different triboelectric layers remains unclear. Moreover, the unique advantages of FC-TENGs in emerging applications such as wireless sensing, human-machine interfaces (HMIs), and modern healthcare have not been fully explored. Given the significant potential and progress of FC-TENGs, a comprehensive review and summary of relevant research findings are of great importance. This review provides a thorough overview and in-depth insights into recent developments in FC-TENGs research, from fundamental material design to some emerging applications of FC-TENGs. The review will be organized as follows: Section 2 introduces the commonly used fiber manufacturing technologies for TENGs, with a primary focus on the most widely used electrospinning technology and spinning materials. Section 3 analyzes the differences among various working modes and equivalent circuit models of TENGs. Section 4 discusses the structural parameters affecting triboelectric layer performance, focusing on interface characteristics, dielectric constants, electron affinity, and crystalline phases. Section 5 explores emerging applications of FC-TENGs, including wearable electronics, self-powered sensors, modern healthcare, wireless communication, and HMI. Finally, Section 6 provides a comprehensive evaluation of the current challenges in FC-TENGs and offers valuable insights into the future prospects of the field, addressing the need for continued research and development. We aim for this review to highlight potential pathways for the advancement of fiber composite tribovoltaic nanogenerators (FC-TVNG) and inspire a paradigm shift toward self-powered wireless AI-IoT era.

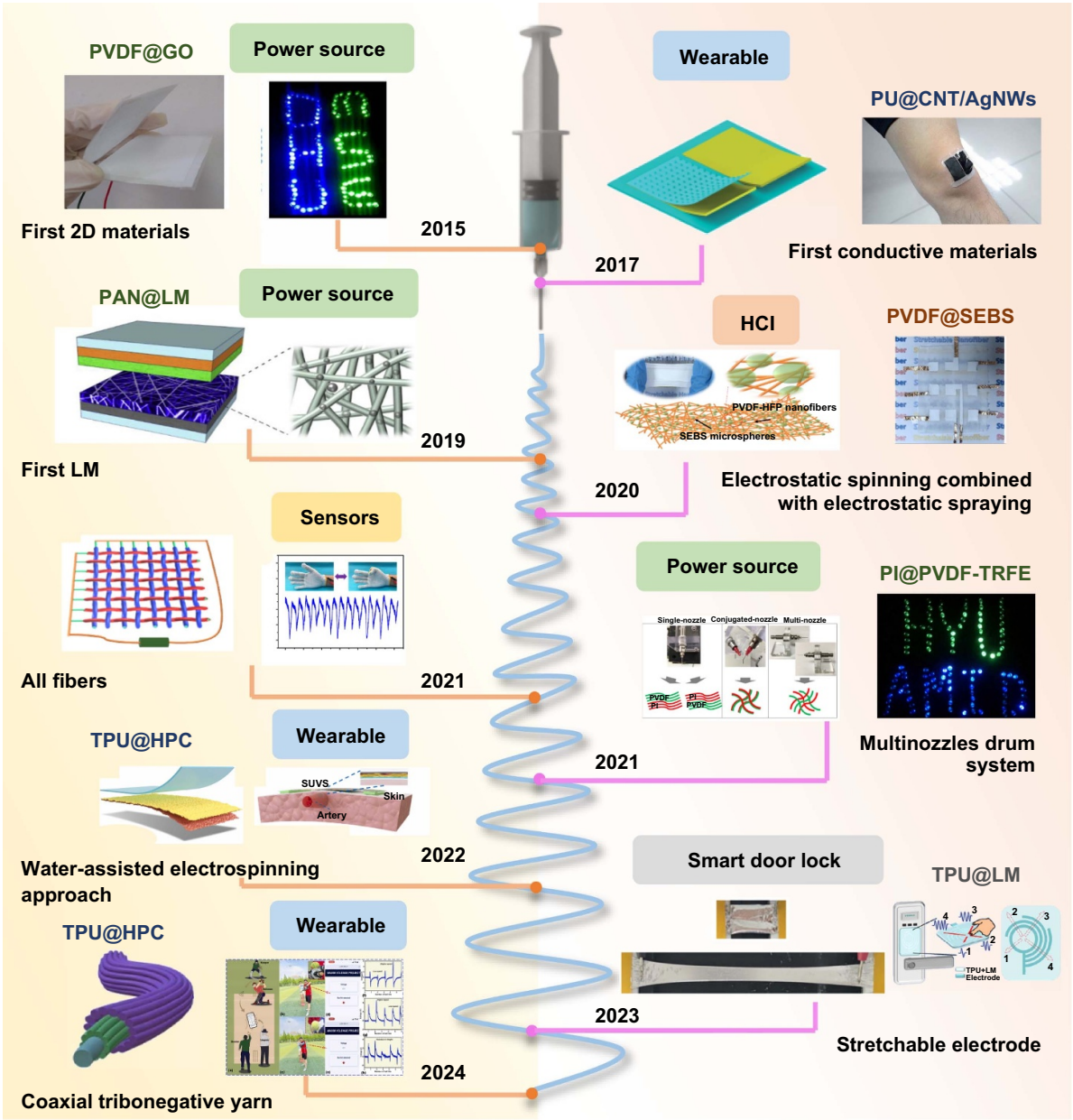

Figure 2. Development of FC-TENG. In 2015, composite fiber for TENG. Reproduced from[122]. CC BY 4.0. In 2017, conductive materials for FC-TENG. Reproduced from[123] with permission from the Royal Society of Chemistry. In 2019, liquid metal (LM) for FC-TENG. Reprinted from[124], Copyright (2019), with permission from Elsevier. In 2020, a combination of electrospinning and electrospraying. Reprinted from[125], Copyright (2020), with permission from Elsevier. In 2021, all-fiber FC-TENG. Reprinted from[126], Copyright (2021), with permission from Elsevier. In 2021, multi-nozzle technology for FC-TENG. Reprinted with permission from[127]. Copyright (2021) American Chemical Society. In 2022, an external factor-assisted electrospinning method for FC-TENG. Reprinted from[116], Copyright (2022), with permission from Elsevier. In 2023, stretchable FC-TENG. Reprinted from[128], Copyright (2023), with permission from Elsevier. In 2024, coaxial triboelectric fibers. Reprinted from[129], Copyright (2024), with permission from Elsevier.

2. Working principle of TENG

To elucidate the influence of fillers on TENGs, it is necessary first to analyze the working principle of TENGs. TENG leverages the principles of triboelectrification and electrostatic induction to facilitate charge transfer, with triboelectrification serving as the core physical process driving it[130]. Based on distinct physical principles and charge transfer mechanisms, TENGs exhibit four distinct operational modes: vertical contact-separation mode (CS)[131,132], lateral sliding mode (LS)[133,134], single-electrode mode (SE)[135,136], and freestanding layer mode (FS)[137,138] (Figures 3(a)–(d), where two polymer materials with differing electron affinities serve as triboelectric layers, or one polymer material and one conductive material acting concurrently as both an electrode and a triboelectric layer). Within these modes, CS and SE are categorized as normal motion modes, while LS and FS are tangential motion modes. In terms of charge transfer, normal motion

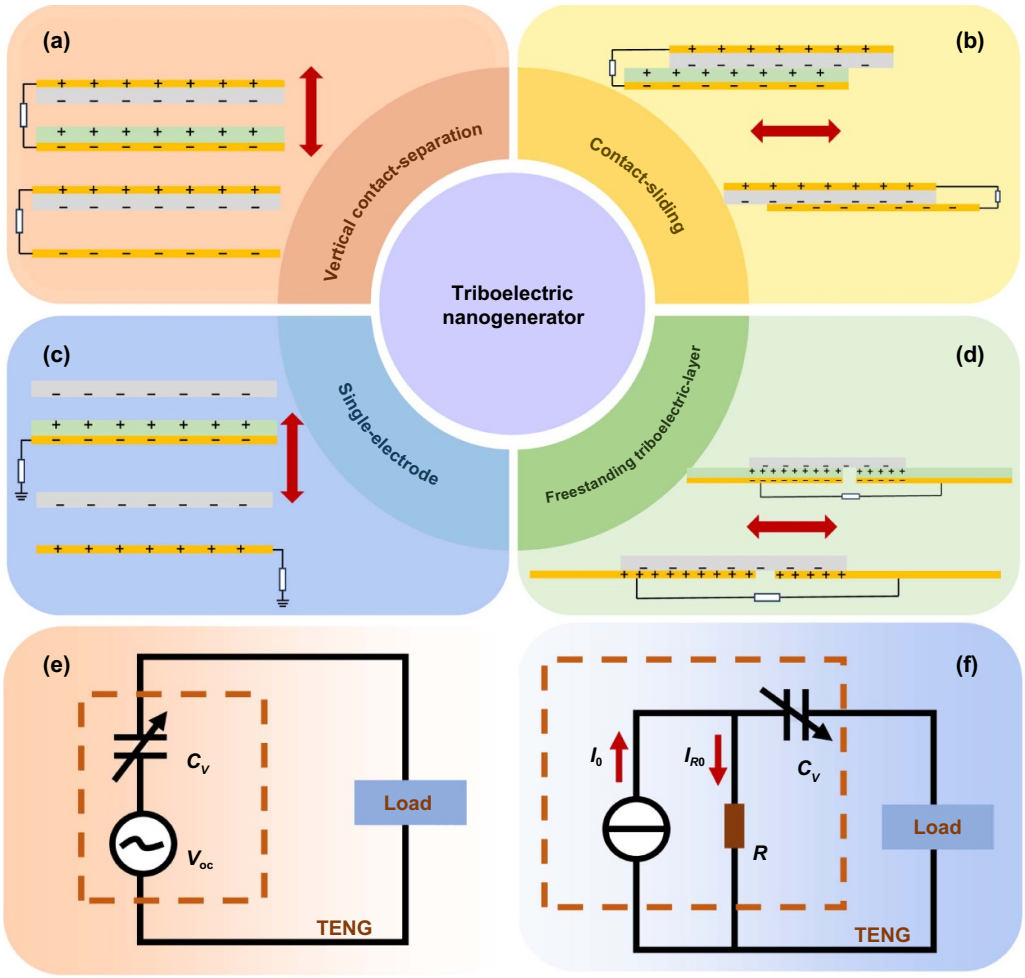

Figure 3. Working principle of TENG. (a) Vertical contact-separation mode. (b) Lateral sliding mode. (c) Single-electrode mode. (d) Freestanding layer mode. (e) Voltage source model. (f) Current source model.

mode generators have brief contact time, resulting in minimal triboelectric charges due to the predominance of small, normal directional micro-displacements and low triboelectric forces. Consequently, their effective output performance is limited, but their durability is enhanced[139–141]. Conversely, tangential motion mode generators, where triboelectric is dynamic, produce higher triboelectric charges and superior effective output performance, but with limited durability[142–144]. Concerning electrical signal output, normal motion mode TENGs undergo electrode polarization followed by instantaneous contact and subsequent charge transfer. As a result, the output electrical signals are pulsed, with rapid changes in current direction. In contrast, tangential motion modes maintain continuous electrode contact, yielding continuous electrical signals with slower current direction changes. Through these four operational modes, TENGs can adapt flexibly to various mechanical stimuli and application scenarios, thus enhancing energy collection efficiency and versatility.

2.1. Four working modes of TENG

2.1.1. CS mode. In Figure 3(a), once the two triboelectric layers physically interact, electron exchange occurs across their interfaces because of varying electron affinities, resulting in the build-up of triboelectric charges with opposite polarities on both surfaces. Upon separation of the two triboelectric layers via external force, an air gap emerges between the formerly contacting surfaces, concurrently inducing a potential difference between the electrodes. When the electrodes are linked via a load, electron movement occurs from one electrode to the other across the external circuit, generating a counter potential that counteracts the electrostatic field. At maximum separation of the electrodes, charge transfer concludes, and the system attains charge equilibrium. Upon recontact of the triboelectric layers, the potential difference induced by triboelectric charges vanishes, causing electrons to move in the reverse direction. The cyclic contact and separation process produces an alternating current (AC) signal[145,146].

2.1.2. LS mode. Figure 3(b) shows that this mode has the same structural configuration as the CS mode. The variation in induced potential difference arises from changes in the tangential contact area among triboelectric layers. LS-TENG can exist in multiple forms, including planar sliding, cylindrical sliding, and disk sliding[147].

Table 1. Comparison of TENGs in different operating modes.

	Advantages	Disadvantages
CS	Simple structure, wide material adaptability	Large vertical displacement required, lower output power
LS	Good output stability, adjustable performance, less sensitive to displacement direction	Complex fabrication, high friction loss
SE	Simple structure, wide application scenarios, flexible contact requirements	Low output performance, easily affected by the environment, low energy collection efficiency
FE	Stable output, non-contact operation, long lifespan	Complex fabrication, high environmental requirements

2.1.3. Single-electrode mode. In certain scenarios, specific parts of the generator are moving components, making it inconvenient to connect them via wires and electrodes. To facilitate easier energy collection, a single-electrode mode has been introduced, where the device has an electrode on only one end. This electrode connects to a reference electrode via a load, with the reference electrode typically grounded (Figure 3(c)). The primary structural distinction between the SE mode and the CS mode is the reduction in electrodes on the dielectric layer. In CS mode, electrons move between different electrodes, whereas in SE mode, only one set of electrodes exchanges charges with ground or a zero-potential point. This leads to the waste of charges on the other electrode, resulting in lower output performance in SE mode. However, during device design, electrode placement is simpler in SE mode, which provides significant advantages in self-powered sensing and solid-liquid energy generation applications[148].

2.1.4. Freestanding layer mode. In most cases, electrodes need to be fixed on the same side, leading to the formation of the FE mode. In the FE mode, the electrodes are placed on the same side (Figure 3(d)), with the dielectric layer moving back and forth between them, resulting in periodic charge variations. Due to the enlarged frictional distance in the FE mode, the induced charge generated from triboelectricity increases, enhancing the output performance. However, this reduces the space efficiency of the device. Compared to other modes, the FE mode offers advantages such as better output performance and more reasonable layout[149,150].

Based on the operating principles and introductions of TENGs in the aforementioned different modes, Table 1 summarizes the advantages and disadvantages of TENGs in different operating modes.

2.2. Electrical model of TENG

Owing to the fact that the interfacial wear induced by tangential motion is significantly more severe than that caused by normal motion, coupled with the unique structural characteristics of FC-TENGs, nearly all FC-TENGs adopt the CS mode and the SE mode. The electrical models of this kind of TENG exhibit similarities. The research of their equivalent circuit models often categorizes them into current source and voltage source equivalent circuit models[151]. Among these, the most classical circuit model is the voltage source equivalent circuit model constructed by Wang et al. in 2013 (Figure 3(e))[152]. The voltage source equivalent circuit model consisted of an internal capacitor and an open-circuit voltage source. An internal capacitor C was formed due to the electrostatic charge induction in the dielectric layer of the TENG. Additionally, a voltage source was incorporated based on the correlation between charge and voltage, thereby establishing the voltage source equivalent circuit model. Using the node method, the capacitance composition and electrical theory for each mode were derived; additionally, the theoretical correlation between the optimal resistance and output performance was calculated, providing important guidance for the structural design of CS-TENGs[153]. That same year, a model for the sliding mode TENG was also created. Through simulations, the potential, electric field, and charge distribution across the metal electrodes were characterized, and the V-Q-x control equations of the generator were studied, providing theoretical guidance for the sliding mode[145,154].

In 2014, a theoretical framework for the SE-TENG was investigated, and the effects of two key structural parameters, electrode spacing and area, on output performance were studied theoretically, providing crucial guidance for rational design of device structures to achieve optimal output in specific applications[155]. In 2015, the theoretical framework of FS-TENG was investigated[149], discussing the performance metrics of standard FS-TENG and elucidating that the suspended layer material, electrode spacing, and suspension height significantly influence the output characteristics of FS-TENG. In summary, the voltage source equivalent circuit model serves as the foundation for the theoretical models of the four basic modes. However, since the power supply characteristics of TENGs have not been fully explored, and the voltage source equivalent circuit does not fully represent the external output characteristics of TENGs, further supplementation is needed in the research on voltage source equivalent circuit models.

According to current research, some scholars have proposed different perspectives on the equivalent power source type of TENGs. Studies have found that TENGs exhibit characteristics more akin to a current source. Zhang et al. compared the theoretical and load characteristics of electromagnetic generators and TENGs[156], determining the control

equations for TENGs and validating their equivalent circuits both theoretically and experimentally. Zhang et al. also conducted a systematic analysis and comparison of the control equations and output metrics, with the goal of establishing complementary uses for the two technologies. Consequently, TENGs can be regarded as current sources with high internal resistance, whereas electromagnetic generators can be equivalently modeled as voltage sources with low internal resistance. In summary, TENGs can be classified as current sources.

To determine whether a TENG is a voltage source or a current source, it is essential to investigate the fundamental theories of generators. The theoretical origin of TENGs is based on the displacement current within Maxwell's equations[150]. According to Maxwell's equations, the electric displacement vector is:

$$D = \varepsilon_0 E + P \tag{1}$$

where E, ε_0, P, are the electric field, the permittivity of free space, and the polarization field density, respectively. For isotropic media, based on Maxwell-Ampère's law, the second term is defined as Maxwell's displacement current:

$$J_D = \frac{\partial D}{\partial t} = \varepsilon_0 \frac{\partial E}{\partial t} + \frac{\partial P}{\partial t}. \tag{2}$$

According to the principle of CS-TENG, the electrostatic field established by triboelectric charges drives the flow of electrons through an external load, leading to the accumulation of free electrons σ_1 and σ_2 in the upper and lower electrodes, respectively. The distance between the two triboelectric layers is a function of z_t, representing the process of converting mechanical energy into electrical energy. The electric fields in triboelectric layers 1 and 2 are given by $E_z = \sigma_1/\varepsilon_1$ and $E_z = \sigma_1/\varepsilon_2$, respectively, while the internal gap electric field is $E_z = (\sigma_1 - \sigma_c)/\varepsilon_0\sigma_c$, where σ_c is the surface charge density.

The relative voltage difference between the two electrodes is:

$$V = \sigma_1 (d_1/\varepsilon_1 + d_2/\varepsilon_2) + z(\sigma_1 - \sigma_c)/\varepsilon_0. \tag{3}$$

Where d_1 and d_2 are the thicknesses of the two triboelectric layers, respectively. Under short-circuit conditions, i.e., $V = 0$,

$$\sigma_1 = \frac{z\sigma_c}{d_1\varepsilon_0/\varepsilon_1 + d_2\varepsilon_0/\varepsilon_2 + z}. \tag{4}$$

From Equation (4), the displacement current density within the material is:

$$J_D = \frac{\partial D_z}{\partial t} = \frac{\partial \sigma_1}{\partial t} = \sigma_c \frac{dz}{dt} \frac{d_1\varepsilon_0/\varepsilon_1 + d_2\varepsilon_0/\varepsilon_2}{[d_1\varepsilon_0/\varepsilon_1 + d_2\varepsilon_0/\varepsilon_2 + z]^2} + \frac{d\sigma_c}{dt} \frac{z}{d_1\varepsilon_0/\varepsilon_1 + d_2\varepsilon_0/\varepsilon_2 + z}. \tag{5}$$

According to Ohm's law, the output current equation is:

$$RA\frac{d\sigma_c}{dt} = z\sigma_c/\varepsilon_0 - \sigma_1 [d_1/\varepsilon_1 + d_2/\varepsilon_2 + z/\varepsilon_0]. \tag{6}$$

Where R is the load resistance, and A can be equivalently regarded as the effective contact area of the triboelectric layer.

The transfer charge within the TENG's internal circuit is fundamental to its output, and a variable capacitance exists inside the TENG. Therefore, the TENG and the external load form a resistor-capacitor (RC) load circuit. Additionally, the root cause of the TENG's operation is the triboelectric charge and the internal current source it forms. The parameters related to the transfer charge and the internal power source directly influence the output of the generator[157].

Based on the output characteristics of the TENG, the internal circuit of the TENG mainly consists of a variable capacitor, an internal equivalent resistance, and multiple constant capacitors. By simplifying the circuit, combining the capacitors and resistors, and adding a current source, Zhao et al. proposed the current source equivalent circuit model of the TENG[158], as shown in Figure 3(f). This model includes a current source I_0, an internal equivalent resistance R_0, and an internal capacitor C_0. Each generation mode can be equivalently represented by this current source equivalent circuit model. It is evident that the internal equivalent resistance is in parallel with the current source and in series with the internal variable capacitor. Compared to the voltage source equivalent circuit model, the current source equivalent circuit model not only clarifies the origin of the internal resistance of the TENG and the composition of the internal circuit but also provides a theoretical foundation for the study of TENGs normalization methods.

3. Fiber manufacturing technologies for TENGs

Fiber manufacturing technologies have brought numerous possibilities for the performance improvement and application expansion of TENGs. This section will focus on elaborating the specific application performances of different fiber manufacturing technologies in TENGs.

3.1. Electrospinning-based TENGs

Electrospinning utilizes strong electric fields to elongate polymer solutions/melts into fibers with diameters ranging from micrometers to nanometers, as shown in Figure 4[159,160]. The system primarily comprises a high-voltage power supply, a syringe, and a collector. In 2015, Wang et al. quantitatively measured the charge density generated by triboelectrification of different triboelectric materials using mercury, that was the electron-gain and -loss situations of various materials. They then ranked these triboelectric materials according to the strength of their electron-gain and -loss abilities[161]. Figure 4 depicts the common triboelectric polymers used in electrospinning. Among them, the electron affinity gradually increases from EC to PET. In the second row, PTFE follows PET with a further increase in electron affinity, and PVB has the strongest electron affinity. During the triboelectric charging process, materials with greater electron affinity tend to attract electrons and become negatively charged[162–165]. By introducing functional groups containing

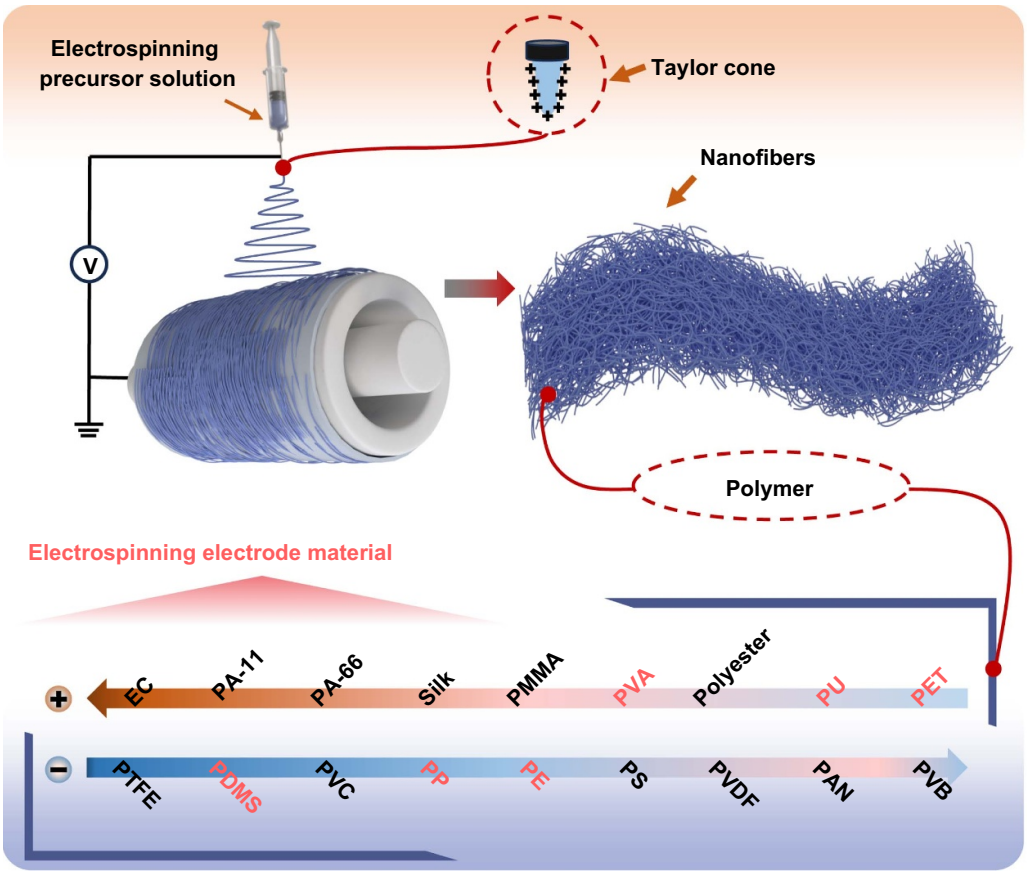

Figure 4. Electrospinning-based TENGs and functional materials. Ethyl cellulose (EC), nylon (PA), polymethyl methacrylate (PMMA), polyvinyl alcohol (PVA), polyurethane (PU), polyethylene terephthalate (PET), polytetrafluoroethylene (PTFE), polydimethylsiloxane (PDMS), polyvinyl chloride (PVC), polypropylene (PP), polyethylene (PE), polystyrene (PS), polyvinylidene fluoride (PVDF), polyacrylonitrile (PAN), polyvinyl butyral (PVB).

oxygen atoms, such as hydroxyl and oxide groups, the polarity of the bottom material can be increased, making it more electron-attracting[166–168]. Materials exhibiting less electron affinity are prone to shedding electrons and acquiring a positive charge. This can be achieved by incorporating conductive impurities like metal particles, conductive polymers, or conductive carbon nanomaterials, which provide additional electron conduction pathways, enhancing conductivity and electron mobility, thus causing the material to lose more electrons[169,170]. The greater the electron affinity difference between triboelectric layers is, the greater the corresponding amount of charge transfer. Materials in red font gain conductivity by adding conductive materials and are commonly used as electrode materials in flexible TENGs. A voltage is applied between the syringe and the collector (usually spanning from several kilovolts to hundreds of kilovolts), creating a high-voltage electric field. When the voltage at the needle tip reaches a certain threshold, the polymer solution surmounts surface tension due to the electric field, leading to the formation of a Taylor cone. The fine stream jetting from the tip of the Taylor cone is rapidly stretched and dried under the action of the electric field, forming nanofibers. These nanofibers are attracted to the grounded or negatively charged collector plate by the electric field force and deposit into a non-woven fabric-like fibrous structure. Depending on the type of collector, the morphology of the nanofiber film can vary. When using a flat-plate collector, nanofibers are randomly arranged due to multiple factors such as jet instability, environmental factors, and solution properties. Some researchers have achieved the patterning of nanofiber thin-films by using a patterned flat-plate collector[171]. If methods such as using a rapidly rotating drum collector or magnetic field assistance are employed, nanofiber thin-film with oriented arrangement can be obtained[172,173]. In addition, Li et al. used a conical collector and successfully obtained micron-scale fiber long-lines composed of nanofibers[174]. Duan et al. have comprehensively analyzed the influence of collector type on the morphology of nanofibers[33], so further elaboration will not be provided here.

3.2. *Wet spinning*

Wet spinning forms solid fibers through the controllable phase separation of polymer solutions (Figure 5(a)). Similar to the preliminary preparations for electrospinning, it is necessary to prepare a uniform spinning solution with a

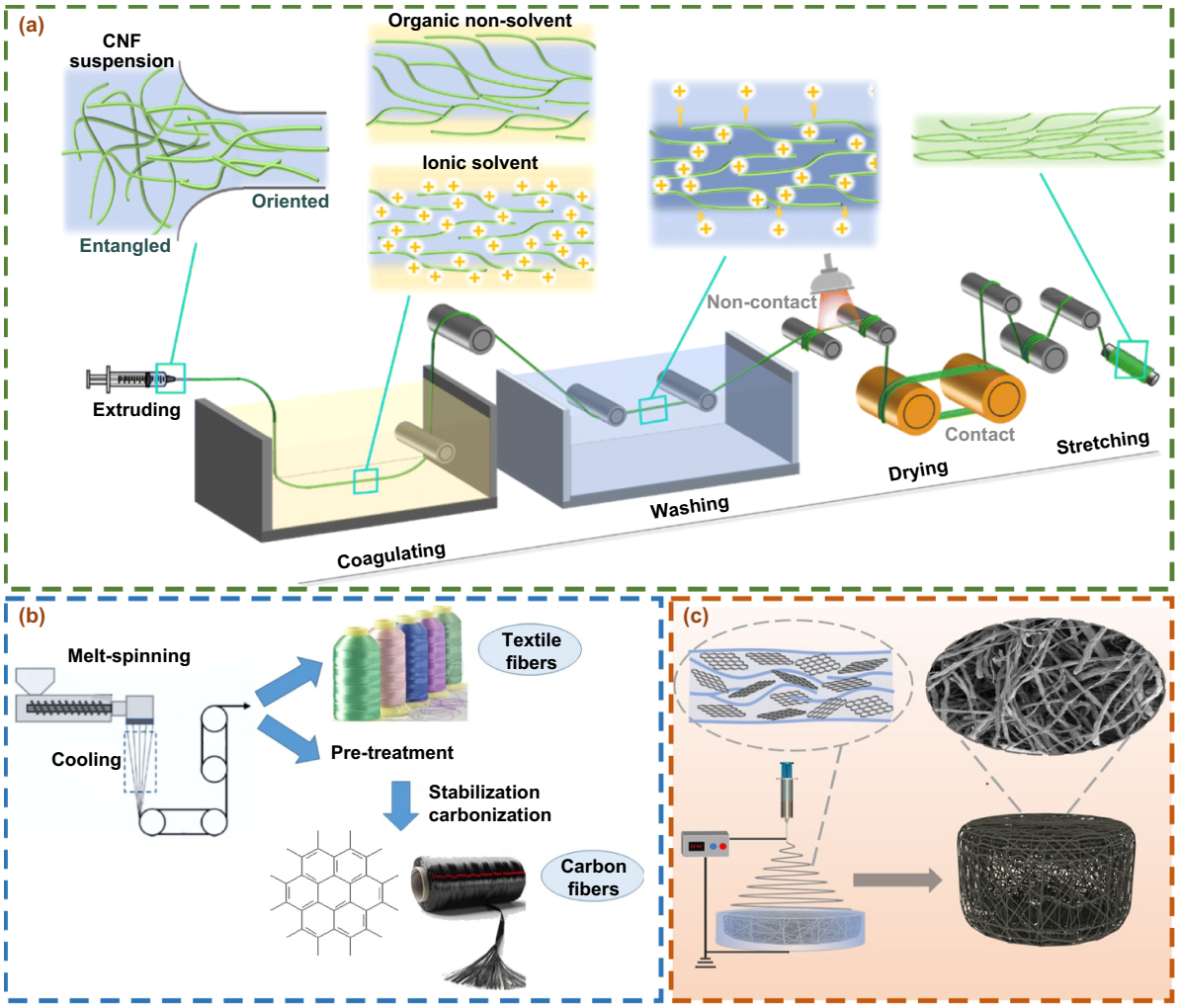

Figure 5. Different spinning technologies. (a) Wet spinning. Reproduced from[182] with permission from the Royal Society of Chemistry. (b) Melt spinning. Reproduced from[183]. CC BY 4.0. (c) Hybrid technology. Reprinted from[184], Copyright (2024), with permission from Elsevier.

certain concentration, viscosity, and stability that can form fibers[175,176]. Subsequently, the solution is extruded through a spinneret into a coagulation bath (usually a non-solvent or a medium that is partially miscible with the solvent). In the coagulation bath, the solvent in the spinning solution undergoes diffusion and exchanges with the non-solvent, causing the polymer chains to gradually precipitate due to the decrease in solubility, ultimately forming continuous fibers. This process involves the dynamic equilibrium between the solvent and the non-solvent, as well as the rearrangement and solidification of the polymer chains. The morphology and properties of the fibers can be optimized by adjusting parameters such as the spinning solution concentration, coagulation bath composition, temperature, and drawing rate. In the manufacture of TENG, PVDF, PVC, PA, and PAN are commonly used materials for wet spinning[177–181].

3.3. Melt spinning

Melt spinning is a technology that stretches molten polymers into nanofibers using high-speed airflow and is suitable for large-scale production (Figure 5(b)). Its advantages lie in high yield, low cost, and the absence of the need for solvents, which give it significant advantages in industrial applications. The fiber membranes prepared by melt spinning have good flexibility and breathability, making them suitable as flexible substrate materials for TENGs. However, the fiber diameter of melt-spun fibers is typically in the micrometer range, and it is difficult to achieve the nanometer scale. Moreover, the fiber morphology is relatively simple, making it challenging to prepare complex structures. In addition, melt spinning is mainly applicable to thermoplastic polymers, resulting in a relatively narrow range of material selection[185–187].

3.4. Hybrid technology and others

Hybrid technology involves combining multiple nanofiber manufacturing techniques to fully leverage their respective advantages. Electrospinning is the most commonly used technique for fabricating TENGs, and it can be used to manufacture the triboelectric layers, electrode layers, and wires

Table 2. The advantages of different fiber manufacturing technologies.

	Advantages
Electrospinning	Nanoscale fibers, high specific surface area, flexible material selection, personalized customization
Wet spinning	Industrialization, low cost
Melt spinning	Industrialization, low cost, without solvents

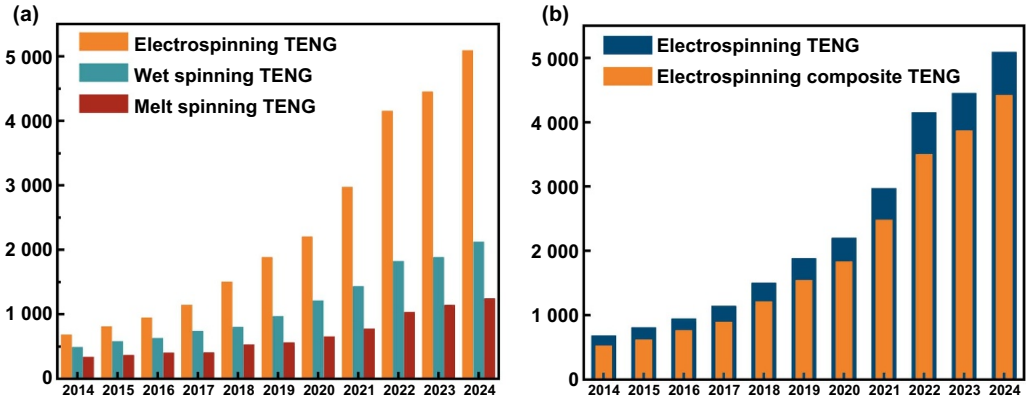

Figure 6. Bibliometric analysis using data from Google Scholar. (a) Keywords: "electrospinning TENG", "wet spinning TENG", and "melt spinning TENG". (b) Keywords: "electrospinning TENG" and "electrospinning composite TENG".

of the TENG system. Table 2 presents the advantages of different spinning technologies. From this, it can be inferred that if the problems associated with industrialization can be resolved, electrospinning technology has the potential to become the primary manufacturing technology for FC-TENGs in the future. Nowadays, hybrid technology usually combines electrospinning with other fiber manufacturing techniques to address the inherent problems of electrospun materials, such as poor mechanical properties and difficulty in controlling fiber alignment. As shown in Figure 5(c)[184], Yang et al. proposed a new technique that combined electrospinning with wet spinning, which can significantly improve the mechanical properties of the materials and maintain good stability even after 3 000 cycles. The advantage of hybrid technology lies in its ability to design TENGs with higher output performance, better flexibility, and durability, while also expanding the range of material selection. However, hybrid technology typically requires multi-step processes, which increases the difficulty and cost of preparation. Moreover, it has higher equipment requirements and a complex optimization process. In TENGs, hybrid technology can be used in the design of high-performance friction layers, multifunctional electrodes, and customized structures, making it suitable for fields with special requirements for performance and application scenarios.

Bibliometric analysis tools were used to explore the hot topics in TENG research. The data were sourced from "Google Scholar" using specific search queries, focusing on articles indexed with relevant information, with publication years limited to 2014–2024. Figure 6(a) shows a clear upward trend in the number of research papers with related keywords since 2014. In particular, the citation volume of the electrospinning technology is far greater than that of other technologies. Moreover, as shown in Figure 6(b), electrospinning composite TENGs dominate the field of TENGs based on electrospinning technology, which indicates that electrospinning composite TENGs will continue to be the focus of future research on flexible TENGs.

4. Optimization of TENG performance through functional materials

From the above discussion, it is evident that the key parameters affecting TENG performance are the effective contact area of the triboelectric materials and the amount of charge transferred between the triboelectric interfaces[188]. Therefore, optimization can be mainly carried out through interface engineering and material selection. Compared to techniques such as solution casting[189,190], spin coating[191,192], sputtering[193,194], and chemical vapor deposition[195,196], the triboelectric layers produced by fiber manufacturing technologies possess a unique fiber structure with a larger specific surface area. This can increase the contact area of the triboelectric interface, thereby optimizing the performance of TENGs. Regarding material selection, according to the triboelectric series, the greater the difference in electron affinity between materials is, the higher the amount of electron transfer during contact. By altering the electron affinity of the triboelectric layers, making the positive triboelectric layer more positively charged and the negative triboelectric layer more negatively charged, the performance of TENGs can be enhanced[197–201]. This chapter will detail the methods for optimizing TENG triboelectric layers by summarizing and comparing the impacts of various methods on the output performance of TENGs, thereby providing material references for enhancing TENG optimization.

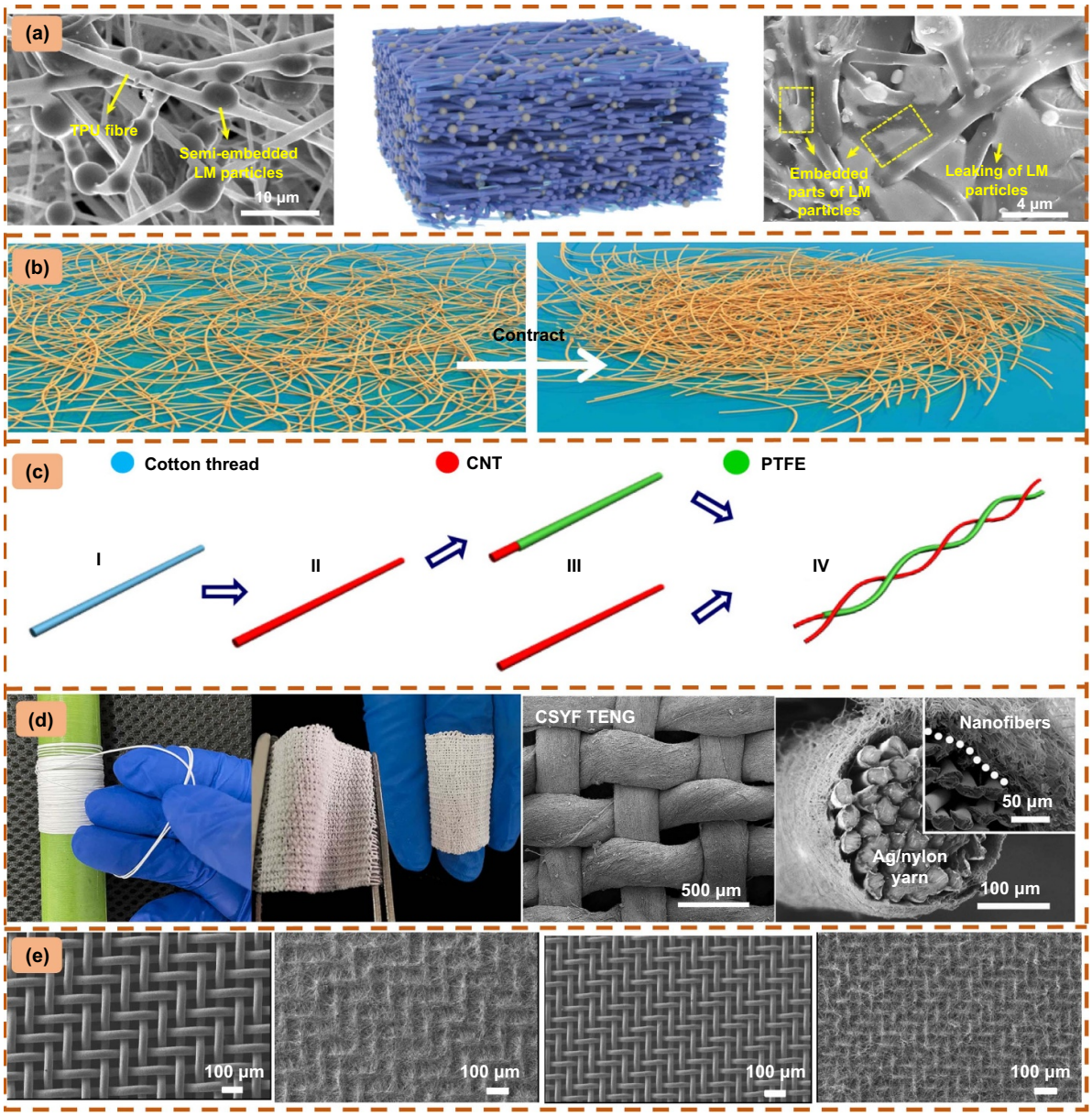

Figure 7. Triboelectric layer materials with interfacial modification. (a) Electrospun LM composite nanofibers. Reproduced from[202], with permission from Springer Nature. (b) Water-assisted electrospun hierarchical nanofiber films. Reprinted from[116], Copyright (2022), with permission from Elsevier. (c) Single composite fiber TENG. Reprinted with permission from[203]. Copyright (2014) American Chemical Society. (d) Core-sheath woven-based TENG. Reprinted from[204], Copyright (2022), with permission from Elsevier. (e) Patterned PVDF-doped $BaTiO_3$ (PVDF/BTO) composite nanofiber films. Reproduced from[205], with permission from Springer Nature.

4.1. Interface properties

The area of the triboelectric interface has a significant impact on the performance of TENGs. Its size determines the efficiency of charge generation and transfer. Generally, during triboelectric motion, a larger contact area leads to a stronger charge separation effect, thereby generating higher energy. Surface micro- and nano- structure design and porous structure are effective methods to increase the contact area. Surface micro- and nano- structure design, also known as surface patterning, includes the design of micro-pattern array structures such as pyramids, cubes, and cylinders[206–210]. There are generally three types of triboelectric layers for FC-TENGs: nanofiber films (Figure 7(b)), single composite fiber long lines (Figure 7(c)), and fabric structures (Figure 7(d)). Such non-smooth surfaces greatly increase the specific surface area of the materials. In addition, the porous structure can effectively increase the specific surface area. Whether it is the nanofiber film prepared by electrospinning or the fabric structure woven by single fibers, the triboelectric layer of FC-TENGs itself has a porous structure, eliminating the need for an additional sacrificial layer step to prepare the porous structure. Similarly, the enhancement of frictional force can also promote the effective generation and separation

of charges, thus optimizing the output performance of TENGs[211,212].

Compared with polymer-based fibers, composite fibers have a larger specific surface area and surface roughness[213,214]. Composites consist of multiple materials with distinct properties, and typical precursor solutions for spinning contain nanoparticles that are either insoluble or poorly soluble in solvents. These include stable metal and inorganic non-metallic materials (gold nanoparticles, silver nanowires, TiO_2, ceramic particles, etc.)[215–218]. The fibers prepared by electrospinning are extremely fine, generally at the nanoscale. The distribution of particles within the electrospun nanofibers can occur in three ways. 1) Particles embedded in the fibers: during the electrospinning procedure, high voltage is applied to the polymer solution/melt, resulting in charge development on its surface. In the electric field, the polymer solution or melt is drawn into fine filaments, and particles are carried into and distributed within the fibers. The diameters of electrospun nanofibers typically range from a few hundred nanometers to several micrometers. If the particles are much smaller than the fibers' diameter, they can be completely embedded within the fibers without altering the fiber morphology. Coaxial electrospinning technology can ensure that nanoparticles are fully distributed inside the nanofibers. 2) Particles semi-embedded on the fiber surface: if the particle size is relatively large, it can affect the surface morphology of the nanofibers (Figure 7(a))[202]. 3) Particles completely on the fiber exterior: by combining electrostatic spray technology, adhesive nanoparticles can be used as binders to connect electrospun polymer nanofibers, achieving interlocking nanofiber structures[125]. Another type of composite fiber does not contain nanoparticles but is composed of two or more polymers. Kun et al. proposed a water-assisted electrospinning technique to generate hierarchical hydroxypropyl cellulose/TPU nanofiber films. Under the influence of Marangoni flow, the electrospun fibers continuously migrated towards the center of the existing nanofiber web on the water surface, driving the web's contraction and forming a continuously growing web mat. By adjusting the spinning process settings, the development and growth of the nanofibers were successfully controlled. A designed drying process was used to achieve surface patterning of the triboelectric layer, resulting in good mechanical properties and high roughness. The output power density of the TENG reached 3.37 $W{\cdot}m^{-2}$ (Figure 7(b))[116].

The fibers prepared by wet spinning and melt spinning are in the form of a single long thread. Electrospinning technology can also use a specialized conical collector to produce nanofibers in the form of long strands. These fibers can be processed into fabrics of different textures (plain, satin, twill) through techniques such as weaving, braiding, and interlacing, which are particularly suitable for multifunctional and wearable electronic devices. The fabric can better conform to the body's contours, achieving conformal attachment. Since these fabrics are composed of long fiber strands, they not only boost the surface area of the woven triboelectric layer but also improve the contact points, thus enhancing the layer's surface area and roughness. In Figure 7(d)[204], Zhou et al. proposed a nanometer/micrometer core-sheath woven-based TENG. Utilizing the co-electrospinning technique, orderly nanofibers are densely wrapped around conductive fibers. Given the hierarchical structure and substantial specific surface area, the prepared TENG demonstrates outstanding electrical performance and robustness, achieving a power density as high as 3.37 $mW{\cdot}m^{-2}$, showing no significant degradation even after 10 000 continuous cycles.

As mentioned above, the micro-patterned structures on the triboelectric layer's surface can significantly enhance the electrical performance of TENGs. The structural parameters of electrospinning also determine the morphology of nanofibers. Research has shown that the voltage of the high-voltage power supply and the receiving distance are positively correlated with the diameter of nanofibers, while the advancing speed of the syringe pump is negatively correlated with the nanofiber diameter. Similarly, different collectors determine the shape of the nanofiber membrane[172]. Similar to the template method, using a collector with a special texture can impart specific patterns to the electrospun nanofiber films. For example, Gu et al. used a metal mesh as a collector to create patterned PVDF/BTO nanofiber films. The preparation process can achieve morphological control using the mesh size, regardless of the film thickness, and maintain the patterns on the fiber film. Under a 100 MΩ load resistance, the prepared TENG achieved an output of up to 434.76 $\mu W{\cdot}m^{-2}$ (Figure 7(e))[205].

4.2. Dielectric constant

In 2013, Niu's team established a theoretical benchmark for TENGs, wherein TENGs are regarded as infinite capacitance models governed by Gauss's law of electric fields[145]. Subsequent researchers have built upon this theoretical foundation, including the team's 2024 proposition of three infinite flat plate models[131]. These models determined the initial charge distribution on the triboelectric layer and the reallocation of all charges across the TENG. Based on this, mathematical derivations were made for the electric field, charge transfer mechanism, external circuit current, and internal displacement current. The TENG's performance metrics and merit were directly derived from the proposed theory. These studies are based on capacitance models, specifically derived from the external circuit using Ohm's law, which characterizes the dynamic transport process under load conditions. In this external setup, the TENG acts like a capacitor, with its output voltage facilitating electron movement between the two terminals. Combined with Maxwell's equations, it is evident that the displacement current is predominant within the internal setup, rendering the external capacitance model a representation of the displacement current's external behavior. For instance, with a dielectric-dielectric CS-TENG, the frictional potential V can be determined via the node method:

$$\begin{aligned} V &= -Q\left(\frac{1}{C_1}+\frac{1}{C_{gap}}+\frac{1}{C_2}\right)+V_{OC} \\ &= -\frac{Q}{S\varepsilon_0}\left[\frac{d_1}{\varepsilon_{r1}}+x(t)+\frac{d_2}{\varepsilon_{r2}}\right]+\frac{\sigma x(t)}{\varepsilon_0}. \end{aligned} \tag{7}$$

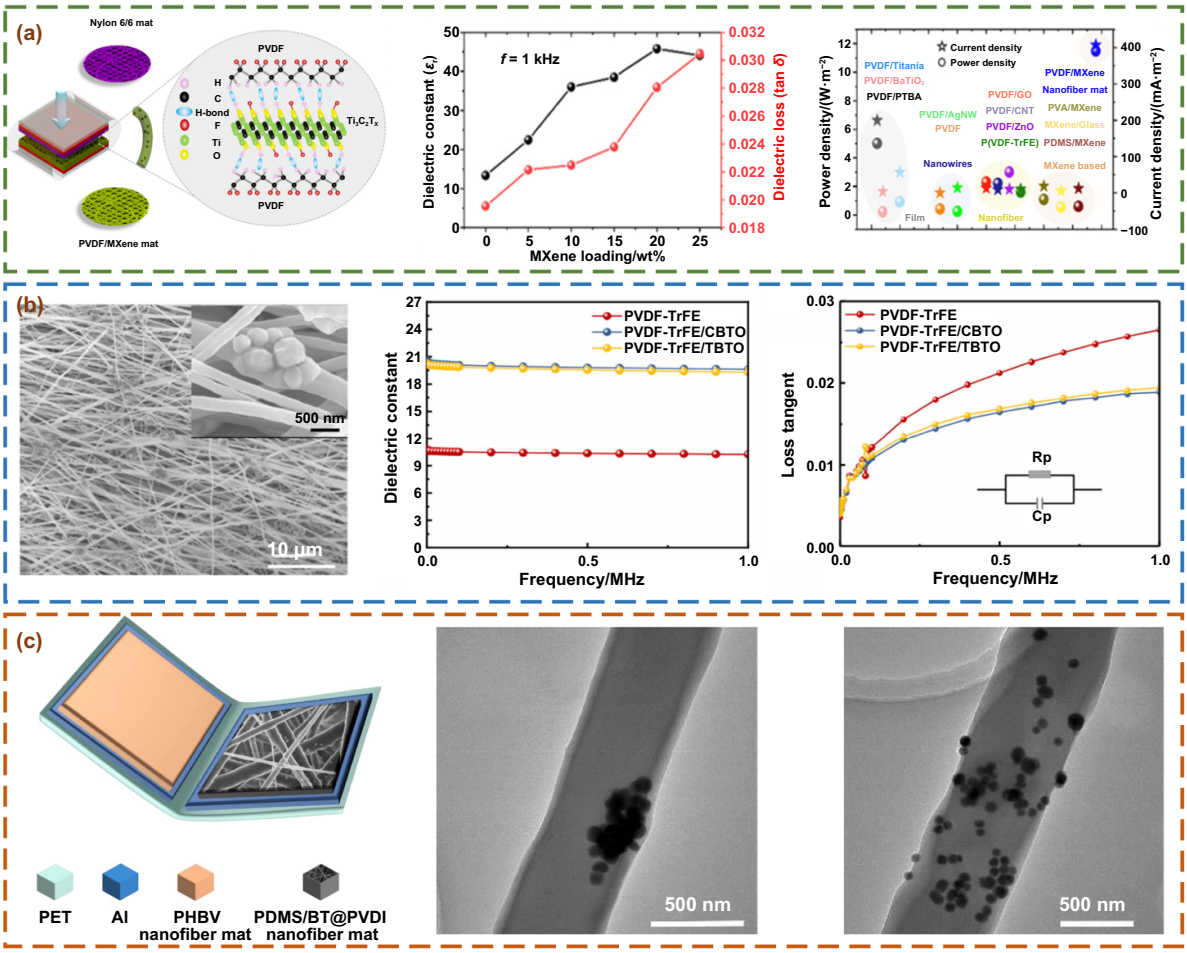

Figure 8. Enhancement of the dielectric constant of triboelectric layers by nanofillers. (a) Dielectric modulation of PVDF nanofibers by MXene nanosheets. Reprinted from[219], Copyright (2021), with permission from Elsevier. (b) Mixing $BaTiO_3$ with 15% concentrated PVDF-TrFE electrospinning precursor solution. Reproduced from[220]. CC BY 4.0. (c) Dielectric and dispersibility modulation of $BaTiO_3$ nanoparticles. Reprinted from[221], Copyright (2020), with permission from Elsevier.

Where C_1 and C_2 are the capacitances of the two positive and negative triboelectric layers, C_{gap} is the capacitance that changes with the distance $x(t)$ between the two triboelectric layers, ε_{r1} and ε_{r2} are the relative dielectric constants of the two triboelectric layers, and d_1 and d_2 are their thicknesses. From Equation (7), it can be seen that the higher the relative dielectric constant of the triboelectric layer is, the higher the output voltage of the TENG. For example, Bhatta et al. proposed using MXene-functionalized PVDF composite fibers as the negative triboelectric layer. After incorporating conductive MXene nanosheets to modulate the dielectric properties of PVDF nanofibers, the dielectric constant increased by 270%. The prepared TENG achieved a peak power of 4.6 mW (power density of 11.213 $W{\cdot}m^{-2}$) at a matched load of 2 MΩ, which was 1.58 times that of the original PVDF nanofibers (Figure 8(a))[219].

MXene nanosheets are two-dimensional materials with excellent conductivity. When doping MXene nanosheets within the PVDF matrix, these conductive nanosheets can form a conductive network, thereby improving the material's electrical conductivity. This conductive network also significantly boosts the dielectric constant, especially at high frequencies. In addition, MXene as a dielectric functional material, promotes interfacial polarization effects by forming microcapacitor structures or penetration systems, thereby achieving high charge induction and charge capture capabilities (Sardana). Some inorganic non-metallic materials with high dielectric constants are also commonly used to prepare triboelectric layers with high dielectric constants. Min et al. mixed different crystalline shapes of $BaTiO_3$ with a PVDF-TrFE electrospinning precursor solution at a concentration of 15%, where $BaTiO_3$ was one-fifth the mass of PVDF-TrFE. The results showed that whether it was cubic $BaTiO_3$ powder or tetragonal $BaTiO_3$ powder, it could significantly increase the dielectric constant of PVDF-TrFE. Among them, tetragonal $BaTiO_3$ powder could increase the power density of the TENG by 3.67 times, reaching 2.75 $W{\cdot}m^{-2}$ (Figure 8(b))[220].

However, at high doping concentrations or during prolonged mechanical deformation, particles such as $BaTiO_3$ may aggregate into clusters in the solution. These clusters can cause the formation of large voids or cavities within the material, reducing the volume fraction of the effective dielectric material. The formation of clusters disrupts the uniformity of the material, leading to uneven electric field distribution

and decreased overall dielectric response. Cluster formation may also introduce internal stresses, degrading the mechanical properties of the material. Such mechanical stresses can affect the distribution and conduction of the electric field, thereby reducing the dielectric constant. To overcome the limitations, Huang et al. proposed a new TENG based on barium titanate-doped coaxial nanofibers with dielectric and dispersibility modulation at the nanoscale. They synthesized tetragonal barium titanate nanoparticles via a sol-gel hydrothermal method, significantly improving their dispersion within PDMS relative to PVDF. During the electrospinning process, the PDMS and barium titanate particles were mixed in situ to form the core of coaxial nanofibers, rather than the traditional composite films. Integrating barium titanate nanoparticles into the PDMS core layer enhanced the dielectric constant of the composite nanofiber membranes and improved the TENG's electrical performance. The optimized TENG delivered a voltage of 1 020 V, a current of 29 μA, and a peak power density of 2.2 $W{\cdot}m^{-2}$ at a 30 MΩ load resistance (Figure 8(c))[221].

The amount of high-dielectric-constant material added is positively correlated with the dielectric constant of the friction layer. However, an increase in the high dielectric constant often results in an increase in dielectric loss, which refers to the energy consumed when the friction layer converts electrical energy into heat energy in an alternating electric field due to factors such as polarization relaxation. An increase in dielectric loss means that more energy is wasted during the power generation process, leading to a decrease in the energy conversion efficiency of the generator. Therefore, when aiming for a high dielectric constant of the friction layer in composite materials, minimizing the dielectric loss is the key to the addition of high-dielectric-constant materials.

4.3. Electronic affinity

In Section 3.1, we discuss a sequence of triboelectric layer materials used in electrospinning, which are ranked based on their electronic affinity strength. The triboelectric layer materials in TENGs are essential for charge generation and transfer processes, with electronic affinity being a key attribute. Electronic affinity refers to the ability of an atom or molecule to gain electrons from the environment to form negative ions. Materials with strong electronic affinity often attract electrons, thereby accumulating negative charges during triboelectric. Conversely, materials with low electronic affinity tend to lose electrons, forming positive charges. This difference in electronic affinity between materials leads to charge separation and transfer, which is the foundation for TENG's electricity generation. Specifically, upon friction between dissimilar materials, electrons migrate from the material with weaker affinity to the one with stronger affinity, resulting in charge separation. The static electric field generated by this process can be captured by an external circuit to produce electric power output[222–224]. Therefore, selecting material combinations with appropriate electronic affinities is crucial for optimizing TENG performance. In practice, common materials like PVDF have moderate electronic affinity and can effectively fix charges, while cellulose, with lower electronic affinity, can effectively release charges. By selecting these material combinations, efficient charge separation and transmission can be achieved. Additionally, doping with high electronic affinity polar materials (such as hydroxyl groups, oxides) or modifying the surface can further adjust the electronic affinity and polarity of the triboelectric layer materials, thus improving the output voltage and current of TENGs[225–227]. In summary, the electronic affinity of materials in triboelectric layers is crucial for TENGs. By reasonably selecting and optimizing material combinations, the effectiveness of charge generation and transfer in TENGs can be significantly improved, thereby enhancing their overall power generation performance.

4.3.1. Negative triboelectric layer. 2D materials not only possess high electronegativity but also offer abundant surface active sites. These surface active sites are uniformly distributed within electrospun nanofibers during the electrospinning process, providing more charge trapping sites. For the negative triboelectric layer, these sites can efficiently capture electrons, thereby improving the charge binding ability of the negative triboelectric material. As shown in Figure 9(a)[228], Shi et al. utilized electrospun PVDF graphene nanosheet composite fibers as the negative triboelectric layer, while spin-coated PVDF fibers were used to form the positive triboelectric layer. Additionally, to better evaluate the electronic affinity of the modified nanofibers, spin-coated PVDF/1.5 wt% graphene and electrospun PVDF nanofibers were employed as counterparts of the negative triboelectric layer for comparative analysis. Experimental results showed that PVDF/PVDF-G achieved an output voltage of 151 V, a short-circuit current density of 7.82 $mA{\cdot}m^{-2}$, and a transferred charge density of 47.42 $\mu C{\cdot}m^{-2}$, indicating that PVDF-G is more electronegative than pure PVDF. Meanwhile, PVDF/PVDF-NF achieved outputs of 299 V, 18.57 $mA{\cdot}m^{-2}$, and 72.36 $\mu C{\cdot}m^{-2}$, nearly double those of the PVDF/G composite. In the case of PVDF/PVDF-G-NF, the respective outputs were 530 V, 42.5 $mA{\cdot}m^{-2}$, and 116.45 $\mu C{\cdot}m^{-2}$. When the connection polarity to the measuring devices was reversed, entirely opposite voltage and current readings were recorded, while the transferred charge density remained constant, further confirming that the observed electrical outputs were due to contact triboelectric charging. These results indicate that only electrospinning can maximize the polarization effect of graphene on PVDF materials. Other 2D materials are also effective in enhancing the electronic affinity of negative triboelectric layer materials. Sardaba et al. prepared composite nanofibers by mixing MXene/MoS_2 within a cellulose matrix (Figure 9(b))[229]. Chemical modification of the prepared nanofiber layers with stearic acid enhanced the hydrophobicity and electronegativity of the MXene/MoS_2 composite material.

While these materials effectively enhance the electron affinity of the negative triboelectric layer, the doping of solid particles has certain limitations. In long-term operation, it can lead to fatigue issues in composite materials; continuous deformation causes nanoparticles to concentrate in deformed areas, leading to clustering and affecting the material's performance. Additionally, there may be stress concentrations

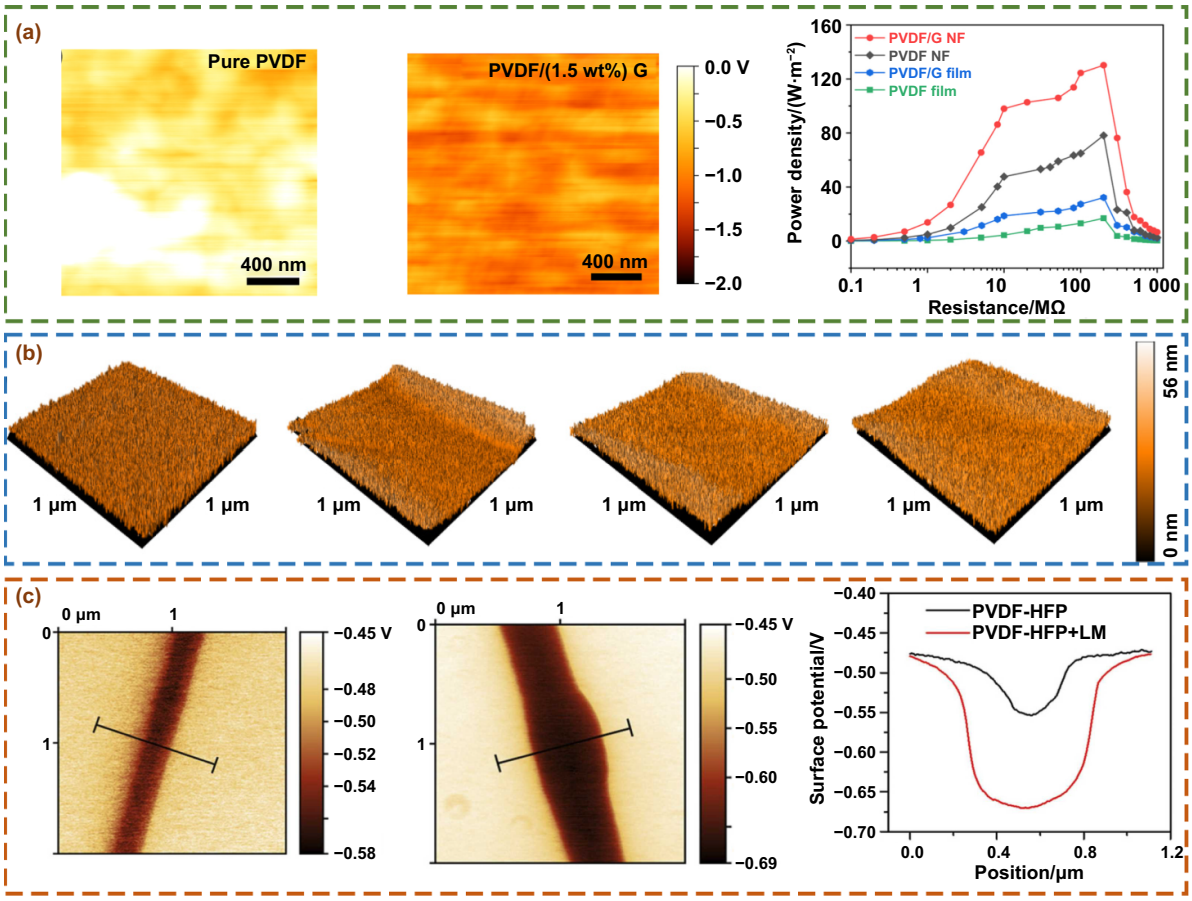

Figure 9. Materials for the negative triboelectric layer. (a) Electrospun PVDF/G nanofibers. Reprinted from[228], Copyright (2021), with permission from Elsevier. (b) Nanofibers of MXene/MoS_2 mixed in a cellulose matrix. Reproduced from[229] with permission from the Royal Society of Chemistry. (c) Electrospun PVDF-HFP/LM composite nanofibers. Reproduced from[230] with permission from the Royal Society of Chemistry.

at the interface between solid nanoparticles and the matrix material, leading to cracks under stress and reducing the material's mechanical properties. Some solid nanoparticles, especially two-dimensional materials, are expensive, making large-scale application challenging. A potential solution is to use liquid-phase nano-fillers. Some metals are liquid at room temperature, such as mercury, but it is toxic and unsuitable for wearable electronic devices. Room-temperature LM, including gallium and its alloys (e.g., gallium-indium and gallium-indium-tin alloys), exhibit fluidity akin to water while retaining metallic conductivity. These materials have low melting points and remain liquid at ambient conditions. They are also called room temperature LMs. Unlike toxic metallic mercury, LM is safe, harmless, and biocompatible, allowing direct skin contact or even injection into the body without harmful effects[231–233]. Recently, owing to their distinct properties, LMs have found extensive use in flexible electronics[234–237].

LM readily reacts with oxygen to create a thin (approximately several nanometers) oxide layer (Ga_2O_3) on its surface. While the LM metal itself is conductive, Ga_2O_3 has semiconductor characteristics. Through methods like ultrasound or shear fragmentation, bulk LM can be broken down into micron- to nano-sized droplets[238,239]. Thus, these core-shell structured nano-droplets can serve as durable, stable, and cost-effective fillers in composite materials, also enhancing TENG output performance. For example, Sha et al. designed an electrospun LM/PVDF-HFP nanofiber film (Figure 9(c))[230]. They doped a small amount of LM into PVDF-HFP (only 2% by weight of PVDF-HFP) to fabricate the fiber mats and TPU, which were used as the negative and positive triboelectric layers, respectively. This configuration enabled the TENG to achieve an output power of 24 $W{\cdot}m^{-2}$ with a peak voltage of 1 680 V. Surface potential of individual nanofibers was characterized using Kelvin probe force microscope, showing a decrease from −0.55 V to −0.67 V. Therefore, a more negative surface potential in the composite nanofiber mat leads to an increased potential difference between the triboelectric layers, facilitating enhanced charge transfer and higher electrical output.

4.3.2. Positive triboelectric layer. As mentioned above, incorporating materials with abundant surface active sites and oxides into the negative triboelectric layer can significantly enhance its electronegativity, thereby enhancing the electrical performance of the TENG. Similarly, optimizing the electropositivity of the positive triboelectric layer can achieve the

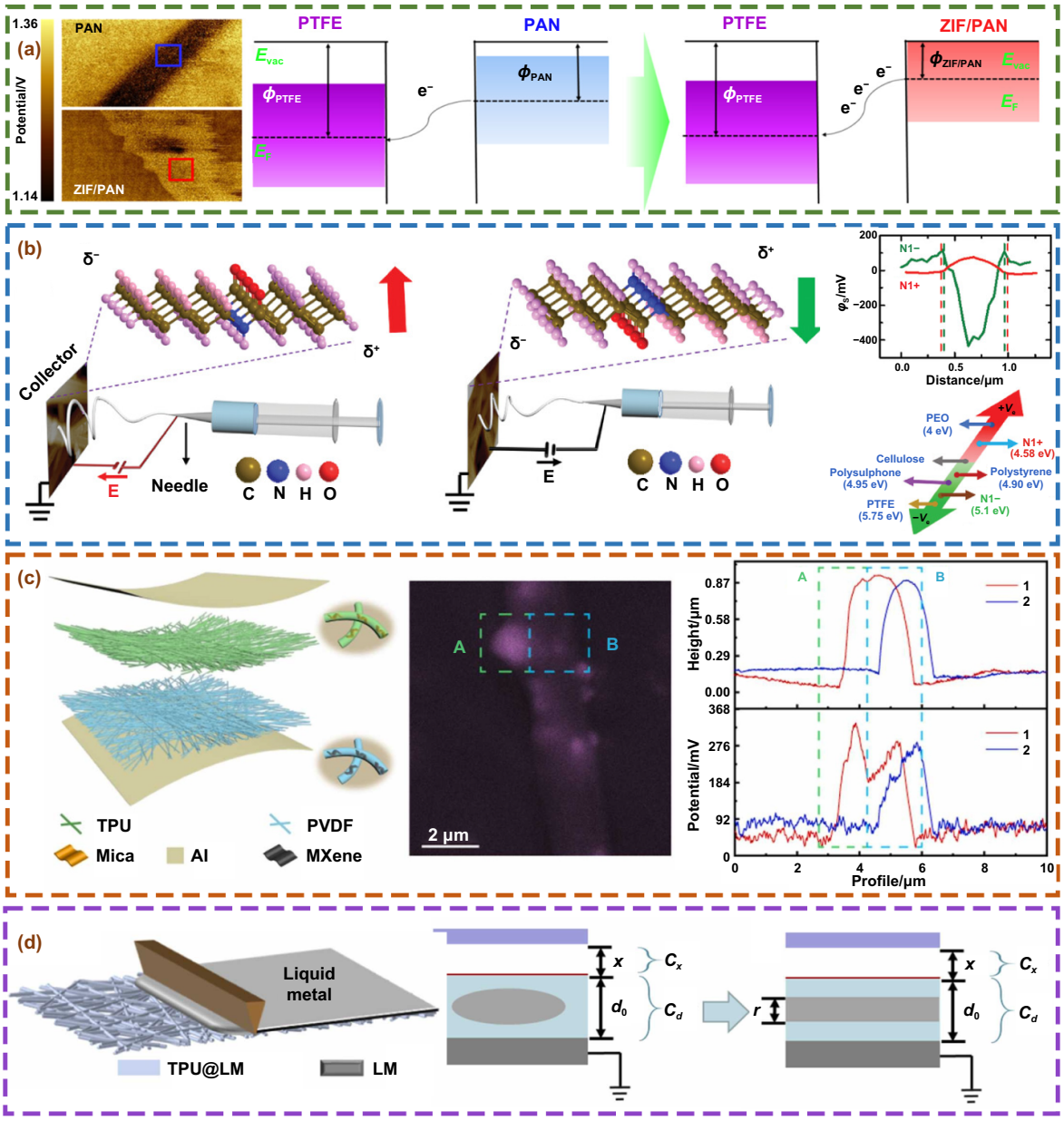

Figure 10. Positive triboelectric layer materials. (a) Electrospun ZIF-8/PAN nanofibers. Reproduced from[42]. CC BY 4.0. (b) Nylon materials with adjustable surface charge density.[240] John Wiley & Sons. © 2022 Wiley-VCH GmbH. (c) Mica nanosheets mixed with stretchable TPU. Reproduced from[112]. CC BY 4.0. (d) TPU nanofibers doped with 2% LM concentration. Reprinted from[128], Copyright (2023), with permission from Elsevier.

same effect. Adding high electropositive nanoparticles to the precursor solution of the positive triboelectric layer before spinning can effectively reduce the electron affinity of the positive triboelectric layer. As depicted in Figure 10(a)[42], zeolitic imidazolate framework (ZIF-8) nanoparticles are mixed with PAN/DMF solution for electrospinning to fabricate ZIF-8-based nanofiber films. The electron affinity level of PAN is 1.19 eV, while that of ZIF-8/PAN is 1.42 eV, which can double the transferred charge between the electrodes.

In addition to using doped nanomaterials to modulate the polarity of the positive triboelectric layer, Babu et al. proposed a tunable single-active-material TENG (Figure 10(b))[240]. During electrospinning, switching the bias voltage polarity from positive to negative can alter the surface charge density of the electrospun nanofibers due to different molecular orientations. They changed the TENG configuration from using two different materials as triboelectric layers to using a single material prepared by positive and negative bias voltages in the electrospinning technique. Both triboelectric layers of the TENG were nylon-11, with work functions of 5.1 eV and 4.58 eV, respectively, for nylon-11+ and nylon-11− triboelectric layers. This technique allowed the preparation of TENG using a single material by achieving different electron affinities in nylon-11.

Additionally, Li et al. exfoliated rigid mica sheets into nanosheets (Figure 10(c)) and mixed them with stretchable TPU[112], which were then electrospun into nanofibers. The findings demonstrated that the mean peak value of electrostatic surface potential for pure TPU nanofibers was approximately 0.2 V, however, the average peak electrostatic surface potential value for TPU/mica nanofibers without mica nanosheet aggregation increased to 218 mV, and the average peak electrostatic surface potential value for the regions with mica nanosheet aggregation increased to 305 mV. The mica sheets significantly enhanced the electrostatic surface potential of the TPU positive triboelectric layer. Mica is a highly robust triboelectrically positive material. Mixing mica nanosheets into TPU, which is less triboelectrically positive than pure mica, can boost the triboelectric positivity of TPU. However, when the concentration of mica exceeds 7.5 wt%, it leads to reduced TENG output, attributed to the reduction in the surface roughness and porosity of the nanofibers. These results indicate that in TENGs, the surface roughness and porosity of the nanofiber membrane have a greater impact on performance than electron affinity in the triboelectric layer. Similarly, LM has also been used to enhance the positive triboelectric characteristics of TPU in the positive triboelectric layer. Song et al. mixed LM nanodroplets with TPU solution for electrospinning (Figure 10(d))[128], and COMSOL simulation results showed that the surface potential of pure TPU was 250 V, which increased to 410 V for TPU doped with 2% LM concentration. However, they attributed the enhanced performance of the TENG to the decreased TPU thickness caused by stretching.

In summary, although the selection of positive and negative triboelectric layers in TENGs relies on their different electron affinities during manufacturing, the impact of electron affinity on TENG performance, i.e., particularly the interfacial charge transfer among the triboelectric layers, seems to be negligible.

4.4. Material crystallinity

The material selection for TENGs most commonly employs PVDF and its derivatives as the negative triboelectric layer. PVDF primarily exhibits four crystal phase structures (α, β, γ, and δ-phase). Different crystal phase structures (α, γ, β, and δ phases) of PVDF have significant impacts on its physicochemical properties. The α phase is the most stable non-polar phase of PVDF. In this phase, the molecular chains are arranged in a zigzag pattern, the polar groups are symmetrically distributed, and the dipole moments cancel each other out. As a result, the piezoelectricity and ferroelectricity of this phase are very weak, the dielectric constant is relatively low, the chemical stability is high, and the surface energy is low. In the γ phase, the molecular chains adopt a TGTG' conformation, which endows them with a certain degree of polarity. Its piezoelectric performance and dielectric constant are superior to those of the α phase, and it also exhibits good chemical stability. However, its stability is slightly weaker compared to the α phase. The δ phase is a polar phase with relatively weak piezoelectricity, ferroelectricity, and pyroelectricity[241–245]. The β-phase has become the most triboelectrically active crystalline phase due to its unique molecular and crystal structures. Its molecular chains exhibit a planar zigzag conformation, with each repeating unit having large dipole moment, strong polarity, and being easily polarized. The highly ordered crystal structure facilitates the directional arrangement and transport of charges. In addition, β-phase PVDF exhibits superior mechanical properties, featuring high toughness and wear resistance. These characteristics enable it to maintain structural integrity during triboelectric processes, thereby enhancing the operational longevity and durability of TENGs. Crystallinity modification can be achieved through physical and chemical methods. Physical methods, such as stretch orientation, can align molecular chains along the stretching direction to promote the formation of the β-phase, and heat treatment can control the crystallization morphology. Chemical methods include blending modification, where the interaction between additives and PVDF induces the arrangement of molecular chains, and changing the synthesis process to increase the proportion of the β-phase. The enhancement of TENG by β-phase modification is mainly based on three mechanisms. Firstly, increasing the β-phase content enhances the polarization ability of the material, making it easier to separate charges at the friction interface and increasing the amount of charge generation. Secondly, the ordered crystal structure provides a stable storage environment for charges, reducing charge recombination and leakage and improving storage efficiency. Thirdly, it improves the internal charge transport channels of the material, reducing transport resistance and facilitating the rapid transport of charges to form current output. For flexible FC-TENGs, in essence, the weakening of the mechanical properties of the material caused by the increase in the β-phase can be ignored.

In summary, elevating the β-phase content in PVDF enhances the energy generation efficiency of FC-TENGs[246–248]. Compared to other thin-film manufacturing methods, the high electric field in electrospinning can induce PVDF molecular chains to align with the direction of the electric field. Given that the β-phase PVDF molecular chains are arranged in a planar zigzag pattern, they are more prone to form this ordered structure under an electric field. Consequently, a high electric field enhances the probability of β-phase formation. Additionally, the stretching effects during electrospinning, such as the stretching of droplets and the fiber formation process, can induce the orientation and alignment of PVDF molecular chains. This stretching effect contributes to the development of a greater β-phase structure fraction[249]. Moreover, electrospinning facilitates the directional alignment of nanofillers within the fibers. This alignment promotes the development of a greater β-phase structure fraction through stretching and whisker elongation mechanisms. Tourmaline is a naturally occurring, eco-friendly material featuring distinctive pyroelectric, piezoelectric, and anion-releasing capabilities. Pan et al. prepared PVDF nanofibers doped with tourmaline (Figure 11(a))[248]. During the electrospinning process, PVDF chains interact synergistically with tourmaline, fostering the formation of highly polar β-phase PVDF crystals. Research findings indicated that a tourmaline concentration of 0.3 wt% can increase the β-phase

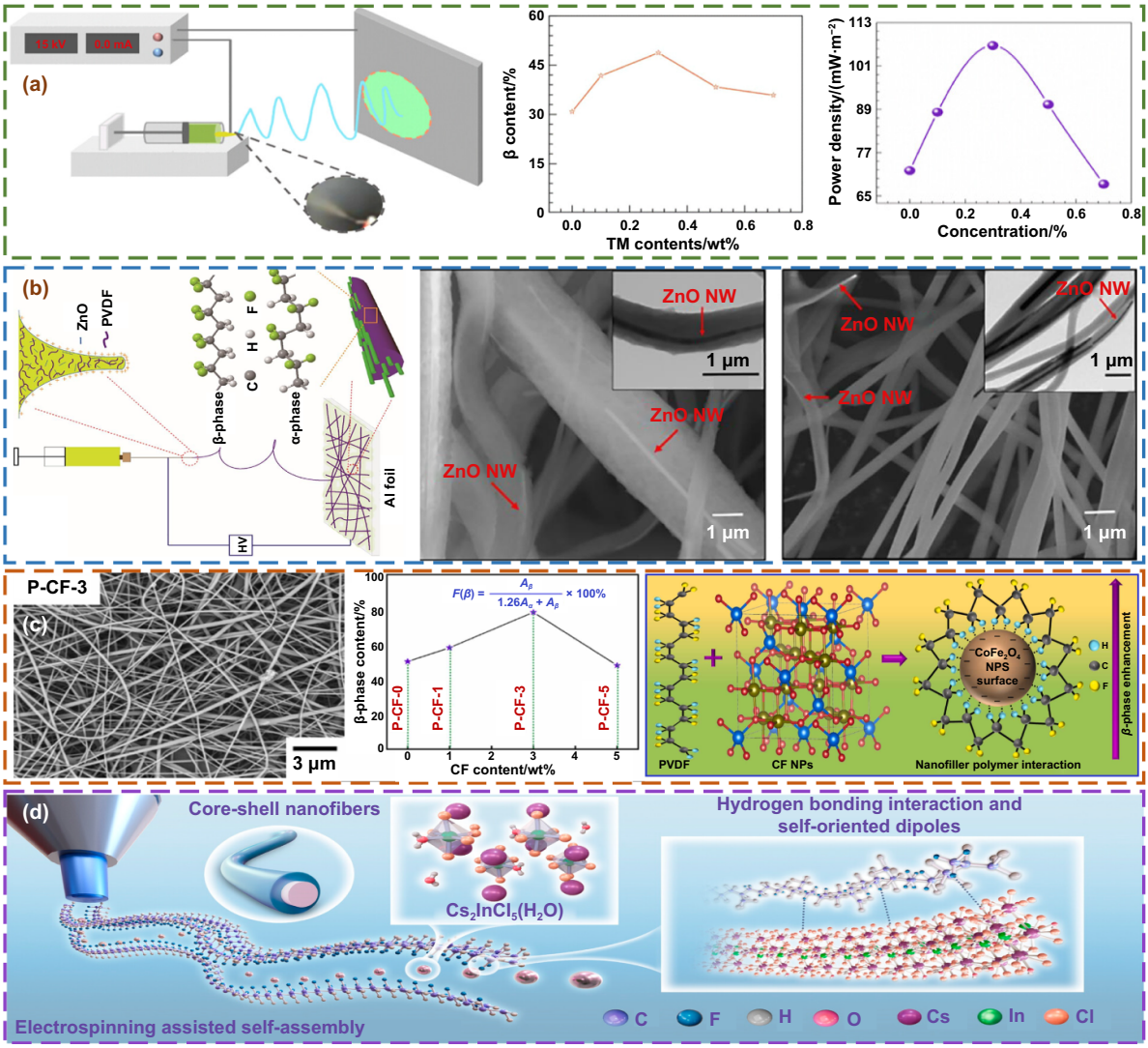

Figure 11. Crystal phase change of fiber materials. (a) PVDF nanofibers doped with tourmaline. Reprinted with permission from[248]. Copyright (2024) American Chemical Society. (b) Electrospun PVDF doped with ZnO nanowires. Reprinted from[111], Copyright (2020), with permission from Elsevier. (c) Flexible electrospun spinel structured CF embedded in PVDF nanofiber membrane. Reprinted from[250], Copyright (2024), with permission from Elsevier. (d) Core-shell structured and biocompatible Cs_2InCl_5 (H_2O)/PVDF-HFP nanofibers. Reprinted with permission from[251]. Copyright (2024) American Chemical Society.

composition in the fibers to 48.76%. The resulting TENG demonstrated a power density of 0.107 $W{\cdot}m^{-2}$ under 40 MΩ.

ZnO is a material with superior piezoelectric properties. The high piezoelectricity and high surface activity of ZnO, along with the mechanical stress and heat treatment effects introduced during the spinning process, contribute to the arrangement and alignment of PVDF chains, thus promoting the formation of the β-phase. Pu et al. achieved a synergistic and aligned configuration of polymer chains with ZnO NWs in fibers through electrospinning (Figure 11(b))[111], facilitating the development of highly polar crystalline β-phase PVDF and δ'-phase in nylon. Under an applied load of 10–20 MΩ, the TENG using ZnO NWs-doped nylon-11/PVDF as the positive and negative triboelectric materials reached a power density of 3.0 $W{\cdot}m^{-2}$. Additionally, materials including CuO, carbon nanotubes (CNT), $BaTiO_3$, ZnO, MXene, and TiO_2 can significantly enhance the β-phase concentration in PVDF electrospun films through various mechanisms, including interfacial effects, mechanical stress, and heat treatment effects. The large specific surface area, superior mechanical properties, and great thermal conductivity of these materials promote the disentanglement and orientation of PVDF molecular chains, thereby increasing the β-phase proportion. Despite enhancements in their electrical properties, these materials face several constraints, including brittleness, diminished mechanical strength, lead toxicity, costly precursors, intricate synthesis processes, chemical instability in harsh environments, and inadequate electrical conductivity. To tackle the challenges, Venkatesan et al. concentrated on creating a soft electrospun spinel cobalt ferrite (CF) embedded PVDF film as a negative triboelectric layer to improve the electrical performance of TENG (Figure 11(c))[250]. Compared to the aforementioned fillers and metal oxides, metal ferrites exhibit enhanced electrical conductivity and compatibility,

with minimal eddy current losses, making them suitable for high-frequency applications such as multifunctional wearable electronics. X-Ray Diffraction (XRD) data indicated that the spinel CF nanoparticles incorporated into the PVDF matrix yielded a face-centered cubic phase in the synthesized nanocomposite, thereby enhancing the β-phase of PVDF and ultimately achieving a threefold boost in the output voltage of the TENG.

In addition to the inorganic filler strategy, establishing synergistic interactions between blended molecules and PVDF nanofiber chains, the utilization of perovskite nanocrystals to trigger the generation of the β-phase is likewise a fruitful approach to augment the β-phase in PVDF nanofibers. Zhi et al. developed Cs_2InCl_5 (H_2O)/PVDF-HFP nanofibers with core-shell structure and biocompatibility via one-step electrospinning-assisted self-assembly technique (Figure 11(d))[251]. By employing lead-free Cs_2InCl_5 (H_2O) as an inducer, the composite nanofibers exhibited enhanced β-phase and self-oriented nanocrystals along the uniaxial axis. This indicated that hydrogen bonding between Cs_2InCl_5 (H_2O) and PVDF-HFP induced the automatic arrangement of dipoles and stabilized the β-phase within the fibers. Fabricated TENG achieved a power density as high as 0.694 $mW{\cdot}cm^{-2}$, showcasing the top-notch output performance in halide-derived TENG systems.

4.5. Electrode materials

Flexible electrodes are a crucial component of flexible TENGs[252]. Common flexible electrodes are made of metal substances like gold, silver, and copper, and these metals can be directly deposited on the triboelectric layer using techniques like thermal evaporation or magnetron sputtering[253–255]. Alternatively, common aluminum or copper foils can also serve as electrodes for flexible TENGs. However, their tendency to fatigue, low functionality, and poor breathability limit the large-scale application of TENGs, especially in wearable electronics. Electrospinning technology offers an effective solution to this problem[256–258]. Electrospun electrodes are typically prepared by mixing conductive materials with polymer substrates to form conductive composites. The concentration and type of conductive material dominate the variations in the electrical conductivity of the composite, while diverse polymer matrices provide the electrodes with various functionalities, such as optical, thermal, and stretchable properties[259]. Common polymer substrates used for electrospun electrodes are indicated in red in Figure 4. TPU is a commonly used substrate material for electrospun electrodes. As shown in Figure 12(a)[123], Zhang et al. prepared an ultra-thin stretchable coplanar electrode TENG using electrospun polyurethane nanofibers along with conductive nano substances (AgNW, CNT) as stretchable electrodes. These electrodes maintained a resistance below 250 $\Omega{\cdot}cm^{-1}$ even when elongated to 100% of their original length, and the TENG could generate an enhanced power density of 3.164 $W{\cdot}m^{-2}$ under folding/stretching conditions. Besides metallic materials, some polymer materials also exhibit certain electrical conductivity, such as polyaniline and polythiophene. To achieve electrodes with both high stability and high conductivity, Karagiorgis et al. designed PEDOT:PSS composites and conducted a detailed study on the effects of PEDOT:PSS and the applied voltage during electrospinning on the fiber's conductive properties (Figure 12(b))[260]. The designed fibers exhibited a sheet resistance of 7 $\Omega{\cdot}sq^{-1}$ and a conductivity of 354 $S{\cdot}cm^{-1}$, with only a slight increase in sheet resistance from 7 $\Omega{\cdot}sq^{-1}$ to 8 $\Omega{\cdot}sq^{-1}$ after 1 000 bending cycles.

Even though conductive polymers possess ideal mechanical characteristics, their poor electrical conductance restricts their real-world applications. Metallic conductive additives exhibit outstanding conductivity performance, yet they often suffer from low strain coefficients and susceptibility to oxidation. In comparison, some conductive two-dimensional materials not only exhibit extremely high electrical conductivity but also possess good chemical stability, such as graphene. Its large aspect ratio makes it an excellent platform for electrical and thermal conductivity across the entire plane. Xing et al. prepared highly stretchable graphene/TPU nanofibers via a one-step electrospinning process (Figure 12(c))[88], achieving ultra-low resistance of 535 $\Omega{\cdot}cm^{-1}$, and demonstrating outstanding durability after over 10 000 stretching-release cycles.

The fluidity of LM and their electrical conductivity are also highly applicable to flexible TENG electrodes. LM has been studied for use in flexible conductors through various approaches, which encompasses incorporating LM particles into elastomers, applying LM onto porous polymeric substrates, blending LM particles with solid conductive filler mixtures, and introducing LM particles into polymer matrices to form biphasic LM structures. Nevertheless, conductors based on liquid metal encounter leakage problems when subjected to external mechanical forces, and this restricts their dependability, consistency, and steadiness. The adoption of coaxial electrospinning technology is an effective approach to address this problem, as depicted in Figure 12(d)[261]. Ma et al. prepared an embedded LM fiber network using coaxial electrospinning to encapsulate LM particles within styrene ethylene butylene styrene (SEBS) nanofibers. This technique enabled the fabrication of electrodes as thin as 10 μm or even thinner, filling the technological gap in producing LM fibers below 100 μm. The LM electrode achieves a conductivity of 1.11 $S{\cdot}mm^{-1}$ with just 3.82 vol% LM. For LM-based flexible electrodes, the oxide layer on LM can lead to changes in conductivity, and generally, sintering methods are needed to disrupt the oxide film and form conductive pathways to enable electrode functionality. As can be seen from the above-mentioned literature, the dielectric constant and interface characteristics are the decisive parameters affecting triboelectric nanogenerators, which should be given key attention in the development of new materials in the future. Many of the aforementioned studies have focused on improving the output of TENGs by enhancing the performance of triboelectric layer materials to promote triboelectric charge generation. However, the output of TENGs highly depends on the crucial dynamic balance of triboelectric charges between generation and decay. Thus, it is difficult

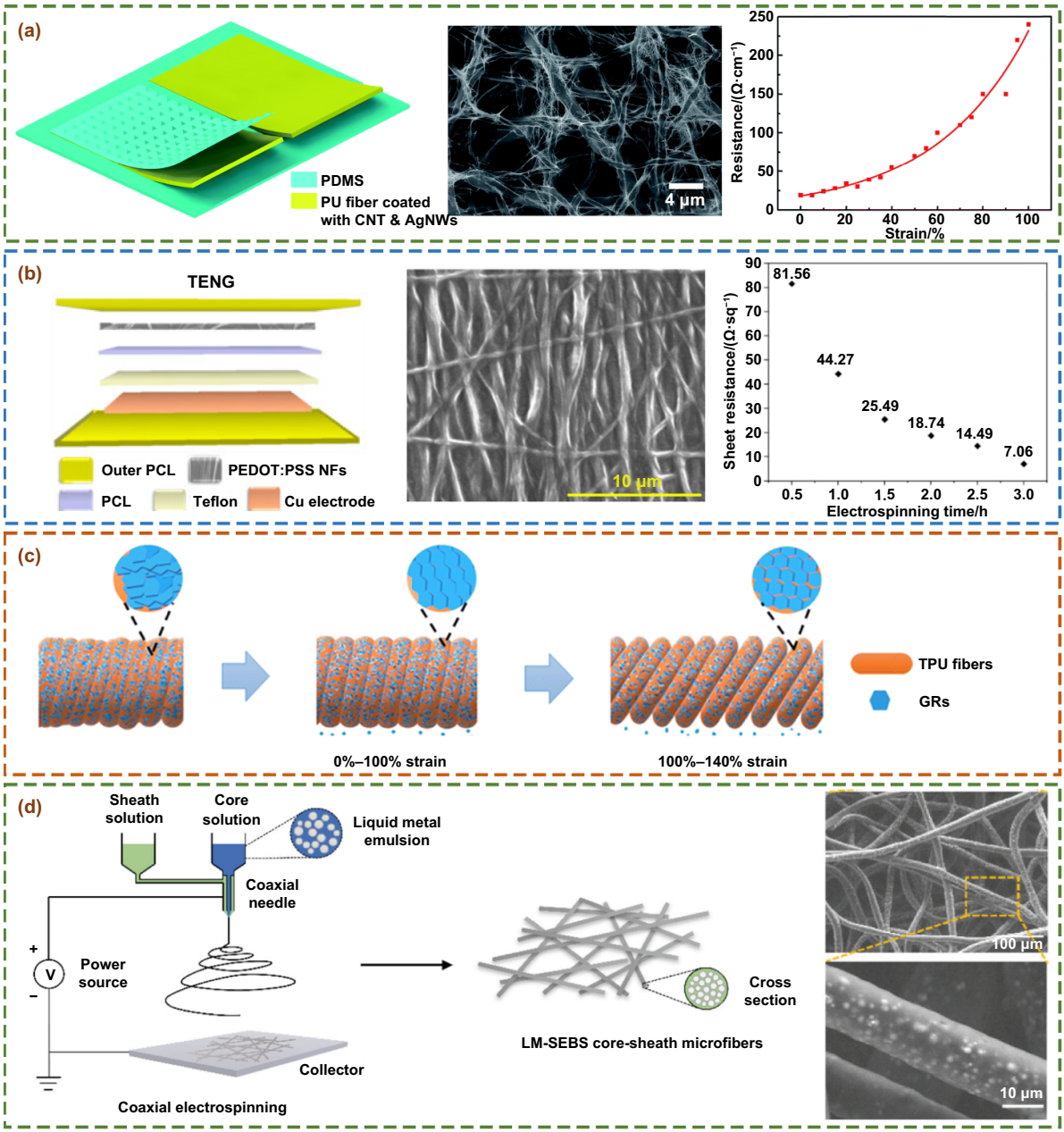

Figure 12. Fiber-based electrode materials. (a) Ultra-thin stretchable coplanar electrode TENG. Reproduced from[123] with permission from the Royal Society of Chemistry. (b) PEDOT:PSS/AgNW composite nanofibers. Reproduced from[260]. CC BY 4.0. (c) Highly stretchable GR/TPU nanofibers. Reproduced from[88] with permission from the Royal Society of Chemistry. (d) Embedded LM fiber network.[261] John Wiley & Sons. © 2023 Wiley-VCH GmbH.

to further improve the output of TENGs merely by promoting triboelectric charge generation. Reducing triboelectric charge decay has often been overlooked in previous studies, but it is also a potential strategy for further improving the output of TENGs in the future[262].

Finally, we have summarized the effects of these composite materials on FC-TENGs, aiming to offer a valuable reference for creating innovative triboelectric layers, as shown in Table 3. It is evident that all parameters, except for the inherent crystal phase improvement of the negative triboelectric layer, are applicable to both positive and negative triboelectric layers.

5. Applications

Through the systematic optimization of strategies such as interface engineering, dielectric regulation, and electron affinity gradient design, FC-TENGs have achieved a leap from basic performance breakthroughs to functional customization. This controllable degree of freedom in material design enables the device characteristics to precisely match the rigid requirements of specific application scenarios. In the wearable field, the inherent flexibility and breathability of FC-TENGs can adapt to the deformation of human motion and ensure wearing comfort. For self-powered sensors, the molecular—level

Table 3. Effect of different composite materials on FC-TENGs.

Matrix	Filler	Parameters	Power density/($W \cdot m^{-2}$)	References
PVDF	ZnO	Crystalline phase	3	[111]
PVDF	Printer ink	Crystalline phase	22	[110]
PVDF	MXene	Crystalline phase, dielectric constant	11.213	[219]
PVDF	Graphene	Crystalline phase, electron affinity	130.2	[228]
PVDF	FEP	Porosity-interface properties, dielectric constant	1.28	[57]
PVDF	PTFE	Fabric-interface properties	0.002 2	[204]
PVDF	Siloxene	Crystalline phase, dielectric constant	13.25	[121]
PVDF	MOFs	Crystalline phase, electron affinity	8.712	[119]
PVDF	Graphene	Electron affinity	11.32	[263]
PVDF	CNCs	Dielectric constant, electron affinity	0.091	[264]
PVDF	$CoFe_2O_4$	Crystalline phase, surface roughness-interface properties		[250]
PVDF	Ag@MXene	Interface properties, electron affinity	18.55	[265]
PVDF	BTO	Fabric-interface properties, electron affinity, crystalline phase	4.348	[205]
PVDF-HFP	SiO_2	Permeability-interface properties	0.445	[117]
PVDF-HFP	BZT	Electron affinity, dielectric constant	47.9	[266]
PVDF-HFP	MXene	Interface properties	0.217	[114]
PVDF-HFP	SiO_2/ZnO	Dielectric constant		[267]
PVDF-HFP	BTO	Crystalline phase, interface properties, dielectric constant	1.9	[268]
PVDF-HFP	Cs_2InCl_5	Crystalline phase, electron affinity	6.94	[251]
PVDF-HFP	LM	Dielectric constant	24	[230]
PVDF-TrFE	BTO	Dielectric constant	2.75	[220]
PVDF-TrFE	MXene	Electron affinity, crystalline phase, dielectric constant	19	[269]
PVDF-TrFE	BTO	Electron affinity, dielectric constant	2.52	[270]
PLLA	Ag-SiO_2	Porosity-interface properties, crystalline phase, dielectric constant		[271]
PEO	Poly-DADMAC	Dielectric constant, crystalline phase	5.6	[89]
PLA	mPEG	Dielectric constant, interface properties, crystalline phase	116.21	[272]
PDMS	BTO	Dielectric constant	2.2	[221]
PAN	BNNS	Permeability-interface properties	3.31	[58]
PVDF	PS	Permeability-interface properties		[273]
PI	AgNPs	Interface properties	1.6	[274]
PLA	MOFs	Porosity-interface properties, dielectric constant		[44]
Nylon-12	A-rGO	Electron affinity	1.3	[115]
CA	Carbon nanotube	Surface roughness-interface properties, electron affinity	0.74	[275]
TPU	AgNW/MnO_2	Interface properties	0.002 12	[276]
TPU	$Gd(OH)_3$	Crystalline phase, interface properties		[277]
TPU	LM			[128]
TPU	Mica	Electron affinity	1.458	[112]
PVDF	MXene			

customization of electron affinity significantly enhances the sensitivity of electrical signal acquisition. In emerging fields such as HMIs, the collaborative optimization of dielectrics and electrodes is breaking through the technical bottleneck of multi-dimensional signal coupling recognition. This chapter will delve into how these material innovations are redefining the application boundaries. By establishing a quantitative mapping relationship between "material properties and scenario requirements", it reveals the crucial role of functional fiber composite materials in modern technology and future society.

5.1. Human wearable electronics

Wearable electronic devices relying on TENG can primarily be categorized into 2 kinds: one where TENG serves as an

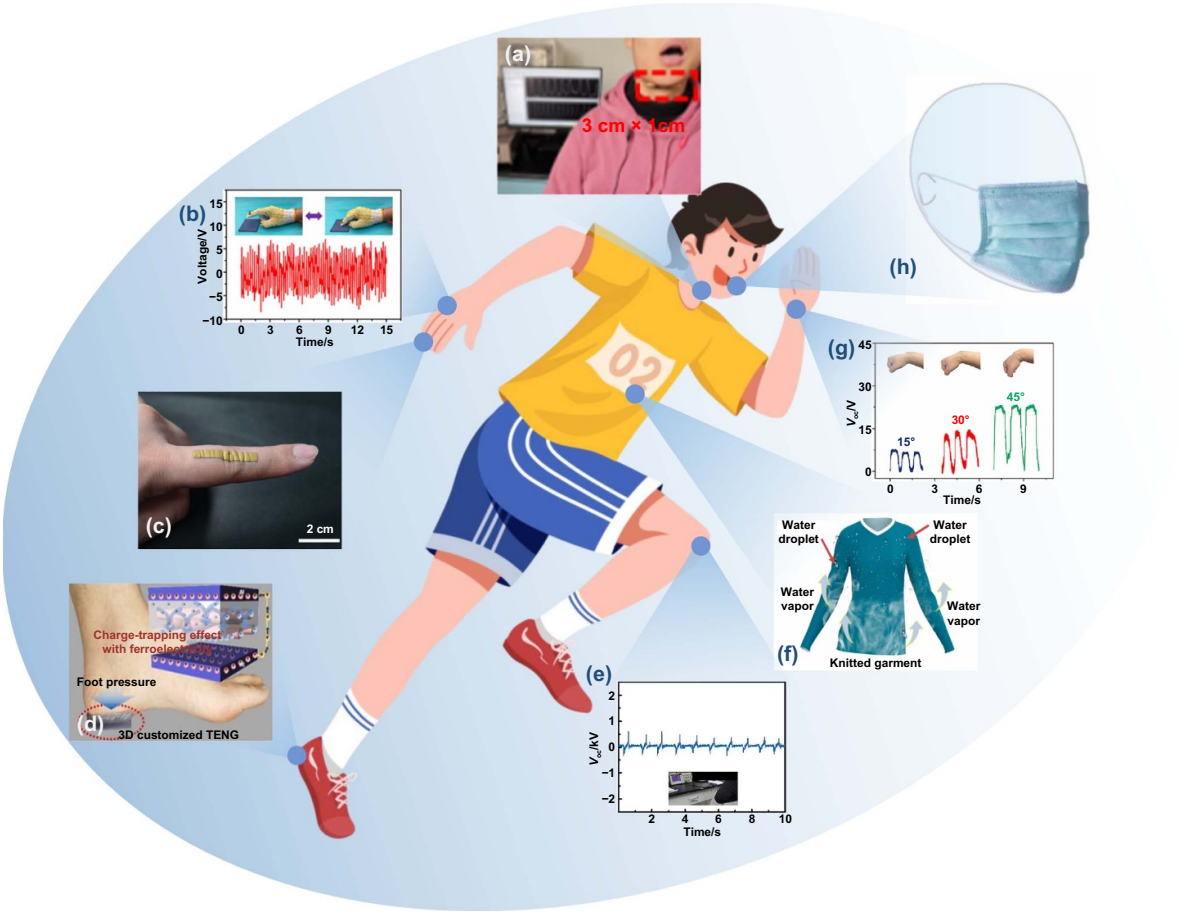

Figure 13. Human-wearable flexible electronic devices based on TENG. (a) Throat. Reprinted with permission from[278]. Copyright (2024) American Chemical Society. (b) Gloves. Reprinted from[126], Copyright (2021), with permission from Elsevier. (c) Finger.[279] John Wiley & Sons. © 2023 Wiley-VCH GmbH. (d) Shoes. Reprinted from[280], Copyright (2022), with permission from Elsevier. (e) Knee. Reprinted from[281], Copyright (2024), with permission from Elsevier. (f) Clothes. Reprinted from[282], Copyright (2022), with permission from Elsevier. (g) Wrist. Reprinted from[275], Copyright (2023), with permission from Elsevier. (h) Mask. Reprinted from[273], Copyright (2023), with permission from Elsevier.

energy source to power wearable electronics[283–286], and the other where TENG is directly employed as a sensor[287–289]. However, the poor output stability has limited the development of TENG as a power supply for wearable electronics. Despite this, TENG has shown significant application prospects in areas such as health monitoring, motion tracking, and environmental sensing. The long-term safety of TENGs in direct contact with human tissues (e.g., skin, organs) is critical for wearable and implantable applications. FC-TENG possesses inherent breathability. Therefore, only its biotoxicity needs to be considered for FC-TENG materials. Polymer matrices (e.g., PDMS, PVDF) are generally regarded as biocompatible. Some fillers, especially LM and certain molecular ferroelectric materials with high piezoelectric responses, have been proven suitable for long-term use in implantable electronics and skin electronics[290,291]. Consequently, human wearable electronic devices based on FC-TENG have become a focal point of research.

The structure of TENG films produced through electrospinning is highly sensitive to acoustic vibrations. Moreover, electrospun films can easily conform to the throat area, adapting to its curvature and movements (such as speaking and swallowing), thereby reducing discomfort. These films generate electrical signals from throat movements, allowing for the immediate tracking of throat well-being, such as detecting inflammation, tumors, or other abnormalities (Figure 13(a))[278]. Additionally, when affixed to various locations on the human body, they are capable of fulfilling varied sensing functions, including motion health monitoring (Figure 13(e)) and pulse monitoring (Figure 13(g))[275–278,281,283–291]. Human skin perceives the surrounding environment by converting mechanical stimuli into bio-signals. Similarly, TENG converts mechanical impulses into electric signals that are used to fabricate electronic skin for environmental perception. Therefore, biocompatible materials can be directly adhered to human epidermis or used to fabricate e-skin for robots to sense their surroundings (Figure 13(c))[279].

Electrospinning technology can be employed to manufacture woven TENG structures. As illustrated in Figure 13(b)[126], Guan et al. designed a breathable and washable woven TENG by sewing multiple TENGs (each with an area of approximately 2 cm^2) onto a commercially

available knitted cotton glove, creating a smart textile glove capable of detecting finger movements in various situations. Similarly, Chen et al. produced a durable, superhydrophobic, wearable nanometer-micrometer structured triboelectric yarn (Figure 13(f))[282]. They enhanced electrical output performance by incorporating electrospun nylon 11/ZnO nanofibers as an intermediate layer and wrapping them with ring-spun polyester fibers as the sheath to enhance wear resistance. Due to the unique interconnected loop structure of the knitted fabric, the resulting electronic textiles exhibited excellent breathability (147.3 $mm{\cdot}s^{-1}$), water vapor permeability (3.470 $kg{\cdot}m^{-2}{\cdot}day^{-1}$), and skin-friendly properties. They demonstrated a power density of 0.488 $W{\cdot}m^{-2}$ at a load resistance of 700 MΩ, indicating their potential for commercialization as self-powered sensors for monitoring body movements. In addition to clothing, shoes and insoles (Figure 13(d)) are among the most common applications of TENG[280]. The contact and separation movements formed during human walking can effectively facilitate charge transfer between the triboelectric layers of TENG interfaces.

Rapid industrial development has long concerned people greatly regarding environmental pollution and human health. Luo et al. prepared PVDF/PS blends using the torque blending method (Figure 13(h))[273]. The PVDF/PS electrospun film obtained through electrospinning can be used to fabricate triboelectric nanogenerators with high output performance. Compared with the commercial PP melt-blown non-woven membrane filter layer, the PVDF/PS electrospun films exhibit better filtration effects on airborne particles of different sizes. Moreover, after losing their charges, the PVDF/PS electrospun films can be recharged through friction to restore their filtration performance. The recharged PVDF/PS membranes still provide good protection, with a filtration rate of up to 95% for airborne particles in the size range of 0.3–10 μm.

5.2. Self-powered sensors

Considering the inherent power-free nature of PENG/TENG and the unlimited material options for TENG, which endow it with high-performance and eco-friendly power generation capabilities as well as self-powered sensing functionality, the excellent compressibility of electrospun films further expands their applicability. They can simultaneously detect dynamic and static pressures while being self-powered[17]. Increasing pressure enhances the contact area and closeness between the triboelectric layers, thus augmenting charge generation and accumulation. The charge density is proportional to the contact pressure, meaning higher pressure yields more generated charges. Moreover, pressure aids in enhancing the effectiveness of charge transfer between materials since greater pressure leads to more intimate surface contact, reducing charge loss. Bhatta et al. designed a silicene/PVDF composite nanofiber membrane for high-performance TENG and self-powered static and dynamic pressure sensing uses (Figure 14(a))[121]. The TENG, composed of S-PVDF membrane and nylon-66, could provide an outstanding power density of 1.325 $mW{\cdot}cm^{-2}$ and facilitate the operation of low-power electronics and IoT devices. By effectively integrating the TENG with a capacitive pressure sensor, it exhibited excellent dynamic pressure sensitivity of 12.062 $V{\cdot}kPa^{-1}$ (<3 kPa) and 2.58 $V{\cdot}kPa^{-1}$ (3–25 kPa), as well as static pressure sensitivity of 25.07 $mV{\cdot}kPa^{-1}$ (<3 kPa) and 5.96 $mV{\cdot}kPa^{-1}$ (3–25 kPa).

TENGs applied in structural health monitoring systems can effectively monitor deformations, vibrations, and stresses in buildings, bridges, pipelines, and other facilities. In Figure 14(b)[292], Meng and colleagues fabricated a self-powered flexible vibration sensor for detector for assessing the sealing security of railway track fasteners, employing an electrospun nanofiber self-powered vibration detector relying on high-performance TENG to set up a real-time and effective security detection system for railway track fasteners. Under matched loads, it achieved a power density of 4.28 $W{\cdot}m^{-2}$. Additionally, it exhibited outstanding operational steadiness, excellent environmental suitability, and rapid reaction time. Similarly, self-powered TENGs are capable of guaranteeing the steady functioning of mechanical equipment (Figure 14(c)) and human health monitoring (Figure 14(d))[293,294].

The variation in TENG output due to changes in the surrounding environment endows TENGs with self-driving characteristics, making them suitable for automatic alarm systems. As shown in Figure 14(e)[295], Yuan and colleagues proposed a high-biomimetic, hollow double-layer structured high-temperature alarm which, upon thermal deformation, drives PVDF and PA66 to undergo triboelectric interaction jointly, producing an electrical signal to realize self-perception and acquire related data regarding the stimulus. With the development of IoT technologies, smart homes have gradually garnered researchers' attention, such as smart keyboards, curtains, and anti-theft doors. Figure 14(f) shows a self-powered sensing anti-theft door[296], where TENGs prepared are deployed at different locations on the door to generate power when the door is opened, knocked, or kicked. Furthermore, when a TENG is installed on the door handle, it can play doorbell music based on different compressive forces. Additionally, utilizing the contact electrification mode of TNEGs, TENGs can be integrated into carpets and floors to produce luminous floors (Figure 14(g))[169].

Besides the TENG-based wearable electronic devices for humans mentioned in the previous section, TENGs with certain adhesive properties, or materials directly written onto the roots, stems, and leaves of plants, can overcome the inherent hydrophobicity of plants and be used as plant-wearable sensors (Figure 14(h)) to ensure the healthy growth of plants or enhance crop production[297].

5.3. Modern healthcare

With the rapid advancement of technology, modern medical techniques are undergoing an unprecedented transformation. Traditional medical devices and methods are gradually being replaced by more intelligent, portable, and efficient solutions. Textile-based TENG wearable sensors inherently fit well with conventional garments, which have the ability to transform mechanical or electrical stimuli into an electrical

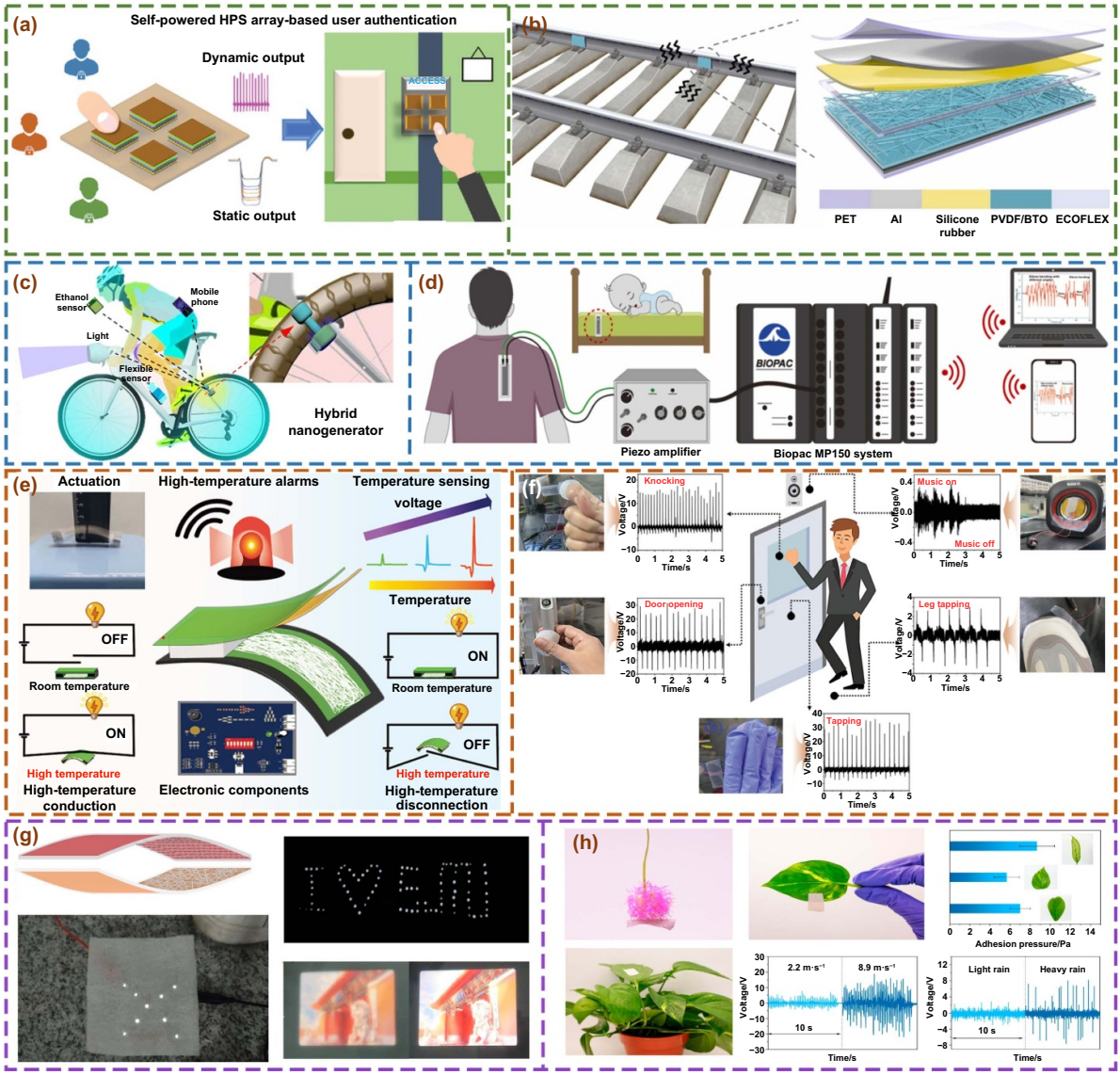

Figure 14. Self-powered sensors based on TENG. (a) Dynamic and static pressure sensors.[121] John Wiley & Sons. © 2022 Wiley-VCH GmbH. (b) Railway track fastener sealing safety detection sensor. Reprinted from[292], Copyright (2022), with permission from Elsevier. (c) Cycling safety protection sensor. Reprinted from[293], Copyright (2022), with permission from Elsevier. (d) Human health monitoring sensor. Reprinted from[294], Copyright (2023), with permission from Elsevier. (e) Automatic alarm sensor. Reprinted from[295], Copyright (2023), with permission from Elsevier. (f) Smart home.[296] John Wiley & Sons. © 2023 Wiley-VCH GmbH. (g) Luminous pavement. Reprinted from[169], Copyright (2022), with permission from Elsevier. (h) Plant wearable sensor. Reprinted with permission from[297]. Copyright (2021) American Chemical Society.

signal, enabling non-intrusive tracking of diverse physiological indicators[298]. This article will delve into the applications of TENG in modern healthcare, focusing on its innovative uses in self-powered wearable medical devices, biosensors, and implantable devices. Figure 15(a) shows a plain-weave fabric smart insole based on TENG[299], which features high sensitivity, antibacterial properties, breathability, and washability. The designed TENG exhibits ultra-high sensitivity (8.36 V·kPa^{-1}) and a low detection limit (0.01 kPa). By strategically positioning 15 TENG stress-sensing elements in the areas corresponding to the key pressure points of the foot, the pressure changes in the TENG output are utilized to analyze gait changes in real-time. Thus, it can detect ulcers caused by abnormal plantar pressure distribution in patients with diabetic feet, providing an innovative solution for the early detection and continuous monitoring of diabetic feet.

The healing process of chronic wounds is frequently hindered by bacterial contagions and feeble transepithelial voltage. Dressings featuring electrical stimulation and antimicrobial capabilities might resolve this problem. Figure 15(b) shows a TENG assembled with an electrospun polymer friction layer and a polypyrrole electrode prepared by chemical vapor deposition[300]. It has excellent flexibility, breathability, and wettability, with a power density as high as 48.7 mW. By collecting mechanical motion and applying electrical stimulation with positive charges on the surface of polypyrrole, more

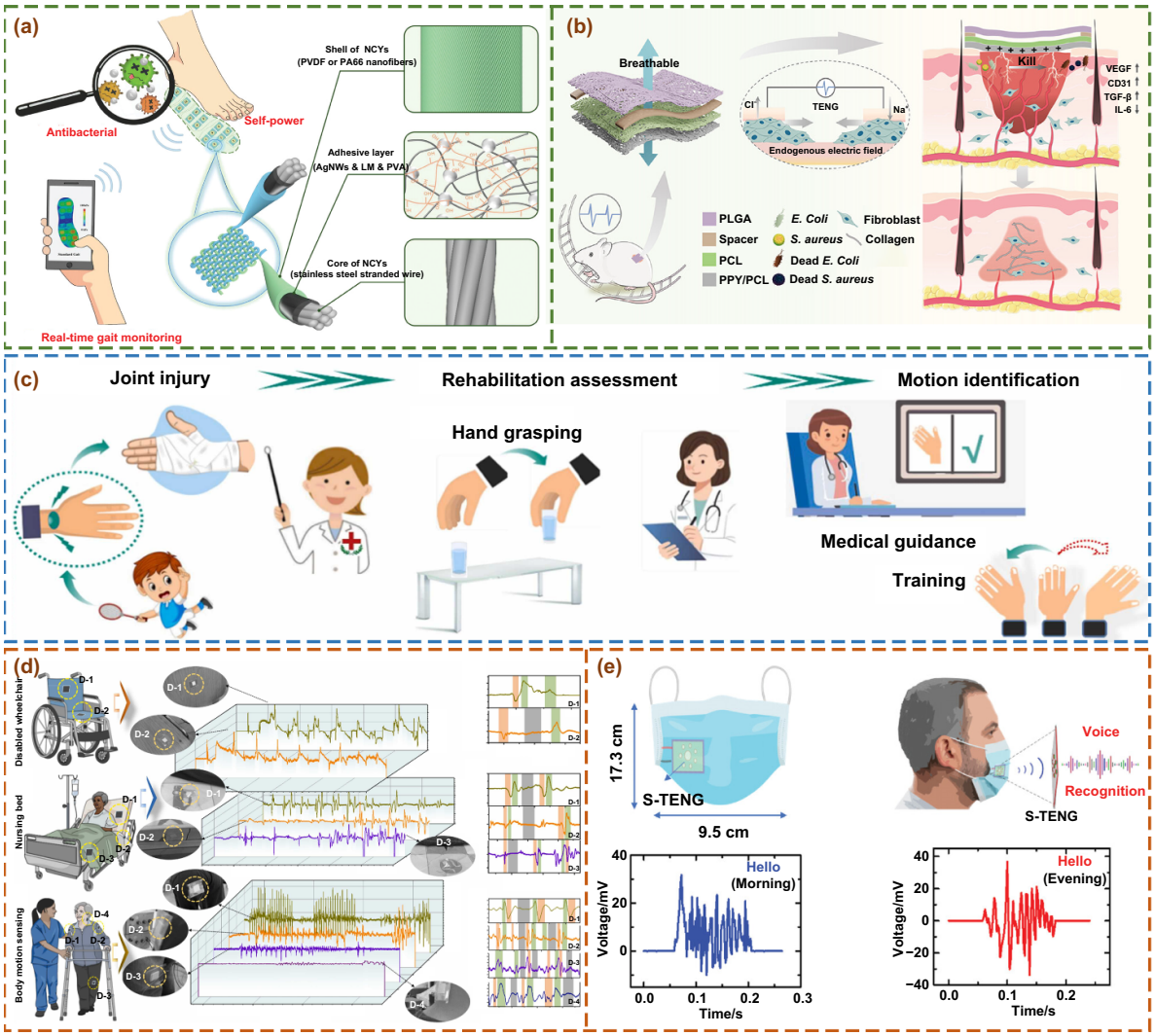

Figure 15. Modern medical devices based on TENG. (a) TENG-based intelligent insole made from plain weave fabric. Reproduced from[299]. CC BY 4.0. (b) Self-powered and intrinsically antibacterial patch based on TENG. Reprinted with permission from[300]. Copyright (2023) American Chemical Society. (c) TENG for auxiliary joint rehabilitation training. Reprinted from[301], Copyright (2024), with permission from Elsevier. (d) TENG for energy harvesting and health monitoring. Reprinted from[120], Copyright (2022), with permission from Elsevier. (e) Mask for speech disorder rehabilitation training.[240] John Wiley & Sons. © 2022 Wiley-VCH GmbH.

than 96% of bacteria can be killed due to its synergistic effect on cell membrane rupture. Cell culture and animal experiments have shown that electrical stimulation can enhance the expression of growth factor genes in mice, thereby accelerating wound healing.

Apart from accelerating wound healing, TENG can also be used for auxiliary joint rehabilitation training. Specifically, TENG integrated into wearable sensors can be employed to collect real-time joint motion and pressure data. Based on these real-time monitoring data, rehabilitation physicians or AI algorithms can develop personalized rehabilitation training programs. By adjusting the intensity, frequency, and methods of training, this approach can optimize rehabilitation outcomes, reduce recovery time, and minimize risks (Figures 15(c) and (d))[120,301]. This methodology can also be extended to the field of speech disorder rehabilitation (Figure 15(e)). Mandal et al. adjusted the surface potential of nanofibers by changing the voltage polarity in the electrospinning device[240]. The designed TENG has been proven to be an ultra-high-sensitivity acoustic sensor, which can generate electrical energy using the tiny mechanical movements produced by vocal organs such as the mouth, throat, and lips during speaking. It has high sensitivity (27 500 mV·Pa^{-1}) in medium-to-low-decibel (60–70 dB) sounds, and thus can identify different sound signals according to the condition of the vocal cords. Patients with language disorders can wear this TENG to adjust their pronunciation and volume in real-time, thereby achieving clearer and more accurate speech, which is crucial for improving their communication ability. Electrospun TENG ensures the breathability of auxiliary medical devices and their conformity with the skin.

5.4. Wireless communication

As the IoT and wireless communication technologies advance rapidly, there's an increasing need for efficient and sustainable energy supply and signal transmission solutions. Traditional battery-powered and externally connected power sources face limitations in certain application scenarios. By modulating the output signals of TENG into radio waves, low-power, short-range wireless power transfer can be achieved, which is an effective strategy to address this challenge[302]. The section will delve into how TENG is utilized in wireless communication, analyzing its working principles, technical advantages, and practical application cases.

Wireless communication systems have significantly enriched the applications of smart homes. Figure 16(a) illustrates a TENG-based smart home system[119], in which triboelectric layers prepared via electrospinning provide more electron traps and a larger specific surface area, effectively enhancing the output of TENG. This results in significant differences in the interval change of TENG output. Initially, a microcontroller unit is utilized for signal processing, followed by a radio frequency module to transmit the final processed signals, enabling the effective control of household appliances. Radio frequency antennas and receivers are commonly used as TENG energy reception modules, effectively assisting in the transmission and reception of TENG output signals. Similarly, some researchers have opted for bluetooth modules for TENG signal transmission. As shown in Figure 16(b)[274], Wang and colleagues designed a TENG for real-time wireless fine-grained biosensing of biological motions and postures. The TENG is connected to a bluetooth module, and the sensing of human movements by TENG can be analyzed using a collection terminal, achieving wireless fine-grained perception of human motion.

The foundation of modern wireless electromagnetic communication is the Maxwell equations. Faraday's law (Equation 8) and the Maxwell-Ampère law (Equation 9) can fundamentally explain the generation of wireless signals[303].

$$\nabla \times E = -\frac{\partial B}{\partial t} \tag{8}$$

$$\nabla \times H = J + \frac{\partial D}{\partial t}. \tag{9}$$

Here, E and D represent the electric field and electric displacement field, respectively, while B and H denote the magnetic induction and magnetic field strength, respectively. J represents the current density. Wireless signals are primarily induced by the variation of the conduction current density J, followed by the conversion between the electric and magnetic fields. Starting from the principle of TENG,

$$\nabla \times H = J + \varepsilon \frac{\partial E}{\partial t} + \frac{\partial P}{\partial t}. \tag{10}$$

The displacement current, corresponding to $\partial D/\partial t$ in Maxwell's equations (Equation (10), is a theoretical quantity that unifies electricity and magnetism. Among the two terms in the displacement current, the second term $\partial P/\partial t$ in the displacement current is caused by the polarization of the medium. Wang reveals that the output current of TENG has a direct correlation with the second term $\partial P/\partial t$ in Maxwell's displacement current, which brings additional displacement current terms to initiate the creation and propagation of wireless signals. Here, ∂P represents the polarization term induced by TENG. Given that TENG can simultaneously and effectively capture mechanical energy and motion signals, no additional power and sensing modules are required. The energy consumption for emitting electromagnetic waves typically falls below 1 mW, and this level of power can be readily supplied by the energy from typical human motion energy collected by TENG, enabling the device to be completely self-powered. Through this integrated setup that cuts down on intermediate processes, additional electronic components and power consumption can be avoided, thereby achieving effective wireless transmission with minimalized devices. However, creating a rapidly varying ∂P within the TENG to produce a sufficiently great $\partial P/\partial t$ for efficient wireless signal propagation poses considerable difficulties. Wang and colleagues designed a self-powered long-distance wireless sensing scheme based on TENG-induced displacement current through discharge-induced displacement current—the TENG-based self-powered wireless sensor electronic label (SWISE, Figure 16(c))[304]. SWISE produces swiftly varying polarization terms P via breakdown discharge and achieves the ability to sense multi-point motion and gas sensing by differentiating signals arising from diverse design parameters and gas compositions. Compared to air, water possesses a higher dielectric constant, which is more favorable for the spread of the polarization electric field. Thus, underwater communication relying on the polarization electric field is feasible in complex water environments. In Figure 16(d)[305], Zhao and colleagues realized underwater wireless communication through Maxwell's displacement current produced by TENG, where connecting wires to TENG can generate an underwater electric field, and underwater receivers at a specific distance are capable of detecting the current signals. The received current signals are essentially unaffected by salinity, turbidity, and underwater obstacles. Even when passing a 100-meter-long spiral water pipe, the electrical signal waveform remains undistorted. Through the modulation and demodulation of the current signals produced by the sound-driven TENG, text and images can be transferred in the tank at a speed of 16 bits per second.

5.5. HMI

HMI has become an indispensable part of modern society[306,307]. From the touchscreens of smartphones to the immersive experiences provided by virtual reality devices, HMI technology continues to drive innovation and advancement in human-computer interfaces(Figure 17(a))[222]. By integrating TENG into HMI systems, not only has the power supply issue of devices been effectively addressed, but user interfaces have become more intelligent and seamless. Wearable HMI has made significant progress in the fields of communication, education, and healthcare, largely due to

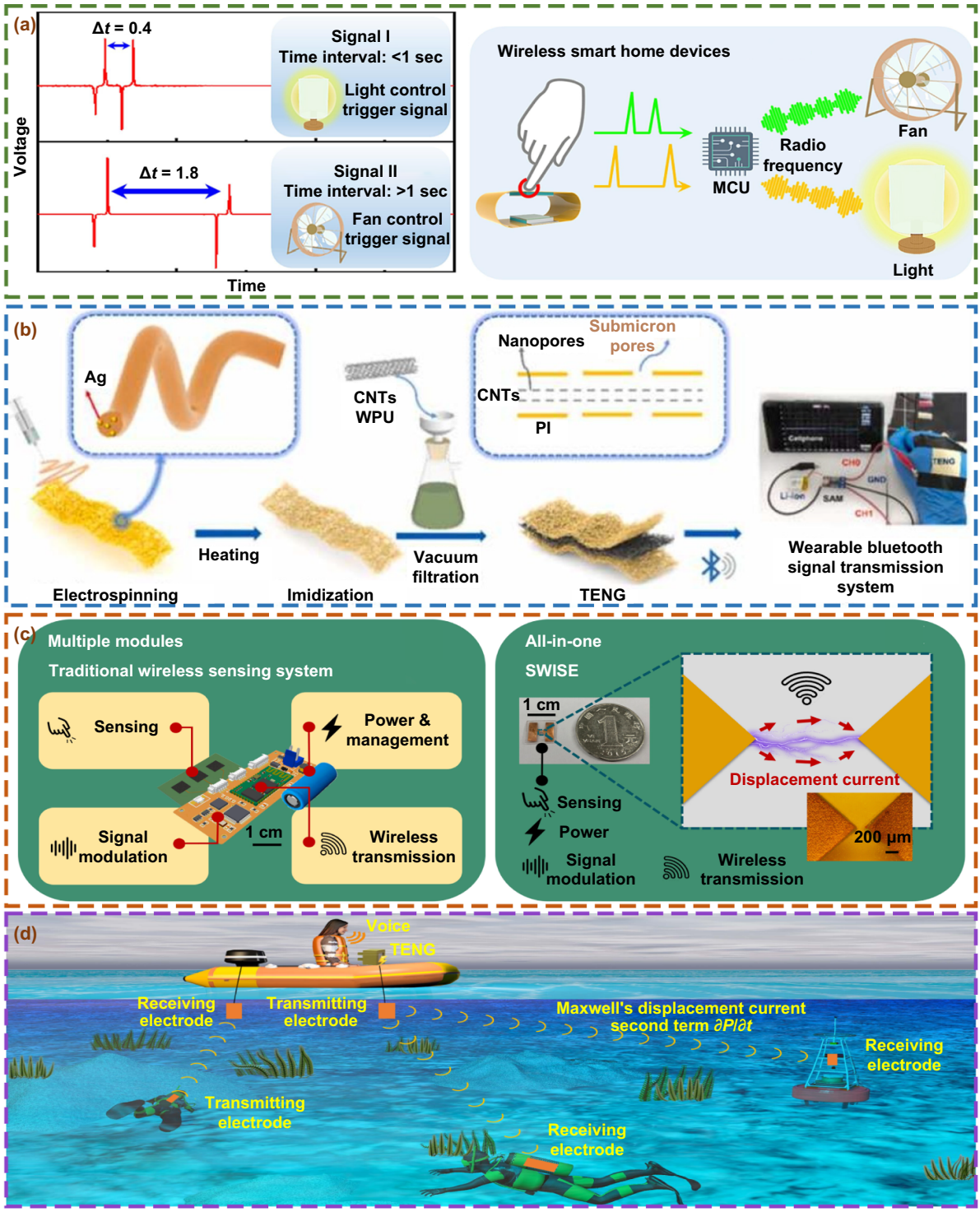

Figure 16. TENG-based wireless communication systems. (a) Wireless smart home system. Reprinted from[119], Copyright (2023), with permission from Elsevier. (b) Wearable bluetooth signal transmission system. Reprinted from[274], Copyright (2024), with permission from Elsevier. (c) Self-powered long-distance wireless sensing via discharge-induced displacement current. Reproduced from[304]. CC BY 4.0. (d) Underwater wireless communication system based on TENG. Reproduced from[305]. CC BY 4.0.

the rapid development of the IoT and 5 generation mobile communication technology. Among the various applications of wearable HMI, there is an urgent need for technologies that assist the visually impaired in communication, enabling them to independently access information. However, progress in research on blind communication has been hindered by challenges related to signal capture limitations and power supply issues. To address these issues, Liu et al. proposed an intelligent finger braille typing system based on a novel TENG (Figure 17(b))[308]. Leveraging the high-impedance

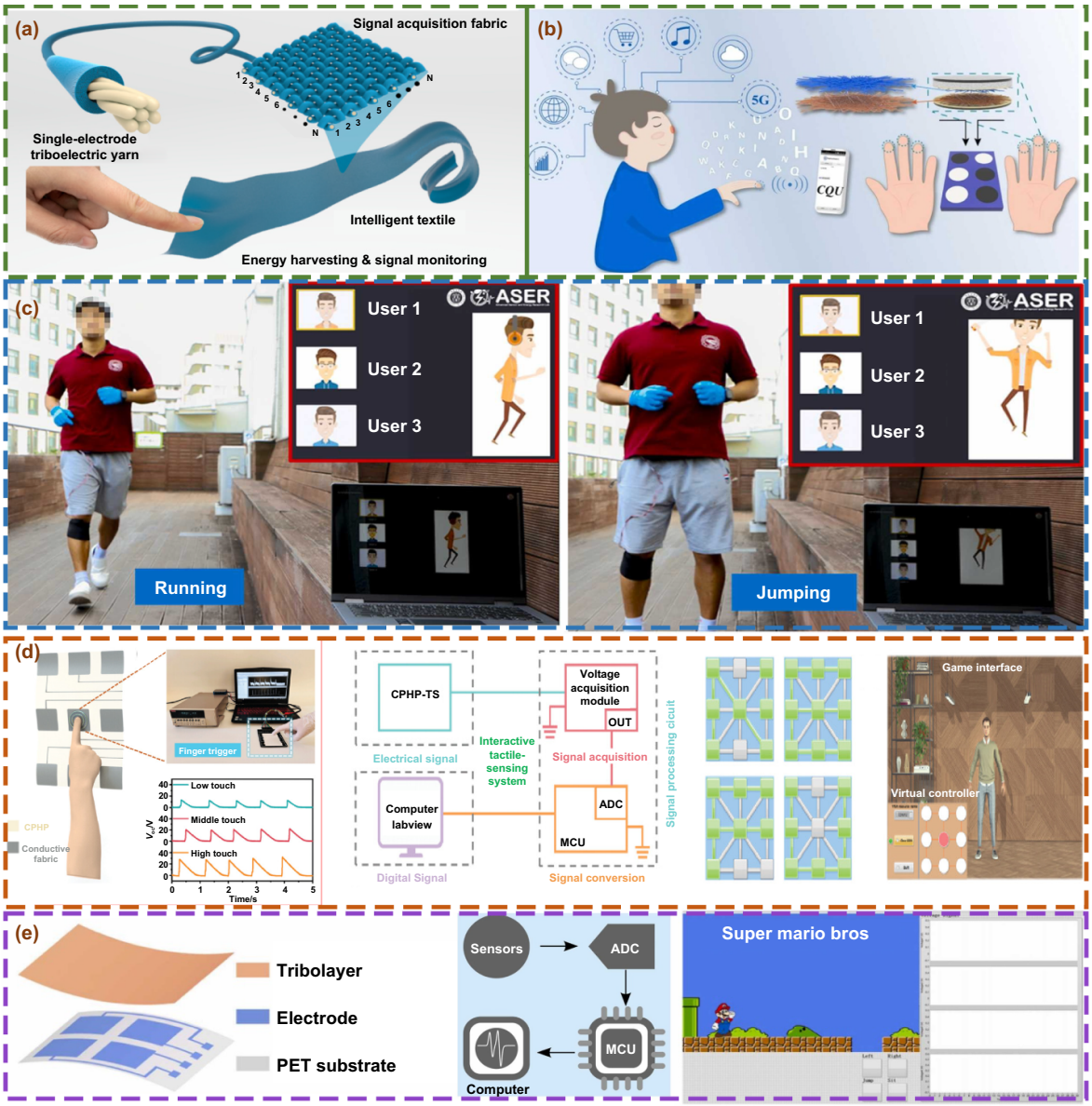

Figure 17. Human-machine interaction systems. (a) Intelligent finger braille typing system. Reprinted with permission from[222]. Copyright (2020) American Chemical Society. (b) Dynamic self-powered tactile perception system. Reprinted from[308], Copyright (2023), with permission from Elsevier. (c) Self-powered sensor for human activity recognition and user identification. Reprinted from[269], Copyright (2023), with permission from Elsevier. (d) TENG for self-powered HMI.[264] John Wiley & Sons. © 2023 Wiley-VCH GmbH. (e) FC-TENG for classic game control. Reprinted from[113], Copyright (2022), with permission from Elsevier.

and low-current characteristics of TENG, specialized weak electrical signal processing circuits were developed to build highly sensitive tactile sensors. The six points of the braille code will be represented by six automatic tactile sensors, and by using different tapping combinations, users can create words, which are then transmitted to a mobile device via bluetooth technology. This system has the potential to significantly enhance the braille literacy of blind or visually impaired individuals, bridging the gap between them and the digital world.

Moreover, TENG is frequently used in motion recognition and motion capture. As shown in Figure 17(c)[269], Shrestha et al. designed an electrospun cellulose-reinforced flexible sensing paper for dynamic self-powered tactile perception. The voltage signals generated by TENG are converted into digital signals via multi-channel voltage acquisition modules and analog-to-digital converters in the signal processing circuit. The microcontroller further filters and processes the signals, and real-time results can be displayed in a LabVIEW-based design program, enabling human-machine interaction functionality and effectively capturing personnel movements for game character control. To improve the accuracy of human-machine interaction, some scholars have begun to introduce algorithmic technologies to enhance accuracy. Shrestha et al. proposed a self-powered sensor for human activity recognition and user identification (Figure 17(d))[264], utilizing

advanced deep learning techniques to analyze TENG sensor data, achieving accuracy rates of 99% in user identification and user activity recognition. Ye et al. proposed TENG for self-powered human-machine interaction (Figure 17(e))[113], achieving a self-powered game controller with signal acquisition and processing circuits. Based on motion recognition of international Morse code, they, for the first time, utilized machine learning to manipulate characters in the Super Mario Bros. game, significantly demonstrating the potential commercial application capabilities of TENG in the field of HMI.

6. Conclusion and future perspectives

In recent years, FC-TENG has made significant progress, and electrospun films modified with nanomaterials have been proven to significantly enhance the specific surface area, porosity, roughness, β-phase transition, dielectric constant, electron affinity, and other properties of the triboelectric layer, thereby effectively improving the output and sensing performance of TENG. Various applications have demonstrated the strong commercial potential of TENG, including energy harvesting, self-powered sensors, wearable electronics for humans/plants, electronic skin, smart homes, wireless communication systems, human-computer interaction interfaces, and medical devices. Despite the notable advancements in material preparation and practical applications of EC-TENG, many scientific and technological challenges still remain in this field (Figure 18).

Material design: in recent years, researchers have focused on the design of novel triboelectric materials, and TENG has seen significant improvements in both energy output and sensing performance. However, as environmental conservation and sustainability concepts become increasingly prominent, the materials for TENG need to possess biodegradability[309,310], biocompatibility[311,312], certain self-healing properties[313,314], and durability[315,316]. The development of biodegradable materials will make TENG more environmentally friendly, especially in applications such as medical devices and wearable electronics. By selecting naturally degradable or body-absorbable biopolymers such as PLA and PHA, the materials can degrade naturally after the lifespan of TENG, reducing environmental pollution[317–319]. These biodegradable materials not only match the performance of traditional polymers but also can fully degrade in specific environments. Notably, as TENG gradually finds applications in implantable medical devices, the materials must be biodegradable and biocompatible. Additionally, materials with certain self-healing properties can enhance the stability and lifespan of TENG. LM can not only serve as a filler in the triboelectric layer of TENG to improve output, but also as an electrode to achieve conformal properties. Extensive research indicates that LM is an ideal material for fabricating self-healing electrodes, but there is no consensus on the enhancement of TENG performance when LM is used as a triboelectric layer[320–323]. In addition, material wear has always been a challenge faced by TENGs. Particularly at the solid-solid interface, it causes severe wear to the friction layer. In recent years, researchers have begun to focus on the study of solid-liquid and gas-solid interfaces to develop TENGs with high durability[324–327]. Therefore, the development of biodegradable, biocompatible materials and LM should be a priority for future TENG research.

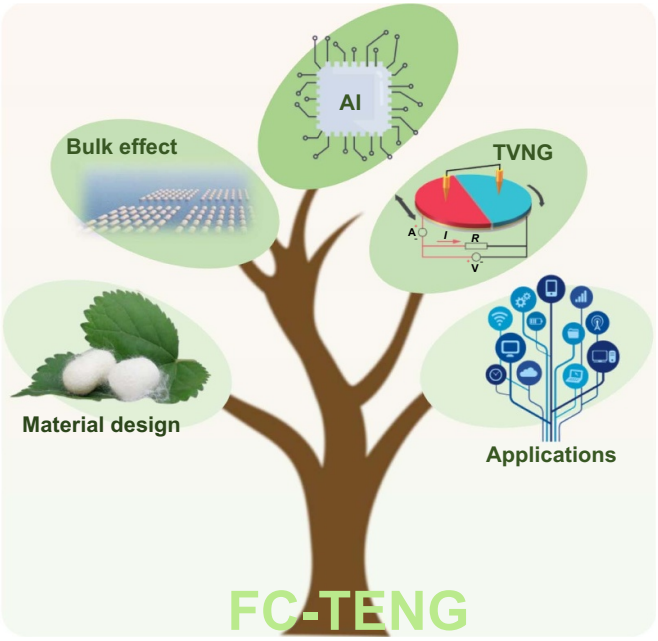

Figure 18. Future Development of FC-TENG. Material design, TVNG[328], application, bulk effect[329], and machine learning algorithm assistance.[328] John Wiley & Sons. © 2023 Wiley-VCH GmbH.[329] John Wiley & Sons. © 2024 Wiley-VCH GmbH.

Tribovoltaic nanogenerators: traditional TENG, lacking rectifying circuits or specialized device structures, can only generate alternating current, and its lower conversion efficiency and output current density have limited its applications. In comparison to energy conversion devices, energy exchange efficiency is nearly as important, as meaningful energy conversion is only possible when the generated power can be maximized and utilized. In this context, designing direct current TENG (DC-TENG) with high output power presents a more economical and rational approach to addressing energy conversion losses and low output power issues. Structural design, phase control, and the use of semiconductor materials are three common methods for constructing DC-TENG. In recent years, spurred by the rapid development of semiconductor materials, tribovoltaic nanogenerators (TVNG) have been developed[330–332]. TVNG is a phenomenon where direct current voltage and current are generated through mechanical friction at semiconductor interfaces. Compared to TENG, TVNG offers the advantages of high current density and low impedance[333–337]. Common semiconductor materials in TVNG include silicon, perovskite, and gallium nitride. The above-mentioned fiber manufacturing technologies can be used to prepare fiber films or long filaments with semiconductor properties. By combining different fiber manufacturing technologies, semiconductor fibers with heterojunction structures can be effectively fabricated,

which have been proven to have significant application values in fields such as photocatalysis[338], energy conversion[339], and environmental remediation[340]. Therefore, the FC-TVNG does not require a rectifier circuit and can be directly used to power micro- and small- sized electronic devices or for energy storage. Compared with TENG, the current output of TVNG can be an order of magnitude higher, making it more commercially promising.

Applications: the FC-TENG has broad application expansion and commercialization prospects, and it will become an important driving force for future technological development. The flexibility and light weight of FC-TENG make it an ideal energy solution for smart clothing and health monitoring devices, which can collect the energy from human motion in real-time and power the sensors[341–343]. In addition, FC-TENG can serve as a distributed energy harvester, providing sustainable power support for wireless sensor networks and promoting the development of smart cities and smart homes[312,344,345]. With the continuous advancement of manufacturing technologies, the production cost of FC-TENG will gradually decrease, and the production efficiency will be significantly improved, laying a foundation for its large-scale commercialization. Through standardized manufacturing processes and optimized material selection, the product consistency and reliability of FC-TENG will be guaranteed to meet the market demand. It can be inferred that FC-TENG is expected to achieve commercial breakthroughs in fields such as consumer electronics, smart textiles, and medical devices, and become an important part of green energy.

Bulk effect: as a clean and sustainable form of energy, the development and utilization of blue energy are of great significance for addressing the global energy crisis and mitigating climate change. The ocean covers 71% of the earth's surface and holds abundant resources of tidal, wave, and current energy, collectively termed blue energy[346]. These resources are not only vast and widely distributed but also have minimal environmental impact. With the gradual depletion of traditional fossil fuels and the increasing global demand for energy, the development and utilization of blue energy have become a core direction for promoting energy transition and achieving green, low-carbon development[347–350]. However, the complexity and vastness of marine environments present numerous technical challenges for blue energy development, particularly in efficient energy collection and long-distance transmission. FC-TENG exhibits excellent mechanical flexibility and charge storage capabilities, enabling the efficient conversion of mechanical energy from the ocean into electrical energy. This technology is not only suitable for small-scale self-powered systems but also provides continuous energy support for marine monitoring equipment and sensor networks. In 2020, Wang et al. attached an aluminum strip electrode to the negative friction layer (PTFE). The impacting water droplets bridged the aluminum strip electrode and PTFE, connecting the originally non-connected components into a closed-loop electrical system. This transformed the traditional interfacial effect into a bulk effect, thereby increasing the instantaneous power density by several orders of magnitude in the equivalent device limited by the interfacial effect[351]. As a result, the instantaneous power density of equivalent devices limited by the interfacial effect was increased by several orders of magnitude. Such remarkable results provide strong clues for subsequent research[352–354]. Therefore, it can be inferred that the bulk effect is very likely to be the key to the future development of blue energy.

Machine learning algorithm assistance: TENG sensors not only convert mechanical energy into electrical energy but also possess high sensitivity, low power consumption, and environmental friendliness, making them suitable for a wide range of applications in environmental monitoring, health monitoring, and IoT[355–359]. However, TENG sensors face challenges in signal processing complexity, data quality, and model optimization during practical applications. TENG sensors often encounter issues such as environmental noise, signal drift, and sensor aging, which can degrade data quality and signal accuracy. Traditional data processing methods often struggle to effectively address these complex issues. Machine learning algorithms, including support vector machines, random forest, and deep learning, can learn from large datasets, automatically extract features, and perform classification and regression analysis, thereby effectively removing noise, correcting signal drift, and improving data quality[360–363]. Furthermore, machine learning algorithms play a crucial role in fault detection and maintenance of TENG sensors[364–366]. Over time, TENG sensors may develop faults that affect their performance and lifespan. Traditional fault detection methods typically rely on manual experience and fixed rules, making it difficult to accurately identify faults in real-time. Machine learning algorithms, particularly unsupervised and semi-supervised learning methods, can analyze real-time sensor data to automatically identify abnormal patterns and provide early fault warnings[367,368]. For instance, Zhang et al. designed a self-powered flexible keyboard capable of identifying users' identities during typing. In combination with machine learning, this keyboard achieves identity authentication through two methods: fixed text input and dynamic text input. It accurately authenticated fixed passwords consisting of 8 characters with a success rate of 95.3%, and precisely authenticated 14 groups of dynamic text containing double-key combinations with an accuracy rate of 100%[369]. Additionally, machine learning algorithms show significant potential in optimizing the energy efficiency and energy management of TENG sensors. The energy output of TENG sensors is influenced by various factors, including mechanical motion frequency, contact material properties, and environmental conditions. Traditional energy management methods are often based on fixed parameters and empirical models, which are less adaptable to complex and dynamic environmental conditions. Machine learning algorithms can dynamically adjust energy management strategies based on real-time data, achieving optimal energy output and storage[370,371].

In summary, although commercialization faces many challenges, TENGs have made significant progress in material design and emerging applications over the past few years. Through close collaboration with other advanced disciplines

and technologies, substantial innovations can be achieved, providing TENGs with a sustainable, versatile, cost-effective, and scalable spinning technology. It can be inferred that the rapid development of FC-TENG will provide significant technical support for the era of wireless artificial intelligence and IoT.

Data availability

No data was used for the research described in the article.

Acknowledgments

This work was financially supported by the National Natural Science Foundation of China (52127811, 51975120), and the Postgraduate Research&Practice Innovation Program of Jiangsu Province (SJCX25_0096).

Confilct of interest

The authors declare that they have no known competing financial interests or personal relationships that could have appeared to influence the work reported in this paper.

CRediT authorship contribution statement

Gang Yu: conceptualization, methodology, formal analysis, writing original draft, visualization, software. **Han Hu**: writing—review & editing, visualization. **Qianguo Yu:** writing—review & editing. **Chun Li:** writing—review & editing. **Dongdong Zhou:** writing—review & editing. **Zuankai Wang:** writing—review & editing, visualization. **Kedong Bi:** project administration, investigation, resources, funding acquisition, writing—review & editing.

ORCID iD

Gang Yu 0000-0002-3418-9257

References

[1] Xue K et al. 2023. Initiatorless solar photopolymerization of versatile and sustainable eutectogels as multi-response and self-powered sensors for human-computer interface. *Adv. Funct. Mater.* **33**, 2305879.
[2] Zhang B B et al. 2024. A three-dimensional liquid diode for soft, integrated permeable electronics. *Nature* **628**, 84–92.
[3] Aliyana A K, Bairagi S, Kumar C, Mulvihill D M and Stylios G K. 2024. Investigating superior performance by configuring bimetallic electrodes on fabric triboelectric nanogenerators (F-TENGs) for IoT enabled touch sensor applications. *Nano Energy* **130**, 110125.
[4] Zhu C Q, Xiang C, Wu M W, Yu C N, Dai S, Sun Q J, Zhou T M, Wang H and Xu M Y. 2024. Recent advances in wave-driven triboelectric nanogenerators: from manufacturing to applications. *Int. J. Extrem. Manuf.* **6**, 062009.
[5] Cui X, Nie J H and Zhang Y. 2024. Recent advances in high charge density triboelectric nanogenerators. *Int. J. Extrem. Manuf.* **6**, 042001.
[6] Lee D, Chae J, Cho S, Kim J W, Ahmad A, Karim M R, La M, Park S J and Choi D. 2024. Bidirectional rotating direct-current triboelectric nanogenerator with self-adaptive mechanical switching for harvesting reciprocating motion. *Int. J. Extrem. Manuf.* **6**, 045502.
[7] Li X W, Zhou Y, Li Z J, Guo H Y, Gong Y, Zhang D, Zhang D, Zhang Q, Wang B and Peng Y. 2023. Vortex-induced vibration triboelectric nanogenerator for energy harvesting from low-frequency water flow. *Energy Convers. Manage.* **292**, 117383.
[8] Wang L, Zhang Y X, Zhang X S, Cheng X J, Zhai S J, Bi X Z, Li H Y, Wang Z L and Cheng T H. 2025. Harvesting broadband breeze vibration energy via elastic bistable triboelectric nanogenerator for in situ, self-powered monitoring of power transmission lines. *Adv. Energy Mater.* **15**, 2403318.
[9] Chen H M et al. 2024. Improved flexible triboelectric nanogenerator based on tile-nanostructure for wireless human health monitor. *Energy Environ. Mater.* **7**, e12654.
[10] Xia Y X, Zhi J Y, Zhang R C, Zhou F, Liu S H, Xu Q and Qin Y. 2024. Synchronous switching strategy to enhance the real-time powering and charging performance of triboelectric nanogenerator. *Adv. Mater.* **36**, 2403361.
[11] Son J-H, Chung S-H, Cha K, Kim S, Lin Z-H, Hong J, Chung J and Lee S. 2023. Ultrahigh performance, serially stackable, breeze driven triboelectric generator via ambient air ionizing channel. *Adv. Mater.* **35**, 2300283.
[12] Hu Y X, Li X Y, Gao Y K, Zhao Z H, Liu X R, He L X, Zhang B F, Zhou L L, Wang Z L and Wang J. 2024. A combined wind harvesting and speed sensing system based on constant-voltage triboelectric nanogenerator. *Adv. Energy Mater.* **14**, 2400672.
[13] Li Y H, Guo Z T, Zhao Z H, Gao Y K, Yang P Y, Qiao W Y, Zhou L L, Wang J and Wang Z L. 2023. Multi-layered triboelectric nanogenerator incorporated with self-charge excitation for efficient water wave energy harvesting. *Appl. Energy* **336**, 120792.
[14] Nan Y B, Wang X T, Xu H, Zhou H, Sun Y N, Wang M X, Liu W L, Ma C Q and Yu T. 2025. Submerged and completely open solid-liquid triboelectric nanogenerator for water wave energy harvesting. *InfoMat* **7**, e12621.
[15] Li Z K, Yu A F, Zhang Q and Zhai J Y. 2024. Recent advances in fabricating high-performance triboelectric nanogenerators via modulating surface charge density. *Int. J. Extrem. Manuf.* **6**, 052003.
[16] Wu P F, Zhao C X, Cui E D, Xu S W, Liu T, Wang F Y, Lee C and Mu X J. 2024. Advances in magnetic-assisted triboelectric nanogenerators: structures, materials and self-sensing systems. *Int. J. Extrem. Manuf.* **6**, 052007.
[17] Zhang B S, Jiang Y C, Ren T C, Chen B J, Zhang R Y and Mao Y C. 2024. Recent advances in nature inspired triboelectric nanogenerators for self-powered systems. *Int. J. Extrem. Manuf.* **6**, 062003.
[18] Liu F, Feng Y, Qi Y C, Liu G X, Zhou H, Lin Y, Fan B B, Zhang Z, Dong S C and Zhang C. 2023. Self-powered wireless body area network for multi-joint movements monitoring based on contact-separation direct current triboelectric nanogenerators. *InfoMat* **5**, e12428.
[19] Meng X C, Xiao X, Jeon S, Kim D, Park B-J, Kim Y-J, Rubab N, Kim S and Kim S-W. 2023. An ultrasound-driven bioadhesive triboelectric nanogenerator for instant wound sealing and electrically accelerated healing in emergencies. *Adv. Mater.* **35**, 2209054.
[20] Wang R, Jin X, Wang Q F, Zhang Q R, Yuan H, Jiao T F, Cao X and Ma J M. 2023. A transparent, flexible triboelectric nanogenerator for anti-counterfeiting based on photothermal effect. *Matter* **6**, 1514–1529.
[21] Chang C-Y, Yang J-R, Liu Y-S and Panda A. 2024. Facile surface functionalization of triboelectric layers *via* electrostatically self-assembled zwitterionic molecules for achieving

efficient and stable antibacterial flexible triboelectric nanogenerators. *Mater. Horiz.* **11**, 646–660.
[22] Patnam H, Graham S A, Manchi P, Paranjape M V, Huh Y S and Yu J S. 2024. Highly flexible and harsh temperature-tolerant single-electrode mode triboelectric nanogenerators via biocompatible ionic liquid electrolytes for wearable electronic applications. *Adv. Compos. Hybrid Mater.* **7**, 56.
[23] Lan S, Chen H and Chen H. 2025. Multimodal perception system with optical feedback based on triboelectric nanogenerator and quantum dot light-emitting synaptic device. *J. Phys. D: Appl. Phys.* **58**, 225110.
[24] Kwon Y H, Meng X C, Xiao X, Suh I-Y, Kim D, Lee J and Kim S-W. 2025. Triboelectric energy harvesting technology for self-powered personal health management. *Int. J. Extrem. Manuf.* **7**, 022005.
[25] Luo L et al. 2025. Constructing high-performance and versatile liquid-solid triboelectric nanogenerator with inflatable columnar units. *Int. J. Extrem. Manuf.* **7**, 015505.
[26] Shen D L, Du T, Dong F Y, Cai H, Noor A, Du X N, Zou Y J, Lee C and Xu M Y. 2025. Advances of wearable silicone rubber-based triboelectric nanogenerators: from manufacturing to application. *Int. J. Extrem. Manuf.* **7**, 032004.
[27] Wang Z, Liu Z R, Zhao G R, Zhang Z C, Zhao X Y, Wan X Y, Zhang Y L, Wang Z L and Li L L. 2022. Stretchable unsymmetrical piezoelectric $BaTiO_3$ composite hydrogel for triboelectric nanogenerators and multimodal sensors. *ACS Nano* **16**, 1661–1670.
[28] Lee C, Cho C and Oh J H. 2023. Highly flexible triboelectric nanogenerators with electrospun PVDF-TrFE nanofibers on MWCNTs/PDMS/AgNWs composite electrodes. *Composites B* **255**, 110622.
[29] Manchi P, Graham S A, Paranjape M V, Kurakula A, Kavarthapu V S and Yu J S. 2024. Calcium copper titanate incorporated polydimethylsiloxane flexible composite film-based triboelectric nanogenerator for energy harvesting and self-powered sensing applications. *J. Mater. Sci. Technol.* **190**, 56–66.
[30] Li Z H, Chen Y M, Hang T Y, Xu C H, Shen J H, Li X P, Zheng J J and Wu Z Y. 2025. Highly flexible and flame-retardant aramid nanofiber composite papers for energy harvesting. *J. Mater. Sci. Technol.* **204**, 81–90.
[31] Nie J H, Chen X Y and Wang Z L. 2019. Electrically responsive materials and devices directly driven by the high voltage of triboelectric nanogenerators. *Adv. Funct. Mater.* **29**, 1806351.
[32] Li Y, Xiao S, Luo Y, Tian S S, Tang J, Zhang X X and Xiong J Q. 2022. Advances in electrospun nanofibers for triboelectric nanogenerators. *Nano Energy* **104**, 107884.
[33] Duan Q S, Peng W Q, He J X, Zhang Z J, Wu Z C, Zhang Y, Wang S F and Nie S X. 2023. Rational design of advanced triboelectric materials for energy harvesting and emerging applications. *Small Methods* **7**, 2201251.
[34] Tao X L, Chen X Y and Wang Z L. 2023. Design and synthesis of triboelectric polymers for high performance triboelectric nanogenerators. *Energy Environ. Sci.* **16**, 3654–3678.
[35] Zhao J and Shi Y J. 2023. Boosting the durability of triboelectric nanogenerators: a critical review and prospect. *Adv. Funct. Mater.* **33**, 2213407.
[36] Potu S, Kulandaivel A, Gollapelli B, Khanapuram U K and Rajaboina R K. 2024. Oxide based triboelectric nanogenerators: recent advances and future prospects in energy harvesting. *Mater. Sci. Eng. R* **161**, 100866.
[37] Belbéoch C, Lejeune J, Vroman P and Salaün F. 2021. Silkworm and spider silk electrospinning: a review. *Environ. Chem. Lett.* **19**, 1737–1763.
[38] Al-Dhahebi A M, Ling J, Krishnan S G, Yousefzadeh M, Elumalai N K, Saheed M S M, Ramakrishna S and Jose R. 2022. Electrospinning research and products: the road and the way forward. *Appl. Phys. Rev.* **9**, 011319.
[39] Si Y F, Shi S and Hu J L. 2023. Applications of electrospinning in human health: from detection, protection, regulation to reconstruction. *Nano Today* **48**, 101723.
[40] Song W L, Tang Y X, Qian C, Kim B J, Liao Y Z and Yu D-G. 2023. Electrospinning spinneret: a bridge between the visible world and the invisible nanostructures. *Innovation* **4**, 100381.
[41] Liu J-H, Wang P, Gao Z H, Li X H, Cui W B, Li R, Ramakrishna S, Zhang J and Long Y-Z. 2024. Review on electrospinning anode and separators for lithium ion batteries. *Renew. Sustain. Energy Rev.* **189**, 113939.
[42] Tabassian R, Rajabi-abhari A, Mahato M, Yoo H, Yoon H Y, Park J Y and Oh I-K. 2024. Metal-organic framework-based nanofibrous film for two different modes of triboelectric nanogenerators. *SmartMat* **5**, e1270.
[43] Zhao L L, Guo X, Pan Y S, Jia S C, Liu L Q, Daoud W A, Poechmueller P and Yang X Y. 2024. Triboelectric gait sensing analysis system for self-powered IoT-based human motion monitoring. *InfoMat* **6**, e12520.
[44] Zhu G Y et al. 2024. Bio-inspired gradient poly(lactic acid) nanofibers for active capturing of $PM_{0.3}$ and real-time respiratory monitoring. *J. Hazard. Mater.* **474**, 134781.
[45] Badmus M, Liu J, Wang N, Radacsi N and Zhao Y. 2021. Hierarchically electrospun nanofibers and their applications: a review. *Nano Mater. Sci.* **3**, 213–232.
[46] Xia C F, Huang L, Yan D F, Douka A I, Guo W, Qi K and Xia B Y. 2021. Electrospinning synthesis of self-standing cobalt/nanocarbon hybrid membrane for long-life rechargeable zinc-air batteries. *Adv. Funct. Mater.* **31**, 2105021.
[47] Hu Y, Zhang Y, Zhu J C and Niu Z Q. 2022. Rational design of continuous gradient composite films for high-performance zinc-ion batteries. *Energy Storage Mater.* **51**, 382–390.
[48] Yang T et al. 2023. *Modulating piezoelectricity and mechanical strength via* three-dimensional gradient structure for piezoelectric composites. *Mater. Horiz.* **10**, 5045–5052.
[49] Sankar S S, Karthick K, Sangeetha K, Karmakar A, Madhu R and Kundu S. 2021. Current perspectives on 3D ZIFs incorporated with 1D carbon matrices as fibers *via* electrospinning processes towards electrocatalytic water splitting: a review. *J. Mater. Chem. A* **9**, 11961–12002.
[50] Han T, Zhou Z H, Du Y H, Wang W F, Wang C, Yang X Q, Liu J W, Yang H B, Cui H Z and Yan J Y. 2024. Advances in radiative sky cooling based on the promising electrospinning. *Renew. Sustain. Energy Rev.* **200**, 114533.
[51] Song Y H, Bao J K, Hu Y, Cai H P, Xiong C X, Yang Q L, Tian H F and Shi Z Q. 2022. Forward polarization enhanced all-polymer based sustainable triboelectric nanogenerator from oriented electrospinning PVDF/cellulose nanofibers for energy harvesting. *Sustain. Energy Fuels* **6**, 2377–2386.
[52] Cha S, Cho Y, Kim J G, Choi H, Ahn D, Sun J Z, Kang D-S, Pak C and Park J-J. 2022. Controllable triboelectric series using gradient positive and negative charge-confinement layer with different particle sizes of mesoporous carbon materials. *Small Methods* **6**, 2101545.
[53] Gao L, Yang J, Zhao Y, Zhao X X, Zhou K K, Zhai W, Zheng G Q, Dai K, Liu C T and Shen C Y. 2025. Multilayer bionic tunable strain sensor with mutually non-interfering conductive networks for machine learning-assisted gesture recognition. *Adv. Funct. Mater.* **35**, 2416911.
[54] Khanh T D, Meena J S, Choi S B and Kim J-W. 2023. Breathable, self-healable, washable and durable all-fibrous triboelectric nanogenerator for wearable electronics. *Mater. Today Adv.* **20**, 100427.
[55] Ning C, Xiang S X, Sun X P, Zhao X Y, Wei C H, Li L L, Zheng G Q and Dong K. 2024. Highly stretchable kirigami-patterned nanofiber-based nanogenerators for harvesting human motion energy to power wearable electronics. *Mater. Futures* **3**, 025101.

[56] Sardana S, Kaur H, Arora B, Aswal D K and Mahajan A. 2022. Self-powered monitoring of ammonia using an MXene/TiO_2/cellulose nanofiber heterojunction-based sensor driven by an electrospun triboelectric nanogenerator. *ACS Sens.* **7**, 312–321.
[57] Xu W K et al. 2022. Laminated triboelectric acoustic energy harvester based on electrospun nanofiber towards real-time noise decibel monitoring. *Nano Energy* **99**, 107348.
[58] Cheng Y, Wang J, Lu X F and Wang C. 2023. An all-nanofibrous Janus textile with directional perspiration for triboelectric nanogenerator and self-powered e-skin sensor. *Nano Energy* **117**, 108852.
[59] Cui M J, Guo H, Zhai W, Liu C T, Shen C Y and Dai K. 2023. Template-assisted electrospun ordered hierarchical microhump arrays-based multifunctional triboelectric nanogenerator for tactile sensing and animal voice-emotion identification. *Adv. Funct. Mater.* **33**, 2301589.
[60] Jo H, Park D, Joo M, Choi D, Kang J S, Ha J-M, Kim K H, Kim K H and An S. 2023. Performance-enhanced eco-friendly triboelectric nanogenerator via wettability manipulation of lignin. *Ecomat* **5**, e12413.
[61] Liu Y, Zhao C L, Xiong Y, Yang J H, Jiao H S, Zhang Q, Cao R, Wang Z L and Sun Q J. 2023. Versatile ion-gel fibrous membrane for energy-harvesting iontronic skin. *Adv. Funct. Mater.* **33**, 2303723.
[62] Rajaboina R K, Khanapuram U K and Kulandaivel A. 2024. 2D layered materials based triboelectric self-powered sensors. *Adv. Sens. Res.* **3**, 2400045.
[63] Shi Y P, Wei X L, Wang K M, He D D, Yuan Z H, Xu J H, Wu Z Y and Wang Z L. 2021. Integrated all-fiber electronic skin toward self-powered sensing sports systems. *ACS Appl. Mater. Interfaces* **13**, 50329–50337.
[64] Sun J Z, Ahn D, Kim J, Ahn S, Hwang J S, Kwon J Y, Lee J S, Oh J M, Nam K and Park -J-J. 2021. Surface-control enhanced crater-like electrode in a gelatin/polyvinyl alcohol/carbon composite for biodegradable multi-modal sensing systems with human-affinity. *J. Mater. Chem. A* **9**, 9145–9156.
[65] Gunasekhar R, Sathiyanathan P, Reza M S, Prasad G, Prabu A A and Kim H. 2023. Polyvinylidene fluoride/aromatic hyperbranched polyester of third-generation-based electrospun nanofiber as a self-powered triboelectric nanogenerator for wearable energy harvesting and health monitoring applications. *Polymers* **15**, 2375.
[66] Amrutha B, Yoon J U K, Woo I, Gajula P, Prabu A A and Bae J W. 2024. Performance optimization of MoS_2-doped PVDF-HFP nanofiber triboelectric nanogenerator as sensing technology for smart cities. *Appl. Mater. Today* **41**, 102503.
[67] Zhao P F et al. 2018. Emulsion electrospinning of polytetrafluoroethylene (PTFE) nanofibrous membranes for high-performance triboelectric nanogenerators. *ACS Appl. Mater. Interfaces* **10**, 5880–5891.
[68] Yang Z Q, Zhang X, Deng T J and Xiang G. 2023. Mechanically robust and electrically stable high-performance triboelectric nanogenerator based on fluffy-free EC/Nylon-11 and PTFE/PVDF nanofibers. *ACS Appl. Mater. Interfaces* **15**, 52696–52704.
[69] Han Y, Wang W Q, Zou J D, Li Z, Cao X and Xu S M. 2020. Self-powered energy conversion and energy storage system based on triboelectric nanogenerator. *Nano Energy* **76**, 105008.
[70] Lei R, Shi Y X, Ding Y F, Nie J H, Li S Y, Wang F, Zhai H, Chen X Y and Wang Z L. 2020. Sustainable high-voltage source based on triboelectric nanogenerator with a charge accumulation strategy. *Energy Environ. Sci.* **13**, 2178–2190.
[71] Chen J H, Wei X L, Wang B C, Li R N, Sun Y G, Peng Y T, Wu Z Y, Wang P and Wang Z L. 2021. Design optimization of soft-contact freestanding rotary triboelectric nanogenerator for high-output performance. *Adv. Energy Mater.* **11**, 2102106.
[72] Roy S, Maji P K and Goh K-L. 2021. Sustainable design of flexible 3D aerogel from waste PET bottle for wastewater treatment to energy harvesting device. *Chem. Eng. J.* **413**, 127409.
[73] Wang N N, Feng Y G, Zheng Y B, Zhang L Q, Feng M, Li X J, Zhou F and Wang D A. 2021. New hydrogen bonding enhanced polyvinyl alcohol based self-charged medical mask with superior charge retention and moisture resistance performances. *Adv. Funct. Mater.* **31**, 2009172.
[74] Makarov D. 2021. Energy supply from magnetoelastic composites. *Nat. Mater.* **20**, 1589–1590.
[75] Ren M X and Xu J J. 2022. Quantum dot nanocomposites for flexible retina. *Nat. Nanotechnol.* **17**, 819–820.
[76] Nepal D et al. 2023. Hierarchically structured bioinspired nanocomposites. *Nat. Mater.* **22**, 18–35.
[77] Isaac J A, Devaux D and Bouchet R. 2022. Dense inorganic electrolyte particles as a lever to promote composite electrolyte conductivity. *Nat. Mater.* **21**, 1412–1418.
[78] Li Z H et al. 2023. Ultrastrong conductive in situ composite composed of nanodiamond incoherently embedded in disordered multilayer graphene. *Nat. Mater.* **22**, 42–49.
[79] Han D L et al. 2023. Molecular interface regulation enables order-disorder synergy in electrocaloric nanocomposites. *Joule* **7**, 2174–2190.
[80] Olhan S and Behera B K. 2024. Development of GNP nanofiller based textile structural composites for enhanced mechanical, thermal, and viscoelastic properties for automotive components. *Adv. Compos. Hybrid Mater.* **7**, 25.
[81] Winkless L. 2014. Exfoliating 2-D materials for printable electronics. *Mater. Today* **17**, 53
[82] Yuan S Q, Shen F, Chua C K and Zhou K. 2019. Polymeric composites for powder-based additive manufacturing: materials and applications. *Prog. Polym. Sci.* **91**, 141–168.
[83] Wu H, Wang S, Wang Z K and Zi Y L. 2021. Achieving ultrahigh instantaneous power density of 10 MW/m^2 by leveraging the opposite-charge-enhanced transistor-like triboelectric nanogenerator (OCT-TENG). *Nat. Commun.* **12**, 5470.
[84] Du J Y, Liu Z Q, Luo H, Li S Y, Tao X L, Zheng L, Yang D and Chen X Y. 2022. Tunable polarity reversal phenomenon at the initial working state of triboelectric nanogenerator. *Nano Energy* **102**, 107651.
[85] Peng Z H et al. 2022. Improving relative permittivity and suppressing dielectric loss of triboelectric layers for high-performance wearable electricity generation. *ACS Nano* **16**, 20251–20262.
[86] Sun D J, Song W Z, Li C L, Chen T, Zhang D S, Zhang J, Ramakrishna S and Long Y Z. 2022. High-voltage direct current triboelectric nanogenerator based on charge pump and air ionization for electrospinning. *Nano Energy* **101**, 107599.
[87] Xing F J, Ou Z Q, Gao X B, Chen B D and Wang Z L. 2022. Harvesting electrical energy from high temperature environment by aerogel nano-covered triboelectric yarns. *Adv. Funct. Mater.* **32**, 2205275.
[88] Xing L, Li L Z, Liu Y, Ren J Y, Guo G L, Chen Y F, Zheng Y and Sun B. 2024. Highly stretchable GR/TPU strain sensor based on one-step electrospun fibrous yarns for wearable devices. *J. Mater. Chem. A* **12**, 10905–10912.
[89] Islam M R, Faruk O, Rana S M S, Pradhan G B, Kim H, Reza M S, Bhatta T and Park J Y. 2024. Poly-DADMAC functionalized polyethylene oxide composite nanofibrous mat as highly positive material for triboelectric nanogenerators and self-powered pressure sensors. *Adv. Funct. Mater.* **34**, 2403899.

[90] Shi K M, Chai B, Zou H Y, Wen Z, Liu Y J, He M, Chen J, Jiang P K and Huang X Y. 2024. Direct-current triboelectric nanogenerators based on contact-separation mode and conductive-adhesive interface. *Adv. Funct. Mater.* **34**, 2400204.
[91] Sun Q Z et al. 2024. Charge dispersion strategy for high-performance and rain-proof triboelectric nanogenerator. *Adv. Mater.* **36**, e2307918.
[92] Hu S M et al. 2022. Biodegradable, super-strong, and conductive cellulose macrofibers for fabric-based triboelectric nanogenerator. *Nano-Micro Lett.* **14**, 115.
[93] Cui S N, Zhou L L, Liu D, Li S X, Liu L, Chen S Y, Zhao Z H, Yuan W, Wang Z L and Wang J. 2022. Improving performance of triboelectric nanogenerators by dielectric enhancement effect. *Matter* **5**, 180–193.
[94] Li Q Y, Fu S K, Li X C, Chen H L, He W C, Yang Q X, Zhang X M, Yang H K, Ren D H and Xi Y. 2023. Overall performance improvement of direct-current triboelectric nanogenerators by charge leakage and ternary dielectric evaluation. *Energy Environ. Sci.* **16**, 3514–3525.
[95] Wu H Y, Wang J, He W C, Shan C C, Fu S K, Li G, Zhao Q H, Liu W L and Hu C G. 2023. Ultrahigh output charge density achieved by charge trapping failure of dielectric polymers. *Energy Environ. Sci.* **16**, 2274–2283.
[96] Wang J et al. 2024. Effectively inhibiting charge injection and dielectric loss of high permittivity inorganic materials by rationally coating organic polymer for achieving high output charge density. *Adv. Energy Mater.* **14**, 2400429.
[97] Wang J, Zhang B F, Zhao Z H, Gao Y K, Liu D, Liu X R, Yang P Y, Guo Z T, Wang Z L and Wang J. 2024. Boosting the charge density of triboelectric nanogenerator by suppressing air breakdown and dielectric charge leakage. *Adv. Energy Mater.* **14**, 2303874.
[98] Kim M, Choi C, Lee J P, Kim J and Cha C. 2022. Multiscale engineering of nanofiber-aerogel composite nanogenerator with tunable triboelectric performance based on multifunctional polysuccinimide. *Small* **18**, 2107316.
[99] Che Z Y, O'Donovan S, Xiao X, Wan X, Chen G R, Zhao X, Zhou Y H, Yin J Y and Chen J. 2023. Implantable triboelectric nanogenerators for self-powered cardiovascular healthcare. *Small* **19**, 2207600.
[100] Tan X Q, Wang S T, You Z Y, Zheng J M and Liu Y. 2023. High performance porous triboelectric nanogenerator based on silk fibroin@MXene composite aerogel and PDMS sponge. *ACS Mater. Lett.* **5**, 1929–1937.
[101] Li C, Luo R Z, Bai Y, Shao J J, Ji J Y, Wang E G, Li Z, Meng H Y and Li Z. 2024. Molecular doped biodegradable triboelectric nanogenerator with optimal output performance. *Adv. Funct. Mater.* **34**, 2400277.
[102] Liao J Q, Shamshina J L, Wang Y Y, Sun D, Shen X P, Zhao D W and Sun Q F. 2024. Emerging cellulosic materials for sustainable mechanosensing and energy harvesting devices: advances and prospect. *Nano Today* **56**, 102232.
[103] Sheng F F, Zhang B, Zhang Y H, Li Y Y, Cheng R W, Wei C H, Ning C, Dong K and Wang Z L. 2022. Ultrastretchable organogel/silicone fiber-helical sensors for self-powered implantable ligament strain monitoring. *ACS Nano* **16**, 10958–10967.
[104] Liu S J, Liang X, Chen P F, Long H R, Jiang T and Wang Z L. 2023. Multilayered helical spherical triboelectric nanogenerator with charge shuttling for water wave energy harvesting. *Small Methods* **7**, 2201392.
[105] Zhang X H, Xu J W, Zhang X M, Chao G J, Cao Q X, Liu T X and Liu Y. 2023. Simultaneous evaporation and foaming for batch coaxial extrusion of liquid metal/polydimethylsiloxane porous fibrous TENG. *Adv. Fiber Mater.* **5**, 1949–1962.
[106] Miao Y, Zhou M J, Yi J, Wang Y Y, Tian G J, Zhang H X, Huang W L, Wang W H, Wu R H and Ma L Y. 2024. Woven fabric triboelectric nanogenerators for human-computer interaction and physical health monitoring. *Nano Res.* **17**, 5540–5548.
[107] Yu X K, Fu S K, Zuo X L, Zeng J, Shan C C, He W C, Li W P and Hu C G. 2022. Moisture resistant and stable wireless wind speed sensing system based on triboelectric nanogenerator with charge-excitation strategy. *Adv. Funct. Mater.* **32**, 2207498.
[108] Wen H Y, Yang X Y, Huang R Y, Zheng D, Yuan J B, Hong H X, Duan J L, Zi Y L and Tang Q W. 2023. Universal energy solution for triboelectric sensors toward the 5G era and Internet of Things. *Adv. Sci.* **10**, 2302009.
[109] Xin C F, Xu Z F, Xie X, Guo H Y, Peng Y, Li Z J, Liu L L and Xie S R. 2023. Structure-crack detection and digital twin demonstration based on triboelectric nanogenerator for intelligent maintenance. *Adv. Sci.* **10**, 2302443.
[110] Tayyab M, Wang J, Wang J M, Maksutoglu M, Yu H D, Sun G Z, Yildiz F, Eginligil M and Huang W. 2020. Enhanced output in polyvinylidene fluoride nanofibers based triboelectric nanogenerator by using printer ink as nano-fillers. *Nano Energy* **77**, 105178.
[111] Pu X, Zha J-W, Zhao C-L, Gong S-B, Gao J-F and Li R K Y. 2020. Flexible PVDF/nylon-11 electrospun fibrous membranes with aligned ZnO nanowires as potential triboelectric nanogenerators. *Chem. Eng. J.* **398**, 125526.
[112] Li W J, Lu L Q, Yan F, Palasantzas G, Loos K and Pei Y T. 2023. High-performance triboelectric nanogenerators based on TPU/mica nanofiber with enhanced tribopositivity. *Nano Energy* **114**, 108629.
[113] Ye G M, Wan Y F, Wu J M, Zhuang W B, Zhou Z Q, Jin T S, Zi J Y, Zhang D D, Geng X M and Yang P. 2022. Multifunctional device integrating dual-temperature regulator for outdoor personal thermal comfort and triboelectric nanogenerator for self-powered human-machine interaction. *Nano Energy* **97**, 107148.
[114] Wu S X, Kan H, Gao J Q, Yue W J, Zhang C W, Gao S and Li Y. 2024. Convolutional neural networks-motivated high-performance multi-functional electronic skin for intelligent human-computer interaction. *Nano Energy* **122**, 109313.
[115] Gajula P, Yoon J U, Woo I, Oh S-J and Bae J W. 2024. Triboelectric touch sensor array system for energy generation and self-powered human-machine interfaces based on chemically functionalized, electrospun rGO/Nylon-12 and micro-patterned Ecoflex/MoS_2 films. *Nano Energy* **121**, 109278.
[116] Wang S, Tian M H, Hu S Y, Zhai W, Zheng G Q, Liu C T, Shen C Y and Dai K. 2022. Hierarchical nanofibrous mat via water-assisted electrospinning for self-powered ultrasensitive vibration sensors. *Nano Energy* **97**, 107149.
[117] Fan C H, Long Z W, Zhang Y X, Mensah A, He H F, Wei Q F and Lv P F. 2023. Robust integration of energy harvesting with daytime radiative cooling enables wearing thermal comfort self-powered electronic devices. *Nano Energy* **116**, 108842.
[118] Chang K-B et al. 2023. A triboelectric nanogenerator-based tactile sensor array system for monitoring pressure distribution inside prosthetic limb. *Nano Energy* **111**, 108397.
[119] Sohn S-H, Choi G-J and Park I-K. 2023. Metal-organic frameworks-induced Self-Poling effect of polyvinylidene fluoride nanofibers for performance enhancement of triboelectric nanogenerator. *Chem. Eng. J.* **475**, 145860.
[120] Graham S A, Patnam H, Manchi P, Paranjape M V, Kurakula A and Yu J S. 2022. Biocompatible electrospun fibers-based triboelectric nanogenerators for energy harvesting and healthcare monitoring. *Nano Energy* **100**, 107455.
[121] Bhatta T, Sharma S, Shrestha K, Shin Y, Seonu S, Lee S, Kim D, Sharifuzzaman M, Rana S S and Park J Y. 2022. Siloxene/PVDF composite nanofibrous membrane

for high-performance triboelectric nanogenerator and self-powered static and dynamic pressure sensing applications. *Adv. Funct. Mater.* **32**, 2202145.
[122] Huang T, Lu M X, Yu H, Zhang Q H, Wang H Z and Zhu M F. 2015. Enhanced power output of a triboelectric nanogenerator composed of electrospun nanofiber mats doped with graphene oxide. *Sci. Rep.* **5**, 13942.
[123] Chen X X, Song Y, Chen H T, Zhang J X and Zhang H X. 2017. An ultrathin stretchable triboelectric nanogenerator with coplanar electrode for energy harvesting and gesture sensing. *J. Mater. Chem. A* **5**, 12361–12368.
[124] Ye Q K et al. 2019. Effects of liquid metal particles on performance of triboelectric nanogenerator with electrospun polyacrylonitrile fiber films. *Nano Energy* **61**, 381–388.
[125] Li Y, Xiong J Q, Lv J, Chen J, Gao D C, Zhang X X and Lee P S. 2020. Mechanically interlocked stretchable nanofibers for multifunctional wearable triboelectric nanogenerator. *Nano Energy* **78**, 105358.
[126] Guan X Y, Xu B G, Wu M J, Jing T T, Yang Y J and Gao Y Y. 2021. Breathable, washable and wearable woven-structured triboelectric nanogenerators utilizing electrospun nanofibers for biomechanical energy harvesting and self-powered sensing. *Nano Energy* **80**, 105549.
[127] Kim Y, Wu X W, Lee C and Oh J H. 2021. Characterization of PI/PVDF-TrFE composite nanofiber-based triboelectric nanogenerators depending on the type of the electrospinning system. *ACS Appl. Mater. Interfaces* **13**, 36967–36975.
[128] Song W-Z, Zhang T-T, Zhang D-S, Li C-L, Sun D-J, Zhang J, Ramakrishna S and Long Y-Z. 2023. Highly stretchable conductors reveal the effect of dielectric layer thickness on triboelectric nanogenerator output. *Nano Energy* **114**, 108621.
[129] Akram W, Chen Q, Zhang X L, Ren S, Niu L and Fang J. 2024. Coaxial tribonegative yarn TENG with aromatic polyimide as charge entrapment layer for real-time edge ball assessment in cricket sports. *Nano Energy* **131**, 110275.
[130] Fan F-R, Tian Z-Q and Wang Z L. 2012. Flexible triboelectric generator. *Nano Energy* **1**, 328–334.
[131] Zhao H F, Wang H, Yu H Y, Xu Q H, Li X S, Guo J, Shao J J, Wang Z L, Xu M Y and Ding W B. 2024. Theoretical modeling of contact-separation mode triboelectric nanogenerators from initial charge distribution. *Energy Environ. Sci.* **17**, 2228–2247.
[132] Shen F, Zhang Q, Guo H Y, Cao C, Gong Y, Wang J L, Peng Y and Li Z J. 2024. Investigation of power density amplification in stacked triboelectric nanogenerators. *Energy Environ. Mater.* **7**, e12697.
[133] Hu C F, Wang F, Cui X H and Zhu Y T. 2023. Recent progress in textile-based triboelectric force sensors for wearable electronics. *Adv. Compos. Hybrid Mater.* **6**, 70.
[134] Liu H, Li Y X, Sun Q B, Yang J Q, Zhao Y, Cui X Y and Tian Y. 2024. Triboelectric wearable devices for accelerated wound healing. *Chem. Eng. J.* **497**, 154628.
[135] Liu J Q, Zhou L L, Gao Y K, Yang P Y, Liu D, Qiao W Y, Zhang B F, Zhao Z H, Wang Z L and Wang J. 2023. Achieving ultra-high voltage (≈10 kV) triboelectric nanogenerators. *Adv. Energy Mater.* **13**, 2300410.
[136] Meng J, Zhang L Q, Liu H M, Sun W X, Wang W Q, Wang H C, Yang D, Feng M, Feng Y G and Wang D A. 2024. A new single-electrode generator for water droplet energy harvesting with a 3 mA current output. *Adv. Energy Mater.* **14**, 2303298.
[137] Bu T Z, Deng W L, Liu Y Y, Wang Z L, Chen X C and Zhang C. 2024. Submillimeter-scale superlubric triboelectric nanogenerator. *Adv. Funct. Mater.* **34**, 2404007.
[138] Liu M J et al. 2024. Earthworm-inspired ultra-durable sliding triboelectric nanogenerator with bionic self-replenishing lubricating property for wind energy harvesting and self-powered intelligent sports monitoring. *Adv. Sci.* **11**, 2401636.
[139] Li S X, Zhao Z H, Liu D, An J, Gao Y K, Zhou L L, Li Y H, Cui S N, Wang J and Wang Z L. 2022. A self-powered dual-type signal vector sensor for smart robotics and automatic vehicles. *Adv. Mater.* **34**, 2110363.
[140] Li G et al. 2024. Ultra-stability and high output performance of a sliding mode triboelectric nanogenerator achieved by an asymmetric electrode structure design. *Energy Environ. Sci.* **17**, 2651–2661.
[141] Yu X K, Zhang S Q, Fu S K, Tan B C, Zhou D, Zeng J, Wang Z P, Li W P and Hu C G. 2024. An adaptable charge source enabled by mode-switchable TENG for efficient self-repairing coating. *Adv. Funct. Mater.* **34**, 2316140.
[142] Zhao D, Yu X, Wang J L, Gao Q, Wang Z J, Cheng T H and Wang Z L. 2022. A standard for normalizing the outputs of triboelectric nanogenerators in various modes. *Energy Environ. Sci.* **15**, 3901–3911.
[143] Hou Y, Dong X L, Li D, Shi D Z, Tang W and Wang Z L. 2023. Self-powered underwater force sensor based on a T-shaped triboelectric nanogenerator for simultaneous detection of normal and tangential forces. *Adv. Funct. Mater.* **33**, 2305719.
[144] Li S, Qian J G, Liu J M, Xue Y H, Zhang J J, Liu Y S, Hu X F, Jing X J and Zhang W. 2023. Machine learning-assisted wearable triboelectric-electromagnetic vibration sensor for monitoring human rehabilitation training. *Mech. Syst. Signal Process.* **201**, 110679.
[145] Niu S M, Wang S H, Lin L, Liu Y, Zhou Y S, Hu Y F and Wang Z L. 2013. Theoretical study of contact-mode triboelectric nanogenerators as an effective power source. *Energy Environ. Sci.* **6**, 3576–3583.
[146] Wang Z L and Wang A C. 2019. On the origin of contact-electrification. *Mater. Today* **30**, 34–51.
[147] Wang Z L, Chen J and Lin L. 2015. Progress in triboelectric nanogenerators as a new energy technology and self-powered sensors. *Energy Environ. Sci.* **8**, 2250–2282.
[148] Zhang H L, Yang Y, Zhong X D, Su Y J, Zhou Y S, Hu C G and Wang Z L. 2014. Single-electrode-based rotating triboelectric nanogenerator for harvesting energy from tires. *ACS Nano* **8**, 680–689.
[149] Niu S M, Liu Y, Chen X Y, Wang S H, Zhou Y S, Lin L, Xie Y N and Wang Z L. 2015. Theory of freestanding triboelectric-layer-based nanogenerators. *Nano Energy* **12**, 760–774.
[150] Wang Z L. 2017. On Maxwell's displacement current for energy and sensors: the origin of nanogenerators. *Mater. Today* **20**, 74–82.
[151] Wang X F, Niu S M, Yin Y J, Yi F, You Z and Wang Z L. 2015. Triboelectric nanogenerator based on fully enclosed rolling spherical structure for harvesting low-frequency water wave energy. *Adv. Energy Mater.* **5**, 1501467.
[152] Zhou Y S, Li S M, Niu S M and Wang Z L. 2016. Effect of contact- and sliding-mode electrification on nanoscale charge transfer for energy harvesting. *Nano Res.* **9**, 3705–3713.
[153] Niu S M and Wang Z L. 2015. Theoretical systems of triboelectric nanogenerators. *Nano Energy* **14**, 161–192.
[154] Niu S M, Liu Y, Wang S H, Lin L, Zhou Y S, Hu Y F and Wang Z L. 2013. Theory of sliding-mode triboelectric nanogenerators. *Adv. Mater.* **25**, 6184–6193.
[155] Niu S M, Liu Y, Wang S H, Lin L, Zhou Y S, Hu Y F and Wang Z L. 2014. Theoretical investigation and structural optimization of single-electrode triboelectric nanogenerators. *Adv. Funct. Mater.* **24**, 3332–3340.
[156] Zhang C, Tang W, Han C B, Fan F R and Wang Z L. 2014. Theoretical comparison, equivalent transformation, and conjunction operations of electromagnetic induction

generator and triboelectric nanogenerator for harvesting mechanical energy. *Adv. Mater.* **26**, 3580–3591.
[157] Shao J J, Willatzen M, Shi Y J and Wang Z L. 2019. 3D mathematical model of contact-separation and single-electrode mode triboelectric nanogenerators. *Nano Energy* **60**, 630–640.
[158] Zhao D, Yu X, Wang Z J, Wang J L, Li X, Wang Z L and Cheng T H. 2021. Universal equivalent circuit model and verification of current source for triboelectric nanogenerator. *Nano Energy* **89**, 106335.
[159] Li D et al. 2021. Scalable and hierarchically designed polymer film as a selective thermal emitter for high-performance all-day radiative cooling. *Nat. Nanotechnol.* **16**, 153–158.
[160] Liao M et al. 2022. Industrial scale production of fibre batteries by a solution-extrusion method. *Nat. Nanotechnol.* **17**, 372–377.
[161] Tang W, Jiang T, Fan F R, Yu A F, Zhang C, Cao X and Wang Z L. 2015. Liquid-metal electrode for high-performance triboelectric nanogenerator at an instantaneous energy conversion efficiency of 70.6%. *Adv. Funct. Mater.* **25**, 3718–3725.
[162] Du Z R, Chen K, Zhang Y X, Wang Y F, He P, Mi H-Y, Wang Y M, Liu C T and Shen C Y. 2021. Engineering multilayered MXene/electrospun poly(lactic acid) membrane with increscent electromagnetic interference (EMI) shielding for integrated Joule heating and energy generating. *Compos. Commun.* **26**, 100770.
[163] Hao R F, Yang S, Yang K, Zhang Z Y, Wang T, Sang S B and Zhang H L. 2021. Self-powered air filter based on an electrospun respiratory triboelectric nanogenerator. *ACS Appl. Energy Mater.* **4**, 14700–14708.
[164] Huang J Y, Hao Y, Zhao M, Li W, Huang F L and Wei Q F. 2021. All-fiber-structured triboelectric nanogenerator via one-pot electrospinning for self-powered wearable sensors. *ACS Appl. Mater. Interfaces* **13**, 24774–24784.
[165] Jiang Y, Dong K, An J, Liang F, Yi J, Peng X, Ning C, Ye C Y and Wang Z L. 2021. UV-protective, self-cleaning, and antibacterial nanofiber-based triboelectric nanogenerators for self-powered human motion monitoring. *ACS Appl. Mater. Interfaces* **13**, 11205–11214.
[166] Rana S M S, Rahman M T, Salauddin M, Sharma S, Maharjan P, Bhatta T, Cho H, Park C and Park J Y. 2021. Electrospun PVDF-TrFE/MXene nanofiber mat-based triboelectric nanogenerator for smart home appliances. *ACS Appl. Mater. Interfaces* **13**, 4955–4967.
[167] Xie Y R, Ma Q L, Qi H N, Liu X N, Chen X Y, Jin Y, Li D, Yu W S and Dong X T. 2021. A fluorescent triboelectric nanogenerator manufactured with a flexible janus nanobelt array concurrently acting as a charge-generating layer and charge-trapping layer. *Nanoscale* **13**, 19144–19154.
[168] Lin M-F, Chang K-W, Lee C-H, Wu X-X and Huang Y-C. 2022. Electrospun P3HT/PVDF-HFP semiconductive nanofibers for triboelectric nanogenerators. *Sci. Rep.* **12**, 14842.
[169] Xia J Y, Zheng Z P and Guo Y P. 2022. Mechanically and electrically robust, electro-spun PVDF/PMMA blend films for durable triboelectric nanogenerators. *Composites A* **157**, 106914.
[170] Joseph S, Padmanabhan N T, Jose J and John H. 2023. Antibacterial self-cleaning nylon-11/TiO_2nanofiber membranes as triboelectric nanogenerators. *Results Eng.* **17**, 100869.
[171] Bu J Y, Chen L H and Song J H. 2024. In situ nanofibers patterned deposition based on electrostatic attraction-repulsion induction. *Chem. Eng. J.* **480**, 147997.
[172] Robinson A J, Pérez-Nava A, Ali S C, Betzabe González-Campos J, Holloway J L and Cosgriff-Hernandez E M. 2021. Comparative analysis of fiber alignment methods in electrospinning. *Matter* **4**, 821–844.
[173] Liu Y Q, Zhang X P, Xia Y N and Yang H. 2010. Magnetic-field-assisted electrospinning of aligned straight and wavy polymeric nanofibers. *Adv. Mater.* **22**, 2454–2457.
[174] Li H Y, Qu R X, Ma Z J, Zhou N J, Huang Q Y and Zheng Z J. 2024. Permeable and patternable super-stretchable liquid metal fiber for constructing high-integration-density multifunctional electronic fibers. *Adv. Funct. Mater.* **34**, 2308120.
[175] Chen G Y et al. 2021. Integrated dynamic wet spinning of core-sheath hydrogel fibers for optical-to-brain/tissue communications. *Natl Sci. Rev.* **8**, nwaa209.
[176] Martinez A P, Decker L K, Wang K Y, Kim J B, Murray C B and Yang S. 2024. High-speed and scalable wet spinning of graphene/liquid crystalline elastomer composite filaments. *Adv. Funct. Mater.* **35**, 2422176.
[177] Ye L, Liu L-X, Yin G, Liu Y F, Deng Z M, Qi C-Z, Zhang H-B and Yu Z-Z. 2023. Highly conductive, hydrophobic, and acid/alkali-resistant MXene@PVDF hollow core-shell fibers for efficient electromagnetic interference shielding and Joule heating. *Mater. Today Phys.* **35**, 101100.
[178] Li H R, Qin J Y, Zhao K Y, Guo Y F, Tong B J, Samadiy M, Alimov U and Deng T L. 2024. Novel lithium ion-sieve spinning fiber composite of PVDF-HMO for lithium recovery from geothermal water. *J. Clean. Prod.* **434**, 139997.
[179] Liu C, Li X R, Duan Q M, Yu X P, Guo Y F and Deng T L. 2025. Insight into strontium recovery from oilfield water by porous fiber-supported ammoniated titanium phosphate: adsorption performance and mechanisms. *Chem. Eng. J.* **503**, 158586.
[180] Nisa Q A K, Nasrun R F B and Kim J H. 2025. Rational design and visualization of multifunctional phenothiazine-based self-assembled monolayers for better interface contact in high-efficiency and stable perovskite solar cells. *Small Methods* **9**, 2402104.
[181] Ostertag B and Ross A E. 2023. Wet-spun porous carbon microfibers for enhanced electrochemical detection. *ACS Appl. Mater. Interfaces* **15**, 17601–17611.
[182] Zhang Z H, Kong Y Y, Gao J Q, Han X, Lian Z C, Liu J M, Wang W-J and Yang X. 2024. Engineering strong man-made cellulosic fibers: a review of the wet spinning process based on cellulose nanofibrils. *Nanoscale* **16**, 6383–6401.
[183] Chernikova E V, Osipova N I, Plutalova A V, Toms R V, Gervald A Y, Prokopov N I and Kulichikhin V G. 2022. Melt-spinnable polyacrylonitrile-an alternative carbon fiber precursor. *Polymers* **14**, 5222.
[184] Yang T T, Ma C, Lin C Y, Wang J T, Qiao W M, Ling L C, Yu Z J and Zhang Y X. 2024. Innovative fabrication of ultrasensitive and durable graphene fiber aerogel for flexible pressure sensors. *Carbon* **229**, 119484.
[185] Zapf V S, Lee M and Rosa P F S. 2023. Melted spin ice. *Nat. Phys.* **19**, 17–18.
[186] Tan H, Sun L J, Huang H F, Zhang L Z, Neisiany R E, Ma X P and You Z W. 2024. Continuous melt spinning of adaptable covalently cross-linked self-healing ionogel fibers for multi-functional ionotronics. *Adv. Mater.* **36**, 2310020.
[187] Wang S H, Bian X F and Jia Y B. 2003. Formation of superthick Al-based amorphous ribbon. *Chin. Sci. Bull.* **48**, 2145–2147.
[188] Zhang B P, Xu W H, Peng L, Li Y C, Zhang W and Wang Z K. 2024. Nature-inspired interfacial engineering for energy harvesting. *Nat. Rev. Electr. Eng.* **1**, 218–233.
[189] Brownlee C. 2024. In nano: highlights of recent ACS nano articles. *ACS Nano* **18**, 4613–4616.
[190] Lozano Montero K, Calvo Guzman R, Tewari A, Zou H Y, Wang Z L, Mäntysalo M and Laurila -M-M. 2024. Printed and stretchable triboelectric energy harvester based

on P(VDF-TrFE) porous aerogel. *Adv. Funct. Mater.* **34**, 2312881.
[191] He E F, Sun Y, Wang X W, Chen H J, Sun B Z, Gu B H and Zhang W. 2020. 3D angle-interlock woven structural wearable triboelectric nanogenerator fabricated with silicone rubber coated graphene oxide/cotton composite yarn. *Composites B* **200**, 108244.
[192] Chen H M et al. 2022. Performance-enhanced and cost-effective triboelectric nanogenerator based on stretchable electrode for wearable SpO2 monitoring. *Nano Res.* **15**, 2465–2471.
[193] Ippili S, Jella V, Lee J M, Jung J-S, Lee D-H, Yang T-Y and Yoon S-G. 2022. ZnO-PTFE-based antimicrobial, anti-reflective display coatings and high-sensitivity touch sensors. *J. Mater. Chem. A* **10**, 22067–22079.
[194] Paranjape M V, Lee J K, Manchi P, Graham S A, Kurakula A, Kavarthapu V S and Yu J S. 2024. Phosphor-loaded triboelectric film-based multipurpose triboelectric nanogenerators for highly-efficient energy harvesting, sensing, and self-illumination applications. *Adv. Funct. Mater.* **34**, 2405838.
[195] Liu P L, Sun N, Mi Y Y, Luo X H, Dong X X, Cai J Y, Jia X L, Ramos M A, Hu T S and Xu Q. 2021. Ultra-low CNTs filled high-performance fast self-healing triboelectric nanogenerators for wearable electronics. *Compos. Sci. Technol.* **208**, 108733.
[196] Yang H Q, He J B, Yan J J, Li H, Bai Y L, Wang Q G, Yan H and Yin S G. 2023. Highly sensitive self-powered humidity sensor based on a TaS_2/Cu_2S heterostructure driven by a triboelectric nanogenerator. *ACS Appl. Mater. Interfaces* **15**, 33077–33086.
[197] Kim Y, Wu X W and Oh J H. 2020. Fabrication of triboelectric nanogenerators based on electrospun polyimide nanofibers membrane. *Sci. Rep.* **10**, 2742.
[198] Babu A, Aazem I, Walden R, Bairagi S, Mulvihill D M and Pillai S C. 2023. Electrospun nanofiber based TENGs for wearable electronics and self-powered sensing. *Chem. Eng. J.* **452**, 139060.
[199] Ding Z D, Tian Z J, Ji X X, Wang D X, Ci X, Shao X J and Rojas O J. 2023. Cellulose-based superhydrophobic wrinkled paper and electrospinning film as green tribolayer for water wave energy harvesting. *Int. J. Biol. Macromol.* **234**, 122903.
[200] Han J, Li J Y, Zhang X, Zhao L W and Wang C C. 2024. Enhancing the performance of triboelectric nanogenerator via chitosan films surface modification. *Chem. Eng. J.* **489**, 151493.
[201] Ra Y et al. 2024. Direct electrospinning of reconstructable PVDF-TrFE nanofibrous mat onto conductive cement nanocomposite for triboelectricity-assisted net zero energy structure. *Chem. Eng. J.* **485**, 149662.
[202] Zheng S J, Wang X W, Li W Z, Liu Z Y, Li Q N and Yan F. 2024. Pressure-stamped stretchable electronics using a nanofibre membrane containing semi-embedded liquid metal particles. *Nat. Electron.* **7**, 576–585.
[203] Zhong J W, Zhang Y, Zhong Q Z, Hu Q Y, Hu B, Wang Z L and Zhou J. 2014. Fiber-based generator for wearable electronics and mobile medication. *ACS Nano* **8**, 6273–6280.
[204] Zhou M J, Xu F, Ma L Y, Luo Q L, Ma W W, Wang R W, Lan C T, Pu X and Qin X H. 2022. Continuously fabricated nano/micro aligned fiber based waterproof and breathable fabric triboelectric nanogenerators for self-powered sensing systems. *Nano Energy* **104**, 107885.
[205] Gu J, Lee D, Oh J, Si H and Kim K. 2024. Synergy of polydopamine-assisted additive modification and hierarchical-morphology poly(vinylidene fluoride) nanofiber mat for ferroelectric-assisted triboelectric nanogenerator. *Adv. Fiber Mater.* **6**, 1910–1926.
[206] Chau N M, Tran P M, Le T H, La T T H and Bui V-T. 2023. Ultra-stretchable and shape-memorable ability of an output-boosted triboelectric nanogenerator utilizing highly ordered microdome-crowning thermoplastic polyurethane for a finger-motion detection sensor. *Mater. Adv.* **4**, 6568–6577.
[207] Song J M, Latif M, Jiang Y X Z, Ounaies Z and Kim J. 2024. High-performance flexible triboelectric nanogenerator based on micropatterned allicin-grafted cellulose film. *Mater. Today Nano* **26**, 100475.
[208] Varghese H, Hakkeem H M A, Farman M, Thouti E, Pillai S and Chandran A. 2022. Self-powered flexible triboelectric touch sensor based on micro-pyramidal PDMS films and cellulose acetate nanofibers. *Results Eng.* **16**, 100550.
[209] Wang J Y, Pan L, Guo H Y, Zhang B B, Zhang R R, Wu Z Y, Wu C S, Yang L J, Liao R J and Wang Z L. 2019. Rational structure optimized hybrid nanogenerator for highly efficient water wave energy harvesting. *Adv. Energy Mater.* **9**, 1802892.
[210] Tan D J, Zeng Q X, Wang X, Yuan S L, Luo Y L, Zhang X F, Tan L M, Hu C G and Liu G L. 2022. Anti-overturning fully symmetrical triboelectric nanogenerator based on an elliptic cylindrical structure for all-weather blue energy harvesting. *Nano-Micro Lett.* **14**, 124.
[211] Cui N Y, Dai C H, Liu J M, Gu L, Ge R, Du T, Wang Z and Qin Y. 2020. Increasing the output charge quantity of triboelectric nanogenerators *via* frequency multiplication with a multigap-structured friction layer. *Energy Environ. Sci.* **13**, 2069–2076.
[212] Tang Q, Wang Z, Chang W X, Sun J F, He W C, Zeng Q X, Guo H Y and Hu C G. 2022. Interface static friction enabled ultra-durable and high output sliding mode triboelectric nanogenerator. *Adv. Funct. Mater.* **32**, 2202055.
[213] Pandey P, Thapa K, Ojha G P, Seo M-K, Shin K H, Kim S-W and Sohn J I. 2023. Metal-organic frameworks-based triboelectric nanogenerator powered visible light communication system for wireless human-machine interactions. *Chem. Eng. J.* **452**, 139209.
[214] Zhang J-H, Li Y, Du J H, Hao X H and Huang H T. 2019. A high-power wearable triboelectric nanogenerator prepared from self-assembled electrospun poly(vinylidene fluoride) fibers with a heart-like structure. *J. Mater. Chem. A* **7**, 11724–11733.
[215] Funnell J L, Ziemba A M, Nowak J F, Awada H, Prokopiou N, Samuel J, Guari Y, Nottelet B and Gilbert R J. 2021. Assessing the combination of magnetic field stimulation, iron oxide nanoparticles, and aligned electrospun fibers for promoting neurite outgrowth from dorsal root ganglia in vitro. *Acta Biomater.* **131**, 302–313.
[216] Huang C X, Dong J, Zhang Y Y, Chai S L, Wang X C, Kang S X, Yu D G, Wang P and Jiang Q. 2021. Gold nanoparticles-loaded polyvinylpyrrolidone/ethylcellulose coaxial electrospun nanofibers with enhanced osteogenic capability for bone tissue regeneration. *Mater. Des.* **212**, 110240.
[217] Liu H L, Lai W Q, Shi Y, Tian L, Li K, Bian L P, Xi Z G and Lin B C. 2024. Ag-decorated electrospun polymer/GO fibrous membranes for simultaneous bacterial filtration and termination. *J. Membr. Sci.* **695**, 122498.
[218] Jiang J, Ni N, Xiao W W, Zhao X F, Guo F W, Fan X H, Ding Q, Hao W and Xiao P. 2021. Robust ceramic nanofibrous membranes with ultra-high water flux and nanoparticle rejection for self-standing ultrafiltration. *J. Eur. Ceram. Soc.* **41**, 4264–4272.
[219] Bhatta T, Maharjan P, Cho H, Park C, Yoon S H, Sharma S, Salauddin M, Rahman M T, Rana S S and Park J Y. 2021. High-performance triboelectric nanogenerator based on MXene functionalized polyvinylidene fluoride composite nanofibers. *Nano Energy* **81**, 105670.

[220] Min G B, Pullanchiyodan A, Dahiya A S, Hosseini E S, Xu Y, Mulvihill D M and Dahiya R. 2021. Ferroelectric-assisted high-performance triboelectric nanogenerators based on electrospun P(VDF-TrFE) composite nanofibers with barium titanate nanofillers. *Nano Energy* **90**, 106600.
[221] Zhang X, Lv S S, Lu X C, Yu H, Huang T, Zhang Q H and Zhu M F. 2020. Synergistic enhancement of coaxial nanofiber-based triboelectric nanogenerator through dielectric and dispersity modulation. *Nano Energy* **75**, 104894.
[222] Ma L Y et al. 2020. Continuous and scalable manufacture of hybridized nano-micro triboelectric yarns for energy harvesting and signal sensing. *ACS Nano* **14**, 4716–4726.
[223] Hu G B, Zhao C Y, Yang Y W, Li X and Liang J R. 2022. Triboelectric energy harvesting using an origami-inspired structure. *Appl. Energy* **306**, 118037.
[224] Jia Y J, Guan Q B, Chu C Z, Zhang L Z, Neisiany R E, Gu S J, Sun J F and You Z W. 2024. A fluorine-based strong and healable elastomer with unprecedented puncture resistance for high performance flexible electronics. *Sci. Bull.* **69**, 1875–1886.
[225] Rajabi-Abhari A, Lee J, Tabassian R, Kim J-N, Lee H and Oh I-K. 2022. Antagonistically functionalized diatom biosilica for bio-triboelectric generators. *Small* **18**, 2107638.
[226] Wang J, Xia Z Y, Yao H, Zhang Q L and Yang H. 2023. Self-powered TENG with high humidity sensitivity from PVA film modified by LiCl and MXene. *ACS Appl. Mater. Interfaces* **15**, 47208–47220.
[227] Tian J W, Wang F, Ding Y F, Lei R, Shi Y X, Tao X L, Li S Y, Yang Y and Chen X Y. 2021. Self-powered room-temperature ethanol sensor based on brush-shaped triboelectric nanogenerator. *Research* **2021**, 8564780.
[228] Shi L et al. 2021. High-performance triboelectric nanogenerator based on electrospun PVDF-graphene nanosheet composite nanofibers for energy harvesting. *Nano Energy* **80**, 105599.
[229] Sardana S, Sharma V, Beepat K G, Sharma D P, Chawla A K and Mahajan A. 2023. Flexible, humidity- and contamination-resistant superhydrophobic MXene-based electrospun triboelectric nanogenerators for distributed energy harvesting applications. *Nanoscale* **15**, 19369–19380.
[230] Sha Z, Boyer C, Li G, Yu Y Y, Allioux F-M, Kalantar-Zadeh K, Wang C-H and Zhang J. 2022. Electrospun liquid metal/PVDF-HFP nanofiber membranes with exceptional triboelectric performance. *Nano Energy* **92**, 106713.
[231] Kim M, Lim H and Ko S H. 2023. Liquid metal patterning and unique properties for next-generation soft electronics. *Adv. Sci.* **10**, 2205795.
[232] Cao C Y, Hou C S, Wang X, Lv D, Ai L Q, Feng Y X, Chen P R, Wang X J, He M L and Yao X. 2024. Liquid metal-enhanced highly adhesive electrodes for multifunctional epidermal bioelectronics. *Adv. Funct. Mater.* **34**, 2403671.
[233] Zhou N J, Ji J J, Qu R X, Feng X, Song X K, Chen M J, Chen F G, Ma Z J and Wei Y. 2025. Permeable and durable liquid-metal fiber mat as implantable physiological electrodes with long-term biocompatibility. *Adv. Mater.* **37**, e2413728.
[234] Li X K, Li M J, Xu J, You J, Yang Z Q and Li C X. 2019. Evaporation-induced sintering of liquid metal droplets with biological nanofibrils for flexible conductivity and responsive actuation. *Nat. Commun.* **10**, 3514.
[235] Chen S, Cui Z L, Wang H Z, Wang X L and Liu J. 2023. Liquid metal flexible electronics: past, present, and future. *Appl. Phys. Rev.* **10**, 021308.
[236] Wang Y, Li J B, Sun L Y, Chen H X, Ye F F, Zhao Y J and Shang L R. 2023. Liquid metal droplets-based elastomers from electric toothbrush-inspired revolving microfluidics. *Adv. Mater.* **35**, 2211731.
[237] Luo W M, Wei B J, Luo T L, Li B W and Zhu G M. 2024. 3D network of liquid metal-embedded graphene via surface coating for flexible thermal management. *Small* **20**, 2406574.
[238] Kim J, Kim H-M, Cho S, Avis C and Jang J. 2018. High hall mobility P-type Cu_2SnS_3-Ga_2O_3 with a high work function. *Adv. Funct. Mater.* **28**, 1802941.
[239] Xu D et al. 2023. Intrinsically conductive and nano-scale reconfigurable liquid metal nano-capsules. *Mater. Today Phys.* **38**, 101239.
[240] Babu A, Malik P, Das N and Mandal D. 2022. Surface potential tuned single active material comprised triboelectric nanogenerator for a high performance voice recognition sensor. *Small* **18**, 2201331.
[241] Ippili S, Jella V, Thomas A M, Yoon C, Jung J-S and Yoon S-G. 2021. ZnAl-LDH-induced electroactive β-phase and controlled dielectrics of PVDF for a high-performance triboelectric nanogenerator for humidity and pressure sensing applications. *J. Mater. Chem. A* **9**, 15993–16005.
[242] Patnam H, Dudem B, Graham S A and Yu J S. 2021. High-performance and robust triboelectric nanogenerators based on optimal microstructured poly(vinyl alcohol) and poly(vinylidene fluoride) polymers for self-powered electronic applications. *Energy* **223**, 120031.
[243] Manchi P, Graham S A, Patnam H, Paranjape M V and Yu J S. 2022. High-efficiency poly(vinylidene fluoride-co-hexafluoropropylene) loaded 3D marigold flower-like bismuth tungstate triboelectric films for mechanical energy harvesting and sensing applications. *Small* **18**, 2200822.
[244] Sim D-J, Choi G-J, Sohn S-H and Park I-K. 2022. Electronegative polyvinylidene fluoride/C_{60} composite nanofibers for performance enhancement of triboelectric nanogenerators. *J. Alloys Compd.* **898**, 162805.
[245] Babu A, Ruthvik K, Supraja P, Navaneeth M, Kumar K U, Kumar R R, Prakash K and Raju N. 2023. High-performance triboelectric nanogenerator using ZIF-67/PVDF hybrid film for energy harvesting. *J. Mater. Sci., Mater. Electron.* **34**, 2195.
[246] Guo Y C, Zhang H N, Zhong Y M, Shi S W, Wang Z Z, Wang P H and Zhao Y. 2023. Triboelectric nanogenerator-based near-field electrospinning system for optimizing PVDF fibers with high piezoelectric performance. *ACS Appl. Mater. Interfaces* **15**, 5242–5252.
[247] Mubarak A, Sarsembayev B, Serik Y, Onabek A, Kappassov Z, Bakenov Z, Tsuchiya K and Kalimuldina G. 2025. Quenched PVDF/PMMA porous matrix for triboelectric energy harvesting and sensing. *Energy Environ. Mater.* **8**, e12808.
[248] Pan J and Jin A. 2024. Improvement of output performance of the TENG based on PVDF by doping tourmaline. *ACS Sustain. Chem. Eng.* **12**, 2092–2099.
[249] Deng X S, Wu Z J, Yu X, Wang M, Zang D F, Long Y H, Guo N, Weng L, Liu Y H and Gao J G. 2025. Preparation and properties of triboelectric nanogenerator based on PVDF-TrFE/PMMA electrospun film. *Adv. Compos. Hybrid Mater.* **8**, 19.
[250] Venkatesan H M, Mohammad S R, Ponnan S, Kim K J, Gajula P, Kim H and Arun A P. 2024. Cobalt ferrite-embedded polyvinylidene fluoride electrospun nanocomposites as flexible triboelectric sensors for healthcare and polysomnographic monitoring applications. *Nano Energy* **129**, 110003.
[251] Zhi C W et al. 2024. Perovskite nanocrystals induced core-shell inorganic-organic nanofibers for efficient energy harvesting and self-powered monitoring. *ACS Nano* **18**, 9365–9377.

[252] Aliyana A K, Jalajamony H M, De S, Bairagi S, Mulvihill D M, Fernandez R E and Stylios G K. 2025. Plasma jet printed AgNP electrodes for high-performance fabric TENGs and adaptive sensing applications. *Chem. Eng. J.* **504**, 158791.

[253] Jing T T, Xu B G, Xin J H, Guan X Y and Yang Y J. 2021. Series to parallel structure of electrode fiber: an effective method to remarkably reduce inner resistance of triboelectric nanogenerator textiles. *J. Mater. Chem. A* **9**, 12331–12339.

[254] Xie Y B, Wang Z H, Ren X Y, Antwi-Afari M F, Wang Y M, Mi H-Y, Yang B, Liu C T and Shen C Y. 2023. An internal electrode strategy for enhancing the stability and durability of triboelectric nanogenerator. *Compos. Sci. Technol.* **237**, 110014.

[255] Li G et al. 2025. Transverse-asymmetric electrode structure design to eliminate charge transfer loss for enhancing output performance of sliding mode TENG. *Adv. Funct. Mater.* **35**, 2413359.

[256] Sun J, Wu M C, Jiang H R, Fan X Z and Zhao T S. 2021. Advances in the design and fabrication of high-performance flow battery electrodes for renewable energy storage. *Adv. Appl. Energy* **2**, 100016.

[257] Yadav S et al. 2021. Fabrication of high surface area ribbon electrodes for use in redox flow batteries via coaxial electrospinning. *J. Energy Storage* **33**, 102079.

[258] Han Z, Wang T D, Cai Y C, Rong S D, Ma J, Hou L and Ji Y. 2024. Electrospun porous carbon nanofiber-based electrodes for redox flow batteries: progress and opportunities. *Carbon* **222**, 118969.

[259] Ilango P R, Savariraj A D, Huang H J, Li L L, Hu G Z, Wang H S, Hou X D, Kim B C, Ramakrishna S and Peng S J. 2023. Electrospun flexible nanofibres for batteries: design and application. *Electrochem. Energy Rev.* **6**, 12.

[260] Karagiorgis X, Shakthivel D, Khandelwal G, Ginesi R, Skabara P J and Dahiya R. 2024. Highly conductive PEDOT:PSS: ag nanowire-based nanofibers for transparent flexible electronics. *ACS Appl. Mater. Interfaces* **16**, 19551–19562.

[261] Ma J X, Liu Z H, Nguyen Q-K and Zhang P. 2024. Lightweight soft conductive composites embedded with liquid metal fiber networks. *Adv. Funct. Mater.* **34**, 2308128.

[262] Wang C Y, Guo H Y, Wang P, Li J W, Sun Y H and Zhang D. 2023. An advanced strategy to enhance TENG output: reducing triboelectric charge decay. *Adv. Mater.* **35**, 2209895.

[263] Jiao Y et al. 2024. High-performance triboelectric nanogenerators based on blade-coating lead halide perovskite film and electrospinning PVDF/graphene nanofiber. *Chem. Eng. J.* **483**, 149442.

[264] Niu Z X, Wang Q X, Lu J Q, Hu Y, Huang J Q, Zhao W, Liu Y J, Long Y-Z and Han G P. 2024. Electrospun cellulose nanocrystals reinforced flexible sensing paper for triboelectric energy harvesting and dynamic self-powered tactile perception. *Small* **20**, 2307810.

[265] Zhang S G, Jiang T Y, Li M, Sun H X, Wu H, Wu W L, Li Y and Jiang H Y. 2024. Multifunctional wearable triboelectric nanogenerators prepared by combined crystallization and diffusion method: high-output, breathable, antimicrobial, and Janus-wettability for smart control and self-powered biosensing. *Nano Energy* **131**, 110214.

[266] He Y L et al. 2024. Bulk Schottky junctions-based flexible triboelectric nanogenerators to power backscatter communications in green 6G networks. *Adv. Sci.* **11**, 2305829.

[267] Yu Y T, Wu H Y, Yu Y L, Yan J W, Shi J, Morikawa H, Lyu W and Zhu C H. 2024. Acid- and alkali-resistant, UV-shielding, and photocatalytic self-cleaning nanofiber membrane-based wearable triboelectric nanogenerator for ultra-low-frequency energy-harvesting and self-powered sensors. *Chem. Eng. J.* **490**, 151546.

[268] Zhi C W, Wu H B and Hu J L. 2024. In-situ welding and thermal activation enabled robust nanofibers based triboelectric nanogenerator for sustainable energy harvesting. *Nano Energy* **127**, 109705.

[269] Shrestha K, Pradhan G B, Bhatta T, Sharma S, Lee S, Song H, Jeong S and Park J Y. 2023. Intermediate nanofibrous charge trapping layer-based wearable triboelectric self-powered sensor for human activity recognition and user identification. *Nano Energy* **108**, 108180.

[270] Xi B B, Wang L L, Yang B, Xia Y F, Chen D L and Wang X. 2023. Boosting output performance of triboelectric nanogenerator based on $BaTiO_3$:La embedded nanofiber membrane for energy harvesting and wireless power transmission. *Nano Energy* **110**, 108385.

[271] He X J et al. 2024. Ultralow-resistance and self-sterilization biodegradable nanofibrous membranes for efficient $PM_{0.3}$ removal and machine learning-assisted health management. *J. Hazard. Mater.* **480**, 135862.

[272] Shi X X, Si W J, Zhu J Y and Zhang S D. 2024. Boosting the electrical performance of PLA-based triboelectric nanogenerators for sustainable power sources and self-powered sensing. *Small* **20**, 2307620.

[273] Luo C, Shao Y, Yu H, Ma H-Z, Zhang Y-H, Gu L, Yin B and Yang M-B. 2023. Preparation and application of high performance PVDF/PS electrospinning film-based triboelectric nanogenerator. *Chem. Phys. Lett.* **813**, 140276.

[274] Wang C H, Feng L L, Xu S J, Zhao Y, Yao L R, Ge J L, Sun T and Pan G W. 2024. Fabrication of reusable bioprotective nanofabric with passive nano-Ag/ Joule thermal disinfection properties for real-time wireless fine biomotion and gesture sensing. *Nano Energy* **124**, 109525.

[275] Bai Y K, Zhou Z J, Zhu Q X, Lu S R, Li Y Q and Ionov L. 2023. Electrospun cellulose acetate nanofibrous composites for multi-responsive shape memory actuators and self-powered pressure sensors. *Carbohydrate Polym.* **313**, 120868.

[276] Tao R, Mao Y Y, Gu C D and Hu W B. 2024. Integrating all-yarn-based triboelectric nanogenerator/supercapacitor for energy harvesting, storage and sensing. *Chem. Eng. J.* **496**, 154358.

[277] Zhu X G, Chang Q R, Li H Y, Wang J D, Guo S Y and Zhang X L. 2024. Multifunctional wearable Spider-Silk Inspired fabric for personal protection in extreme environments. *Chem. Eng. J.* **491**, 152011.

[278] Huang L S, Bu X F, Zhang P, Li Y X, Zhang K, Yao Y J, Yang L Q and Yang R R. 2024. The triboelectric nanogenerator with dual functions of sensing and power generation based on electrospinning. *ACS Appl. Energy Mater.* **7**, 8767–8776.

[279] Bai Y Z, Yin L T, Hou C, Zhou Y L, Zhang F, Xu Z Y, Li K and Huang Y N. 2023. Response regulation for epidermal fabric strain sensors via mechanical strategy. *Adv. Funct. Mater.* **33**, 2214119.

[280] Kim Y W, Lee H B, Yoon J and Park S-H. 2022. 3D customized triboelectric nanogenerator with high performance achieved via charge-trapping effect and strain-mismatching friction. *Nano Energy* **95**, 107051.

[281] Joshi S R and Kim S. 2024. High power triboelectric nanogenerator based on nanofibers of silk protein and PVBVA and its motion sensing applications. *Chem. Eng. J.* **489**, 151248.

[282] Chen W C, Fan W, Wang Q, Yu X C, Luo Y, Wang W T, Lei R X and Li Y. 2022. A nano-micro structure engendered abrasion resistant, superhydrophobic, wearable triboelectric yarn for self-powered sensing. *Nano Energy* **103**, 107769.

[283] Dassanayaka D G, Alves T M, Wanasekara N D, Dharmasena I G and Ventura J. 2022. Recent progresses in wearable triboelectric nanogenerators. *Adv. Funct. Mater.* **32**, 2205438.

[284] Tan D, Xu B G, Gao Y Y, Tang Y, Liu Y F, Yang Y J and Li Z H. 2022. Breathable fabric-based triboelectric nanogenerators with open-porous architected polydimethylsiloxane coating for wearable applications. *Nano Energy* **104**, 107873.
[285] Yuan W, Zhang C G, Zhang B F, Wei X L, Yang O, Liu Y B, He L X, Cui S N, Wang J and Wang Z L. 2022. Wearable, breathable and waterproof triboelectric nanogenerators for harvesting human motion and raindrop energy. *Adv. Mater. Technol.* **7**, 2101139.
[286] Zhang H H, Zhang P, Li P F, Deng L, Zhang W K, Liu B C and Yang Z C. 2022. Enhanced performance triboelectric nanogenerator based on porous structure C/MnO_2 nanocomposite for energy harvesting. *Nano Res.* **15**, 7163–7171.
[287] Mao Y P, Wen Y Z, Liu B, Sun F X, Zhu Y S, Wang J X, Zhang R, Yu Z J, Chu L and Zhou A G. 2023. Flexible wearable intelligent sensing system for wheelchair sports monitoring. *iScience* **26**, 108126.
[288] Zhao Z Q, Mi Y J, Lu Y, Zhu Q L, Cao X and Wang N. 2023. From biochemical sensor to wearable device: the key role of the conductive polymer in the triboelectric nanogenerator. *Biosensors* **13**, 604.
[289] Liu C X, Shao T, Hao Z J, Sui Z, Ma Z Y, Wang Y C, Lei K L, Reyes A and Song L G. 2024. Hybrid human energy harvesting method of MTEG-TENG based on a flexible shared substrate. *Mater. Today Sustain.* **26**, 100692.
[290] Zhang H-Y et al. 2024. Biodegradable ferroelectric molecular crystal with large piezoelectric response. *Science* **383**, 1492–1498.
[291] Liu J, Zeng S, Zhang M, Xiong J, Gu H, Wang Z, Hu Y, Zhang X, Du Y and Ren L. 2023. Giant piezoelectric output and stability enhancement in piezopolymer composites with liquid metal nanofillers. *Adv. Sci.* **10**, 2304096.
[292] Meng Y et al. 2022. Nano-fiber based self-powered flexible vibration sensor for rail fasteners tightness safety detection. *Nano Energy* **102**, 107667.
[293] Wang D Y, Zhang D Z, Tang M C, Zhang H, Chen F J, Wang T, Li Z and Zhao P P. 2022. Rotating triboelectric-electromagnetic nanogenerator driven by tires for self-powered MXene-based flexible wearable electronics. *Chem. Eng. J.* **446**, 136914.
[294] Prasad G, Graham S A, Yu J S, Kim H and Lee D-W. 2023. Investigated a PLL surface-modified Nylon 11 electrospun as a highly tribo-positive frictional layer to enhance output performance of triboelectric nanogenerators and self-powered wearable sensors. *Nano Energy* **108**, 108178.
[295] Zhang Z X and Yuan W Z. 2023. Highly biomimetic triboelectric-generating soft actuator with a hollow bilayer structure for sensing, temperature-sensitive switching and high-temperature alarm. *Compos. Sci. Technol.* **242**, 110185.
[296] Rani G M, Ghoreishian S M, Ranjith K S, Park S H, Lee M, Umapathi R, Han Y-K and Huh Y S. 2023. High roughness induced pearl necklace-like ZIF-67@PAN fiber-based triboelectric nanogenerators for mechanical energy harvesting. *Adv. Mater. Technol.* **8**, 2300685.
[297] Lan L Y, Xiong J Q, Gao D C, Li Y, Chen J, Lv J, Ping J F, Ying Y B and Lee P S. 2021. Breathable nanogenerators for an on-plant self-powered sustainable agriculture system. *ACS Nano* **15**, 5307–5315.
[298] Jiang Y, An J, Liang F, Zuo G Y, Yi J, Ning C, Zhang H, Dong K and Wang Z L. 2022. Knitted self-powered sensing textiles for machine learning-assisted sitting posture monitoring and correction. *Nano Res.* **15**, 8389–8397.
[299] Wang Y H, Chu L, Meng S, Yang M X, Yu Y D, Deng X K, Qi C, Kong T T and Liu Z. 2024. Scalable and ultra-sensitive nanofibers coaxial yarn-woven triboelectric nanogenerator textile sensors for real-time gait analysis. *Adv. Sci.* **11**, 2401436.
[300] Tang Q W, Ke Q, Chen Q, Zhang X Y, Su J Y, Ning C Y and Fang L M. 2023. Flexible, breathable, and self-powered patch assembled of electrospun polymer triboelectric layers and polypyrrole-coated electrode for infected chronic wound healing. *ACS Appl. Mater. Interfaces* **15**, 17641–17652.
[301] Guo Y C, Zhang H N, Fang L, Wang Z X, He W, Shi S W, Zhang R Y, Cheng J and Wang P H. 2024. A self-powered flexible piezoelectric sensor patch for deep learning-assisted motion identification and rehabilitation training system. *Nano Energy* **123**, 109427.
[302] Mallineni S S K, Dong Y C, Behlow H, Rao A M and Podila R. 2018. A wireless triboelectric nanogenerator. *Adv. Energy Mater.* **8**, 1702736.
[303] Cao X, Zhang M, Huang J R, Jiang T, Zou J D, Wang N and Wang Z L. 2018. Inductor-free wireless energy delivery via maxwell's displacement current from an electrodeless triboelectric nanogenerator. *Adv. Mater.* **30**, 1704077.
[304] Wang H Y et al. 2021. A paradigm shift fully self-powered long-distance wireless sensing solution enabled by discharge-induced displacement current. *Sci. Adv.* **7**, eabi6751.
[305] Zhao H F et al. 2022. Underwater wireless communication via TENG-generated Maxwell's displacement current. *Nat. Commun.* **13**, 3325.
[306] Lu L J, Hu G S, Liu J Q and Yang B. 2024. 5G NB-IoT system integrated with high-performance fiber sensor inspired by cirrus and spider structures. *Adv. Sci.* **11**, 2309894.
[307] Zhu P C, Niu M J, Liang S Y, Yang W Q, Zhang Y T, Chen K, Pan Z F and Mao Y C. 2025. Non-hand-worn, load-free VR hand rehabilitation system assisted by deep learning based on ionic hydrogel. *Nano Res.* **18**, 94907301.
[308] Liu W Q, Yu W, Li K C, Zhou S Y, Wang Q and Yu H. 2023. Enhancing blind-dumb assistance through a self-powered tactile sensor-based Braille typing system. *Nano Energy* **116**, 108795.
[309] Joo H, Gwak S, Lee M H, Park H, Lee C, Lee J H, Han S A and Lee J-H. 2023. Functionalized thermoplastic polyurethane with tunable tribopolarity and biodegradability for high performance and biodegradable triboelectric nanogenerator. *Sustain. Mater. Technol.* **36**, e00638.
[310] Zhang S, Meng S, Zhang K, Wang Z, Xu X Y, Zhi C W, Shi S and Hu J L. 2023. A high-performance S-TENG based on the synergistic effect of keratin and calcium chloride for finger activity tracking. *Nano Energy* **112**, 108443.
[311] Jin Z H, Wang L L, Zheng K Y, Gao Q Y, Feng W, Hu S K, Yue M and Shan X B. 2024. Microelectronic printed chitosan/chondroitin sulfate/ZnO flexible and environmentally friendly triboelectric nanogenerator. *J. Colloid Interface Sci.* **669**, 275–282.
[312] Tan X Q, Huang Z Y, Pei H R, Jia Z C and Zheng J M. 2024. Highly porous, ultralight, biocompatible silk fibroin aerogel-based triboelectric nanogenerator. *ACS Sens.* **9**, 3938–3946.
[313] Parida K, Kumar V, Jiangxin W, Bhavanasi V, Bendi R and Lee P S. 2017. Highly transparent, stretchable, and self-healing ionic-skin triboelectric nanogenerators for energy harvesting and touch applications. *Adv. Mater.* **29**, 1702181.
[314] Li C Y, Guo H Y, Wu Z Y, Wang P, Zhang D and Sun Y H. 2023. Self-healable triboelectric nanogenerators: marriage between self-healing polymer chemistry and triboelectric devices. *Adv. Funct. Mater.* **33**, 2208372.
[315] Fu S K and Hu C G. 2024. Achieving ultra-durability and high output performance of triboelectric nanogenerators. *Adv. Funct. Mater.* **34**, 2308138.
[316] Li W J, Lu L Q, Zhang C, Loos K and Pei Y T. 2024. Durable and high-performance triboelectric nanogenerator based on an inorganic triboelectric pair of diamond-like-carbon and glass. *Adv. Sci.* **11**, 2309170.

[317] Le T H, Mai U K G, Huynh D P, Nguyen H T, Luu A T and Bui V T. 2022. Surfactant-free GO-PLA nanocomposite with honeycomb patterned surface for high power antagonistic bio-triboelectric nanogenerator. *J. Sci. Adv. Mater. Devices* **7**, 100392.
[318] Kuang T R, Zhang J B, Huang G-M, Liu T and Huang Z-X. 2024. Multifunctional biopolymer poly (lactic acid)-based triboelectric nanogenerator via controlled construction of secondary electron path. *Nano Energy* **128**, 109877.
[319] Wang C M et al. 2024. Extreme orientation of stereocomplexed poly(lactic acid) induced ultrafine electroactive nanofibers for respiratory healthcare and intelligent diagnosis. *ACS Sustain. Chem. Eng.* **12**, 9290–9300.
[320] Hou Y F, Wang F Y, Qin C C, Wu S N, Cao M Y, Yang P K, Huang L and Wu Y P. 2022. A self-healing electrocatalytic system via electrohydrodynamics induced evolution in liquid metal. *Nat. Commun.* **13**, 7625.
[321] Shen Q C et al. 2023. Liquid metal-based soft, hermetic, and wireless-communicable seals for stretchable systems. *Science* **379**, 488–493.
[322] Zhao Y Y et al. 2023. A self-healing electrically conductive organogel composite. *Nat. Electron.* **6**, 206–215.
[323] Ling S H et al. 2024. Tension-driven three-dimensional printing of free-standing Field's metal structures. *Nat. Electron.* **7**, 671–683.
[324] Liu D, Yang P Y, Gao Y K, Liu N, Ye C Y, Zhou L L, Zhang J Y, Guo Z T, Wang J and Wang Z L. 2024. A dual-mode triboelectric nanogenerator for efficiently harvesting droplet energy. *Small* **20**, 2400698.
[325] Gong S, Li K, Sun J, Chen J and Guo H. 2025. Interfacial droplet-based triboelectric nanogenerator with optimized architecture for highly efficient vibrational energy conversion. *Joule* **9**, 101763.
[326] Hu X Y, Feng J R, Liang C J, Ning H, Chen C J, Li J Y, Wen H G, Yao H L, Wan L Y and Liu G L. 2023. Round-trip oscillation triboelectric nanogenerator with high output response and low wear to harvest random wind energy. *Nano Res.* **16**, 11259–11268.
[327] Dong Y, Feng M, Cheng J H, Chang S P, Wang D A and Lu W L. 2024. Ring-shaped single-electrode triboelectric nanogenerator (RSE-TENG) for energy harvesting and liquid flow rate monitoring of gas-liquid two-phase flow. *Nano Energy* **119**, 109083.
[328] Dong S C et al. 2023. Freestanding-mode tribovoltaic nanogenerator for harvesting sliding and rotational mechanical energy. *Adv. Energy Mater.* **13**, 2300079.
[329] Wang J, Zhao Z H, Li L W, Gao Y K, Zhao X J, Zhang B F, Zhou L L, Wang Z L and Wang J. 2025. A self-recovery triboelectric nanogenerator with high breakdown resistance for water wave energy harvesting. *Adv. Energy Mater.* **15**, 2404147.
[330] Luo X X, Liu L D, Wang Y C, Li J Y, Berbille A, Zhu L P and Wang Z L. 2022. Tribovoltaic nanogenerators based on mxene-silicon heterojunctions for highly stable self-powered speed, displacement, tension, oscillation angle, and vibration sensors. *Adv. Funct. Mater.* **32**, 2113149.
[331] Qiao W Y, Zhao Z H, Zhou L L, Liu D, Li S X, Yang P Y, Li X Y, Liu J Q, Wang J and Wang Z L. 2022. Simultaneously enhancing direct-current density and lifetime of tribovotaic nanogenerator via interface lubrication. *Adv. Funct. Mater.* **32**, 2208544.
[332] Wang Z Z, Gong L K, Dong S C, Fan B B, Feng Y, Zhang Z and Zhang C. 2022. A humidity-enhanced silicon-based semiconductor tribovoltaic direct-current nanogenerator. *J. Mater. Chem. A* **10**, 25230–25237.
[333] Qiao W Y, Zhou L L, Zhao Z H, Yang P Y, Liu D, Liu X R, Liu J Q, Liu D Y, Wang Z L and Wang J. 2023. MXene lubricated tribovoltaic nanogenerator with high current output and long lifetime. *Nano-Micro Lett.* **15**, 218.
[334] Jiang F, Thangavel G, Zhou X R, Adit G, Fu H B, Lv J, Zhan L X, Zhang Y H and Lee P S. 2023. Ferroelectric modulation in flexible lead-free perovskite schottky direct-current nanogenerator for capsule-like magnetic suspension sensor. *Adv. Mater.* **35**, 2302815.
[335] Liu G et al. 2025. Ultrahigh-current-density tribovoltaic nanogenerators based on hydrogen bond-activated flexible organic semiconductor textiles. *ACS Nano* **19**, 6771–6783.
[336] Sriphan S, Worathat S, Pharino U, Chanlek N, Pakawanit P, Choodam K, Kanjanaboos P, Maluangnont T and Vittayakorn N. 2023. Highly flexible tribovoltaic nanogenerator based-on P-N junction interface: comparative study on output dependency dominated by photovoltaic effect in freestanding-mode. *Adv. Funct. Mater.* **33**, 2305106.
[337] Cao J et al. 2024. A power-managed tribovoltaic nanogenerator and self-powered wireless temperature monitoring system. *Adv. Energy Mater.* **14**, 2400659.
[338] Capilli G, Calza P, Minero C and Cerruti M. 2019. Electrospun core-sheath PAN@PPY nanofibers decorated with ZnO: photo-induced water decontamination enhanced by a semiconducting support. *J. Mater. Chem. A* **7**, 26429–26441.
[339] Ma W J et al. 2021. Smart fibers for energy conversion and storage. *Chem. Soc. Rev.* **50**, 7009–7061.
[340] Yan W and Zhu M F. 2024. High-performing semiconductor fibers set a new stage for ambient intelligence. *Adv. Fiber Mater.* **6**, 332–334.
[341] Jiang J X, Guan Q B, Liu Y N, Sun X H and Wen Z. 2021. Abrasion and fracture self-healable triboelectric nanogenerator with ultrahigh stretchability and long-term durability. *Adv. Funct. Mater.* **31**, 2105380.
[342] Wang W, Yu A F, Zhai J Y and Wang Z L. 2021. Recent progress of functional fiber and textile triboelectric nanogenerators: towards electricity power generation and intelligent sensing. *Adv. Fiber Mater.* **3**, 394–412.
[343] Rastegardoost M M, Tafreshi O A, Saadatnia Z, Ghaffari-Mosanenzadeh S, Serles P, Filleter T, Park C B and Naguib H E. 2023. Highly durable triboelectric nanogenerators based on fibrous fluoropolymer composite mats with enhanced mechanical and dielectric properties. *Mater. Today Energy* **38**, 101431.
[344] Yang T, Wan C W, Zhang X Y, Liu T, Niu L, Fang J and Liu Y Q. 2024. High-efficiency preparation of multifunctional conjugated electrospun graphene doped PVDF/CF yarns for energy harvesting and human movement monitoring in TENG textile. *Nano Res.* **17**, 4478–4488.
[345] Zheng Z P, Ma X C, Lu M Y, Yin H, Jiang L and Guo Y P. 2024. High-performance all-textile triboelectric nanogenerator toward intelligent sports sensing and biomechanical energy harvesting. *ACS Appl. Mater. Interfaces* **16**, 10746–10755.
[346] Jiang Y, Liang X, Jiang T and Wang Z L. 2024. Advances in triboelectric nanogenerators for blue energy harvesting and marine environmental monitoring. *Engineering* **33**, 204–224.
[347] Pang H, Feng Y W, An J, Chen P F, Han J J, Jiang T and Wang Z L. 2021. Segmented swing-structured fur-based triboelectric nanogenerator for harvesting blue energy toward marine environmental applications. *Adv. Funct. Mater.* **31**, 2106398.
[348] Shen S et al. 2021. High-efficiency wastewater purification system based on coupled photoelectric-catalytic action provided by triboelectric nanogenerator. *Nano-Micro Lett.* **13**, 194.
[349] Wei X L, Zhao Z H, Zhang C G, Yuan W, Wu Z Y, Wang J and Wang Z L. 2021. All-weather droplet-based triboelectric nanogenerator for wave energy harvesting. *ACS Nano* **15**, 13200–13208.
[350] Xu Y H, Yang W X, Lu X H, Yang Y F, Li J P, Wen J M, Cheng T H and Wang Z L. 2021. Triboelectric

nanogenerator for ocean wave graded energy harvesting and condition monitoring. *ACS Nano* **15**, 16368–16375.
[351] Xu W H et al. 2020. A droplet-based electricity generator with high instantaneous power density. *Nature* **578**, 392–396.
[352] Gu H J et al. 2021. A bulk effect liquid-solid generator with 3D electrodes for wave energy harvesting. *Nano Energy* **87**, 106218.
[353] Fu S K, Wu H Y, He W C, Li Q Y, Shan C C, Wang J, Du Y, Du S H, Huang Z Y and Hu C G. 2023. Conversion of dielectric surface effect into volume effect for high output energy. *Adv. Mater.* **35**, 2302954.
[354] Li Y et al. 2024. From interface effect to bulk effect: probing the capacitive coupling enhancement mechanism to achieve high performance DC droplet-based nanogenerator. *Nano Energy* **127**, 109743.
[355] Kim W-G, Kim D-W, Tcho I-W, Kim J-K, Kim M-S and Choi Y-K. 2021. Triboelectric nanogenerator: structure, mechanism, and applications. *ACS Nano* **15**, 258–287.
[356] Zhu M L, Yi Z R, Yang B and Lee C. 2021. Making use of nanoenergy from human–nanogenerator and self-powered sensor enabled sustainable wireless IoT sensory systems. *Nano Today* **36**, 101016.
[357] Wang Z H, Jin Y C, Lu C Y, Wang J Y, Song Z W, Yang X, Cao Y D, Zi Y L, Wang Z L and Ding W B. 2022. Triboelectric-nanogenerator-enabled mechanical modulation for infrared wireless communications. *Energy Environ. Sci.* **15**, 2983–2991.
[358] Zhang Q, Xin C F, Shen F, Gong Y, Zi Y L, Guo H Y, Li Z J, Peng Y, Zhang Q and Wang Z L. 2022. Human body IoT systems based on the triboelectrification effect: energy harvesting, sensing, interfacing and communication. *Energy Environ. Sci.* **15**, 3688–3721.
[359] Zhang B S, Li W B, Ge J W, Chen C G, Yu X, Wang Z L and Cheng T H. 2023. Single-material-substrated triboelectric-electromagnetic hybrid generator for self-powered multifunctional sensing in intelligent greenhouse. *Nano Res.* **16**, 3149–3155.
[360] Huang J J, Wang S L, Zhao X K, Zhang W Q, Chen Z M, Liu R, Li P, Li H L and Gui C M. 2023. Fabrication of a textile-based triboelectric nanogenerator toward high-efficiency energy harvesting and material recognition. *Mater. Horiz.* **10**, 3840–3853.
[361] Wu H, Xu X A, Xin C F, Liu Y C, Rao R Z, Li Z J, Zhang D, Wu Y X and Han S Z. 2023. Intelligent fault diagnosis for triboelectric nanogenerators via a novel deep learning framework. *Expert Syst. Appl.* **226**, 120244.
[362] Zhang H, Zhang D Z, Mao R Y, Zhou L N, Yang C Q, Wu Y, Liu Y K and Ji Y C. 2024. MoS_2-based charge trapping layer enabled triboelectric nanogenerator with assistance of CNN-GRU model for intelligent perception. *Nano Energy* **127**, 109753.
[363] Zhao C et al. 2024. Coaxial flexible fiber-shaped triboelectric nanogenerator assisted by deep learning for self-powered vibration monitoring. *Small* **20**, 2307680.
[364] Huo X Q, Wei X L, Wang B C, Cao X L, Xu J H, Yin J X, Wu Z Y and Wang Z L. 2023. Intelligent electronic passworded locker with unique and personalized security barriers for home security. *Nano Res.* **16**, 7568–7574.
[365] Ouyang W, Luo F Y, Yao Y B, Qu B B, Feng C H, Xie Y Y and Chen B. 2023. A triboelectric sensor with double bubble structure applied in a high security double lock system. *ACS Sens.* **8**, 4615–4624.
[366] Shen C, Chen J Y, Liu Y, Chen Z M and Huang J J. 2024. Triboelectric signal enhancement via interface structural design and integrated with deep learning for real-time online material recognition. *Chem. Eng. J.* **500**, 156874.
[367] Ji X L, Fang P L, Xu B Z, Xie K, Yue H B, Luo X, Wang Z X, Zhao X and Shi P. 2020. Biohybrid triboelectric nanogenerator for label-free pharmacological fingerprinting in cardiomyocytes. *Nano Lett.* **20**, 4043–4050.
[368] Dai K R, Miao X Y, Zhang W L, Huang X H, Zhang H and Kim S-W. 2023. Robust displacement sensing by direct-current triboelectric nanogenerator via intelligent waveform recognition. *Adv. Sci.* **10**, 2204694.
[369] Zhang T T, Manshaii F, Bowen C R, Zhang M Y, Qian W Q, Hu C S, Bai Y N, Huang Z J, Yang Y and Chen J. 2025. A flexible pressure sensor array for self-powered identity authentication during typing. *Sci. Adv.* **11**, 2297.
[370] Luo H, Wang H Q, Yang L J, Wu H, Kang S L, Yong S, Liao R J, Wang J Y and Wang Z L. 2022. In situ nanofluid dispersion monitoring by liquid-solid triboelectric nanogenerator based on tuning the structure of the electric double layer. *Adv. Funct. Mater.* **32**, 2200862.
[371] Zhou Y K, Cui X and Zhang Y. 2024. Self-powered wireless devices and machine learning enable local humidity monitoring. *IEEE Trans. Intell. Transp. Syst.* **25**, 10369–10374.